Resonance behaviour for classes of billiards on the Poincaré half-plane

Phil Howard

Technical Report
RHUL–MA–2007–6
30 May 2007

Department of Mathematics
Royal Holloway, University of London
Egham, Surrey TW20 0EX, England
http://www.rhul.ac.uk/mathematics/techreports

Resonance behaviour for classes of billiards on the Poincaré half-plane

Phil Howard

Department of Mathematics

Royal Holloway College

University of London

A thesis submitted for the degree of

Doctor of Philosophy

in the faculty of science of the University of London

September 2006

Dedication

Το 'Ονειροποιος

I declare that the work presented in this thesis is my own work.

Abstract

The classical and quantum mechanics of two linked classes of open billiard systems on the Poincaré half-plane is studied. These billiard systems are presented as models of arithmetic scattering systems under deformation. An investigation is made of the classical phase space and the stability of a certain family of periodic orbits is investigated. The movement of the positions and widths of the resonances is followed, as the shape of Artin's billiard is deformed. One deformation varies its lower boundary, interpolating between integrable and fully chaotic cases. The other deformation translates the right hand wall of the billiard, thus interpolating between several examples of Hecke triangle billiards. The variation of the statistical properties of the spectra are focussed on and the transitions in the statistics of the resonance positions and widths are mapped out in detail near particular values of the deformation parameters, where the billiard is a fundamental domain for some arithmetic group. Analytic solutions for the scattering matrix and the resonance positions in these particular systems are derived and numerical results are obtained which are in excellent agreement with the predictions.

Away from the arithmetic systems, both generic behaviour according to the predictions of Random Matrix Theory, and non-generic behaviour is found, with deviations occurring particularly in the long range statistics. In the integrable case, semiclassical WKB theory is used to produce accurate wavefunctions and eigenvalues. For the general deformation a number of numerical methods are explored, such as the finite element method, complex absorbing potentials and collocation, in order to find an optimum method to locate the resonance positions.

Acknowledgements

There are many people who deserve my thanks for their role in the production of this thesis. I do not intend to list them all, for inevitably some will be forgotten and others misremembered. But to all those individuals that I have had the fortune to interact with over the past four years - yet do not get mentioned here - I thank you for whatever influence you have had on bringing me to this point. To misquote Chuck Yeager, *"I've had a ball"*.

Before offering more personal thanks though, I must acknowledge the much-appreciated support of the research council EPSRC, who funded me for three years. Their financial support has made all this possible, and I am particularly grateful for the EPSRC and EU funds that have enabled my attendance at several stimulating and enjoyable conferences over my time at Royal Holloway.

Above all though, I must thank my supervisor, Pat O'Mahony. From our initial meeting over four years ago up to the present day, he has never ceased to show interest in and offer encouragement for my work. Whenever I would be dragging my feet in a mire of computational difficulties or such, he would remotivate me with interesting and fruitful discussions of where we could go next, or a shared wonder at the remarkable and fascinating nature of the systems studied in this thesis. Of course, his repeated, exasperated cries of *"get writing!"* over the last year have been much appreciated too, and at long last they have paid off. His pertinent criticism of this document as it grew has been invaluable. For sharing his time and expert knowledge, and for keeping a firm grasp on our goal of a finished product I cannot thank him enough.

I must also thank the other members of the Quantum Dynamics Group at Royal Holloway, for their guidance and encouragement. In particular I must praise their multi-lingual translation skills, and thank them for the enjoyable reading and discussion groups organised on quantum information. Sadly their talents in these areas have not rubbed off on me. Hopefully their kind words and friendly mannerisms will have.

Ville Uski has been a good friend as well as a role-model for where I hope to be in the now not-too-distant future. His 'warm' Finnish exterior belies a charming wit and sharp scientific mind. I owe him a huge debt for being so incredibly helpful, generous and patient in his instruction of me on all matters computational. On that note I must also mention Paula Valença for her role as the Linux reference point in our office for three years. I hope it wasn't my ceaseless barrage of OS difficulties that drove her back to Portugal.

My thanks also to Holger Then, who I met in Cambridge and who kindly shared his Bessel function routines, which are the basis for the routines we use here for the bulk of the numerical calculations.

Paula, Chris, Krassi, Laurence and Tim must also all be thanked for being fantastic to share an office with; as colleagues and as friends. I feel privileged to have shared blackboard space with the instigators of so many fascinating discussions, and have always been sad to wipe their discoveries and creations away. I hope they have appreciated some of mine. To have their companionship on this journey through the PhD has been, as I mentioned before, a ball. I almost feel a little guilty, for being the first to finally submit out of our group.

Outside of the Royal Holloway mathematics department there are even more people who have been sources of encouragement, relief, inspiration, support and medication. Foremost in my thoughts are Wezli and the other Neuromantics, who are sorely missed. Music has been most cathartic for me over these trying years and for that I must

also thank my gigging partners Caroline, Dave and Gideon, amongst others.

Socially, the members of Gamesoc have provided much-needed light relief week-in week-out and in particular I have to thank Matt Stanham for his tireless devotion to our small gaming group. Thanks to him, and to Chris, Ed, Ian and Matt Butler for many great times. Let the dice fall where they may.

Thanks also to my piratey pals in British Sea Power and our mutual friend Barnie who passed away this year. He will be remembered fondly.

Personally I have to offer my thanks to Elizabeth for the past and to Miranda for the present. Miranda's patience and understanding while I have been writing this thesis have been monolithic, and her loving support a constant source of energy and motivation.

Finally I offer my thanks to my family for so much. For twenty-eight years of confidence in me and unfailing support when I have needed it. I can but hope I serve as a reasonable model for my brother Geoffrey, who is just entering the second year of his mathematics undergraduate course. I wish him the best in everything.

Contents

List of Tables

List of Figures

Nomenclature

Greek Symbols

$\sum_j$	The sum over terms indexed by j.
$\prod_j$	The product of terms indexed by j.
$\imath$	Unit imaginary number $\sqrt{-1}$.
π	$4\tan^{-1}(1), \quad \simeq 3.14159\ldots$

Other Symbols

$\Re(z)$	Real part of a complex number z.
$\Im(z)$	Imaginary part of a complex number z.
$\oint_\gamma$	Integration around a curve γ
$f(x)\|_p$	The function $f(x)$, evaluated at the point $x = p$.
$\|z\|$	The absolute value (modulus) of z.
Δ_{LB}	The Laplace-Beltrami operator
$\{q_j\}$	A set of elements q, indexed by j.
$\mathbb{H}$	The set of points making up the Poincaré half-plane.
$\mathbb{Z}$	The set of integers.
$\mathbb{R}$	The set of real numbers.

$\mathrm{SL}(2,\mathbb{R})$ The group of rank two matrices with real elements and unit determinant.

$\mathrm{PSL}(2,\mathbb{R})$ The group of rank two matrices with real elements and unit determinant, modulo plus or minus the identity.

$\mathrm{PSL}(2,\mathbb{Z})$ The Modular group; the group of rank two matrices with integer elements and unit determinant, modulo plus or minus the identity.

$\Gamma(2,n)$ The Hecke group with $\theta = \frac{\pi}{n}$.

Acronyms

RMT Random Matrix Theory

GOE Gaussian Orthogonal Ensemble

GUE Gaussian Unitary Ensemble

CAP Complex Absorbing Potential

FEM Finite Element Method

KAM Kolmogorov-Arnold-Moser theorem

EBK Einstein-Brillouin-Keller theory

WKB Wentzel-Kramers-Brillouin theory

BGS Bohigas-Giannoni-Schmit conjecture

Chapter 1

Introduction

"It was the best of times, it was the worst of times.
- Charles Dickens, *A Tale Of Two Cities*"

The duality expressed above by Dickens is present throughout this thesis. The background area worked in, the world context in which the events here are considered, is the field of Quantum Chaos - a term coined to describe investigation of quantum limits of classical systems displaying chaotic behaviour. In the forty-five years since chaotic dynamics were first investigated by Lorenz (a meteorologist), nearly every area of human investigation has been touched by the advances made in our understanding of these systems. What we are witnessing is the final stages of a paradigm shift started at the beginning of the last century, when the seeds of relativity and quantum mechanics were sown to grow up and overthrow the old world picture of a deterministic, fixed, infinite universe. However, even before those two great revolutions began, mathematicians such as Poincaré had laid the foundations for the explosive volume of work done on chaotic systems once the experimental hardware of electronic computers became widely available. These three threads of human investigation interact beautifully in the systems studied here and it is their paradoxical interplay which initially motivated my studies in this area.

The brave new world of quantum mechanics did not sit easily alongside these early developments in classical chaos. Einstein [Ein17] was quick to fault the emerging probabilistic theory for its apparent limitation to integrable systems.

The standard semiclassical techniques to describe the correspondence principal linking quantum systems to their classical limits (WKB, EBK theory [BB97]) rely on tori in phase space for applicability. Whereas classically the KAM theory [Ott93] of how these tori are destroyed as chaos increases in a system was a huge success, no resolution was forthcoming to the problem of how to treat, in general, the quantum problems corresponding to even the simplest classically chaotic systems, until the work of Gutzwiller in the late sixties [Gut90]. Even today, relatively little is known about generic quantum properties of systems with classically mixed phase space [BTU93].

So just as we still struggle to unify general relativity and quantum mechanics, thus viewing them both as limits of some more general theory, so too are there still many open questions posed when trying to understand classical mechanics as some limit of quantum mechanics. In fact, the question has even been asked [Maj98] as to whether quantum chaos exists at all. That is, does chaos manifest in quantum systems? The name is perhaps at least a little misleading (Berry [Ber89] suggested the term 'quantum chaology' as a less loaded alternative, which is popular in some circles). Classical chaos arises when there are nonlinearities in the dynamical equations governing the evolution of a system. However, the Schrödinger equation which governs quantum systems is linear and thus typical chaotic phenomena such as the exponential divergence of neighbouring trajectories are not seen. Moreover, the very notion of a trajectory is redundant in quantum mechanics. How can two such different descriptions of a system be compatible? This is just the tip of the iceberg. Hence the opening quotation - which continues with *"it was the age of wisdom, it was the age of foolishness, it was the epoch of belief, it was the epoch of incredulity."* Our advances in one theory on the one hand enlighten, yet on the other throw much else into doubt. All the time there are fresh surprises being uncovered. It is from the eventual resolution of these clashes that deeper understanding emerges, and thus the questions keep coming and our quest continues.

In fact exponential sensitivity, though not to initial conditions, can be observed in some quantum systems [SC93; Sch95], though most often disorder is seen to suppress state diffusion, such as in Anderson localization [And58]. Otherwise, there are more generally *traces* of chaotic behaviour detectable in quantum

systems. The most notable and well-studied to date of these are the *scarring* of wavefunctions and the statistical distribution of quantum eigenvalues. Scars were discovered by Heller et al. [Hel84] in 1984 and are a tendency of the quantum probability distribution to cluster around unstable classical periodic orbits. We do not study this phenomenon here and focus more on the statistical properties of the spectra. Also in 1984, Bohigas et al. [BGS84] made a famous conjecture that led to a vast volume of work done on this topic. They conjectured that all suitably chaotic systems have spectra that display the same statistical properties as those of large matrices with entries chosen at random from an appropriate distribution. This suggestion was prompted by, amongst other things, the largely successful application of the Random Matrix Theory (RMT) to nuclear data [PT56]. Indeed, in the years following, this prediction has proved to be remarkably accurate for almost all systems obeying wave equations with underlying chaotic dynamics. More recently, progress has been made in understanding the success from a theoretical point of view [MHB$^+$04] and we expect the agreement to be better in particular for short-range statistics rather than for long-range correlations, due to non-universal features of particular systems.

Returning to our theme of revolution in the scientific picture of the world, another mathematical development important in this work was the discovery of hyperbolic geometry in the early nineteenth century, which turned the millennia-old work of Euclid on its head. If quantum chaos provides the context for consideration of this work, then hyperbolic geometry is the theatre in which the actors play out their roles. Here the actors are the spinless, non-relativistic particles of the two-dimensional Schrödinger equation and the stage is a strangely contorted construction called Artin's billiard, where the players enter and exit from infinitely far away. We will study the changing patterns these characters form as the stage shifts its boundaries, and focus on key moments where fascinating symmetries emerge from what looks at first to be a random configuration. In fact Artin's billiard has even been proposed as a model for the early universe [ALST05]. As such the stage becomes the curved space-time of general relativity and the play becomes one of cosmological significance. However, this is not a line of investigation that shall be pursued here.

Enough with metaphor. What is studied here is a class of systems, unbounded in one direction but constrained by infinitely high walls in all others. The space on which these so-called billiard systems are defined is negatively curved (this is what hyperbolic geometry means), so the constrained motion of classical particles is highly chaotic, as discovered at the turn of the last century by Hadamard [Had98]. Being simply defined and completely describable mathematically, these systems became paradigms of the new theory of chaotic dynamics that arose in the latter half of that century. In fact Artin's first investigations [Art24] of his eponymous billiard established the use of symbolic dynamics in classifying dynamical systems (reducibility to symbolic dynamics is now considered a hallmark of the strongest form of chaos). These fascinating systems are the starting point of our investigation and one is recommended to read the excellent review article by Balazs and Voros [BV86] for a more technical introduction to the area, though all the necessary background material for appreciation of our results will be provided here.

Being so widely and precisely studied in terms of classical mechanics meant that the billiard systems in hyperbolic geometry were natural candidates for investigation of quantum chaos. The startling discovery was that for certain triangular billiards including Artin's billiard, the distribution of spacings between nearest neighbour energy levels obeyed a distribution typical of fully integrable systems [BGS86]. Other triangles showed the expected fit to the distribution for the Gaussian Orthogonal Ensemble of random matrices. It wasn't until several years later that an explanation for these deviations was forthcoming. In fact, the non-universal statistics only occur in billiard systems which are the *fundamental domain* of some *arithmetic group* [BGGS92; BSS92]. These terms will be defined later (see sections 3.1 and 4.2). Suffice to say that these systems are of particular interest to number theorists due to their relation to groups representable by matrices having particular restrictions on their elements. For instance, Artin's billiard is closely related to the Modular group, whose matrix representations have only integer entries. For such systems (and indeed for all billiards which are a fundamental domain of some group) there is in fact an explicit formula - Selberg's trace formula - which allows, in principle, exact calculation of quan-

tum spectral properties from classical quantities derived from the group matrices [ASS88].

While the mathematicians have known much about these systems for years, it is only relatively recently that the physics community has started to pay more attention to them. This is partly because of the violation of universality in the level-spacing statistics mentioned above. But there is one further thread adding colour to the tapestry we are weaving. The above, and indeed most of the work on these systems, has been done on the bound states of billiards. There are however even more fascinating features to be observed in the scattering theory from open billiards. The quantum scattering theory for systems that are classically chaotic has attracted much interest in recent years (see for example, the recent special issue of Journal of Physics A entitled *'Trends in quantum chaotic scattering'* [FKS05]), although there is not the level of knowledge about open systems as there is about bounded ones. It turns out that the scattering theory for arithmetic systems violates the predictions of RMT even more dramatically than the statistics of the bound states do.

In particular, Artin's billiard has the position in energy of its resonances (quasi-bound states which correspond to the eigenfunctions in bound systems) determined by the zeros of Riemann's zeta function on the *critical line* $\Re(z) = \frac{1}{2}$. This leads to two distinct and remarkable features of the resonance spectrum. Most obvious is that the imaginary parts of the momenta, which correspond in some sense to the lifetime of the quasi-bound state, are all equal (to $-\frac{1}{4}$). For generic chaotic scattering systems, RMT predicts a chi-squared distribution for the widths, so this behaviour is quite extraordinary. The second abnormality is in the statistics of the real parts of the resonant momenta. These are positioned according to the values of the Riemann zeros and thus have statistics which follow the predictions of RMT for systems that aren't invariant under the operation of time-reversal, although this symmetry is intact in the system.

The connection between the Riemann zeta function and quantum chaos was first noticed in a fortuitous meeting of Dyson and Montgomery in 1972. Dyson pointed out that the pair-correlation function of the Riemann zeros mentioned to him by Montgomery matched that of the nuclear resonance data he was looking at [Mon73]. This observation sparked a field of application of RMT in number

theory that is still proving to be incredibly fruitful [MS05]. One of the ideas that has emerged and has focussed attention on the systems studied here is the *spectral interpretation* of the Riemann zeros. That is the suggestion that there may be some Hamiltonian system whose quantum spectrum has the Riemann zeros as its eigenvalues [BK99]. The importance of this would be an immediate proof of the celebrated Riemann hypothesis. Obviously Artin's billiard, with its resonance spectrum fulfilling the criterion, is tantalisingly close to meeting the requirements, but a suitable system has yet to be found.

It is also the case for Artin's billiard that a set of bound states exist superimposed on the scattering continuum (so-called *cusp forms* in mathematics). Such states arise in atomic scattering when the parameters of a system conspire to give zero coupling to the continuum, and are extremely sensitive to perturbation of those parameters [Fri98]. Additionally, the Phillips-Sarnak conjecture [PS85] states that an infinite set of cusp forms only exist for the case of arithmetic billiards, and that they should all be destroyed for arbitrary deformations of those billiards. Here the cusp forms are treated as part of the resonance continuum and the variation of the resonance positions on smoothly deforming the boundary of Artin's billiard is studied. Thus we have reasons from both physics and mathematics for expecting that the cusps will immediately evolve into resonances as the billiard shape is varied. Mathematically the task of studying the deformation of cusp forms under perturbation is challenging and only very few recent efforts have been made in this direction [BV98; Ave02]. The results presented here numerically chart the evolution of many resonances under two separately parameterised deformations of Artin's billiard. One parameterisation varies the shape until at one limit a fully-integrable billiard system is reached. This follows the work of Csordás et al. who studied the same deformation but in the context of the bound spectrum with no continuum present. The other parameterisation shifts the walls so that the transitions between three separate arithmetic systems can be traced, as well as including another, non-arithmetic group along the way. The groups encountered as the second deformation is applied are from the class of Hecke groups, of which the Modular group is the simplest. We predict and discover a class of resonance in those systems with fixed width twice that of the

resonances determined by the Riemann zeta function, and with regularly spaced real parts.

1.1 Organization of thesis

In the following three chapters the necessary background material for the appreciation of our results is presented. In chapter 2 we give a brief review of hyperbolic geometry and introduce the classical and quantum mechanics for free motion in the particular model studied here, the Poincaré half-plane.

In chapter 3 the concept of compactification of a region to obtain a billiard system is defined. The dramatic differences in the classical and quantum mechanics for billiards as opposed to those for free systems are discussed. A detailed analysis of the scattering theory for Artin's billiard is presented.

Chapter 4 introduces the two different deformations to Artin's billiard that we consider. Also, an explanation is given of the structure of the groups we encounter. These are groups for which a fundamental domain corresponds to one of the billiard systems at some particular values of the deformation parameters. Two explicit methods of calculating the scattering parameters are presented.

Then we move on to a discussion of our results in chapter 5. We start with an investigation of the classical mechanics. We examine the variation of phase space and the stability of a class of periodic orbits, as the deformation progresses from an integrable case to the fully chaotic case of Artin's billiard. Then there is a discussion of the various numerical methods we have tried in solving the full quantum problem, and we present some detailed statistics on the resonances obtained by a modified collocation method developed specifically for tackling this problem. Both short and long-range correlations are investigated, in both the real and imaginary parts of the resonance spectra, and their variation as the deformation progresses is followed.

The results for the second deformation are presented similarly, though we restrict our attention to short-range correlations, where the dramatic spectral reorganisations due to the transitions to arithmetic systems are most vividly displayed. A derivation of the scattering matrix for these arithmetic systems is performed and its predictions confirmed by our data. This is most notable in the

discovery of a class of resonance in those systems with fixed width and regularly spaced real parts.

A comparison of our results with those already available in the literature is made in table 5.1, at least for cases where there are results available. Excellent agreement is found. Concluding remarks and a summary of our main results can be found in chapter 6.

Chapter 2

Classical and quantum mechanics in hyperbolic geometry

2.1 Hyperbolic geometry

Euclid's fifth postulate in his axiomatisation of geometry states: 'If a line segment intersects two straight lines forming two interior angles on the same side that sum to less than two right angles, then the two lines, if extended indefinitely, meet on that side on which are the angles less than the two right angles.'

This statement, the 'parallel postulate' was the cause of much discomfort until the nineteenth century when the two alternatives, leading to spherical and hyperbolic geometries, were actively investigated. In the hyperbolic case which is the setting for investigations here, the two lines do not necessarily meet, and there are an infinite number of straight lines through a given point parallel to another. The spherical case corresponds to the geometry of lines on a sphere, the earth's surface for instance, and much of our intuition about its properties can be carried over to the less intuitive hyperbolic case. For example while the angles in a triangle on a sphere add up to more than 180 degrees, in hyperbolic geometry they add up to less. For this reason, hyperbolic geometry was also called acute geometry.

As the surface of a sphere models spherical geometry, so there is a pseudo-sphere which models the hyperbolic case. A sphere in three dimensional Euclidean space is given by the equation $x_1^2 + x_2^2 + x_3^2 = R^2$, where R is the radius of the

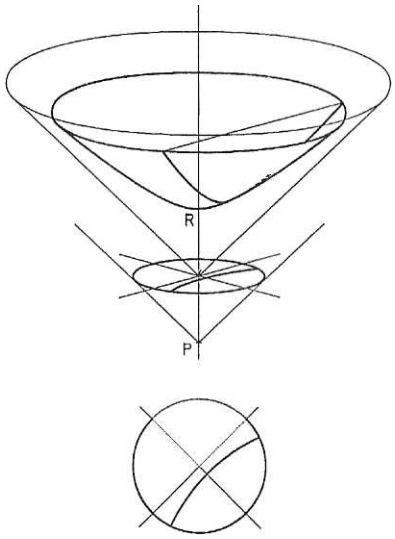

Figure 2.1: Geometry of the transformation from pseudo-sphere to disk variables. The upper figure shows the pseudo-sphere, or hyperboloid, and the lower figure the Poincaré disk. A single geodesic and its projection onto the disk is indicated. Reproduced from [BV86].

sphere. That is to say it is the set of points a constant Euclidean distance from the origin. The pseudo-sphere has equation $x_1^2+x_2^2-x_3^2 = -R^2$, which is constant distance from the origin if a non-Euclidean (Minkowskian, specifically) measure of distance (metric) is used, $\mathrm{d}s^2 = \mathrm{d}x_1^2 + \mathrm{d}x_2^2 - \mathrm{d}x_3^2$. Here we only consider the case $R = 1$, so that the Gaussian curvature ($-1/2$ of the scalar curvature) is -1 everywhere (the surface is clearly homogeneous). This corresponds to using R as the unit of distance [BV86]. The existence of this fixed scale has important ramifications for the geometry, one of which will be seen in section 3.1.

Just as it is convenient to map the surface of the earth onto flat two-dimensional paper, it is easier to work with projected models of the pseudo-sphere for most purposes. Two models due to Poincaré are widely used; the disk and the half-plane. The Poincaré disk is obtained by stereographically projecting the top half of the pseudo-sphere down onto the unit disk in the x_1x_2 plane via the mapping (obtained by similar triangles with base $P = (0, 0, -1)$)

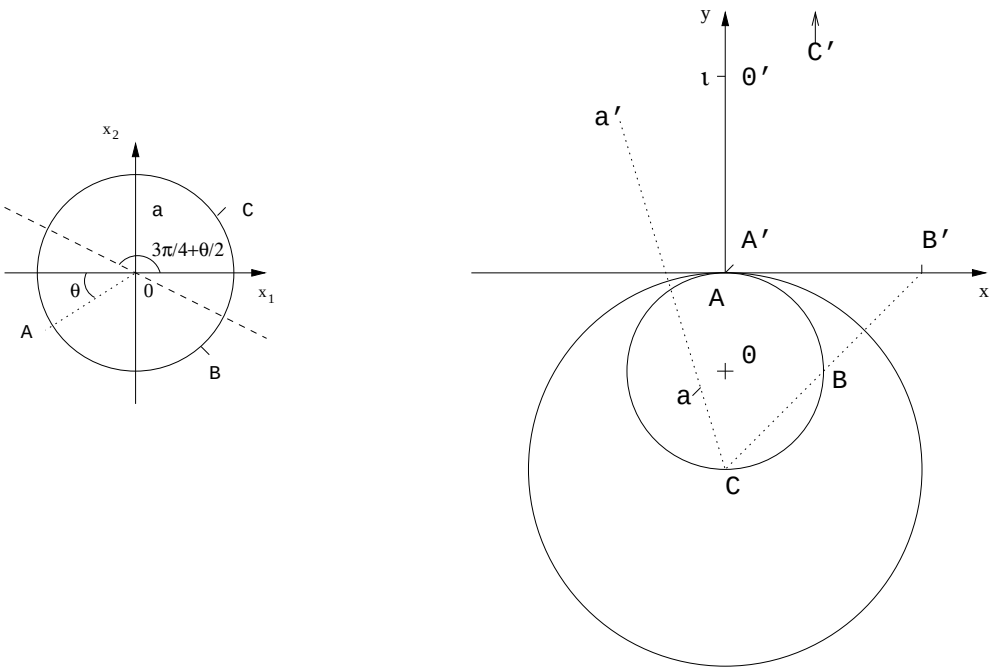

Figure 2.2: Geometry of the transformation from disk to half-plane variables. To the left is shown the reflection of the disk in the line $\arg(w) = 3\pi/4 + \theta/2$ and to the right its inversion across the circle $|w - \imath| = 1$.

$$\begin{aligned} x_1 &\mapsto x_1' = x_1/(1+x_3) \\ x_2 &\mapsto x_2' = x_2/(1+x_3) \end{aligned} \tag{2.1}$$

(See figure 2.1 for a picture of the geometry). Thus the metric on the disk becomes

$$\mathrm{d}s^2 = \frac{4(\mathrm{d}x_1'^2 + \mathrm{d}x_2'^2)}{(1-(x_1'^2+x_2'^2))^2} \tag{2.2}$$

by substitution of variables. The base of the top sheet maps to the origin, and the points at infinity map to the boundary of the disk, which has unit radius.

It becomes convenient for describing transformations to use a complex notation, $w = x_1' + \imath x_2'$ and the mapping of the disk to the Poincaré half-plane model is given by the conformal (angle preserving) Möbius transformation

$$z = x + \imath y = -\imath \frac{w + e^{\imath\theta}}{w - e^{\imath\theta}}. \tag{2.3}$$

This takes the origin of the disk to the point $z = \imath$ and θ is the angle of an arbitrary rotation of the disk around that point. The geometry of the transformation is shown in figure 2.2 with reference to how points a, A, B and C transform to the corresponding points a', A', B' and C'. First the disk is reflected in the line $\arg(w) = 3\pi/4 + \theta/2$ (shown on the left of the figure; this is equivalent to a clockwise rotation of the disk by θ and then reflection in the line $x_1 = -x_2$). Next its dimensions are reduced by a factor of two and it is translated to sit as it is displayed in the right hand of the figure, with its centre at the point $-\frac{\imath}{2}$. Then it is inverted across the circle $|w - \imath| = 1$ as indicated. That is to say, a point at a distance s from C, the centre of the inversion, maps to a point a distance $1/s$ from C along the same radial direction. The boundary of the unit circle is taken to the real axis and one point at complex infinity (the point C in the figure).

The metric now becomes

$$\mathrm{d}s^2 = \frac{\mathrm{d}x^2 + \mathrm{d}y^2}{y^2} = \frac{\mathrm{d}z\mathrm{d}\overline{z}}{y^2}, \tag{2.4}$$

which can also be written

$$\mathrm{d}s^2 = g_{ij}x^i x^j; g_{ij} = y^{-2}\delta_{ij} \tag{2.5}$$

Using Einstein's notation for summing over indices and where δ_{ij} is the Kronecker delta. Geodesics (straight lines) in this metric are determined (by minimization over paths of the integral $\int_{z_1}^{z_2} \mathrm{d}s$ giving the arclength between two points) by the equation [Sch80b]

$$\frac{\mathrm{d}^2 x^i}{\mathrm{d}t^2} + \Gamma^i_{jk} \frac{\mathrm{d}x^j}{\mathrm{d}t} \frac{\mathrm{d}x^k}{\mathrm{d}t} = 0, \tag{2.6}$$

where here the Christoffel symbol

$$\Gamma^i_{jk} = \frac{1}{2} g^{im} \left(\frac{\partial g_{mj}}{\partial x^k} + \frac{\partial g_{mk}}{\partial x^j} - \frac{\partial g_{jk}}{\partial x^m} \right), \tag{2.7}$$

so the only non-zero symbols are

$$\Gamma^1_{21} = \Gamma^1_{12} = \Gamma^2_{22} = -1/y \tag{2.8}$$

and

$$\Gamma^2_{11} = 1/y. \tag{2.9}$$

Equation (2.6) thus becomes the pair

$$\frac{\mathrm{d}^2 y}{\mathrm{d}t^2} - \frac{1}{y}\left(\frac{\mathrm{d}y}{\mathrm{d}t}\right)^2 + \frac{1}{y}\left(\frac{\mathrm{d}x}{\mathrm{d}t}\right)^2 = 0 \tag{2.10}$$

and

$$\frac{\mathrm{d}^2 x}{\mathrm{d}t^2} - \frac{2}{y}\left(\frac{\mathrm{d}x}{\mathrm{d}t}\frac{\mathrm{d}y}{\mathrm{d}t}\right) = 0. \tag{2.11}$$

As can be seen from direct substitution, these have solutions

$$\begin{aligned} x &= q + r\tanh(t), \\ y &= r\,\mathrm{sech}(t), \end{aligned} \tag{2.12}$$

which are the equations of circles crossing the real axis orthogonally, with centre $(q, 0)$ and radius r, or vertical straight lines ($r = 0$). Figure 2.3 shows some examples.

Finding $\int_{z_1}^{z_2} \mathrm{d}s$ along the unique geodesic connecting the two points z_1 and z_2, using this canonical parameterisation (t can have a scalar prefactor), gives the distance $\rho(z_1, z_2)$ between them as

$$\begin{aligned} \rho(z_1, z_2) &= t(z_2) - t(z_1) \\ &= \cosh^{-1}\left(\frac{r}{y_2}\right) - \cosh^{-1}\left(\frac{r}{y_1}\right) \\ &= \ln\left(\frac{r}{y_2} + \sqrt{\left(\frac{r}{y_2}\right)^2 - 1}\right) - \ln\left(\frac{r}{y_1} + \sqrt{\left(\frac{r}{y_1}\right)^2 - 1}\right) \\ &= \ln\left(\frac{\frac{r}{y_2} + \frac{x_2 - q}{y_2}}{\frac{r}{y_1} + \frac{x_1 - q}{y_1}}\right). \end{aligned} \tag{2.13}$$

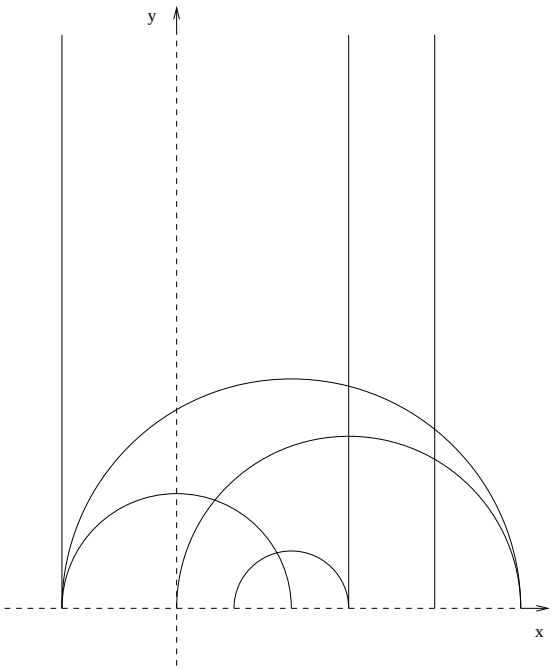

Figure 2.3: Some geodesics on the Poincaré half-plane.

Here the subscripts label the different points, not the components of some tensor as they do in (2.6).

Elementary trigonometry shown in figure 2.4 provides the following relations

$$\frac{r}{y_2} = \text{cosec}(\beta), \quad \frac{r}{y_1} = \text{cosec}(\alpha) \tag{2.14}$$

and

$$\frac{x_2 - q}{y_2} = \cot(\beta), \quad \frac{x_1 - q}{y_1} = \cot(\alpha), \tag{2.15}$$

as well as

$$A = |z_1 - z_2| = 2r\sin\left(\frac{\alpha - \beta}{2}\right), \quad B = |z_1 - \overline{z_2}| = 2r\sin\left(\frac{\alpha + \beta}{2}\right) \tag{2.16}$$

and

$$A^2 = 2r^2\left(1 - \cos(\alpha - \beta)\right); B^2 = 2r^2\left(1 - \cos(\alpha + \beta)\right). \tag{2.17}$$

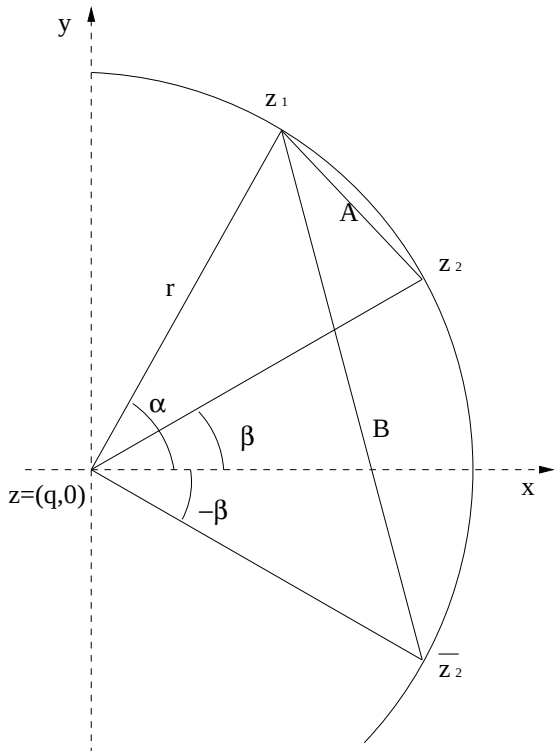

Figure 2.4: Geometry for finding the geodesic distance between two points z_1 and z_2 on the Poincaré half-plane.

Using these and some simple trigonometrical identities leads to the following equivalent expressions seen in the literature [BV86; Cox65] for the distance

$$\begin{aligned}
\rho(z_1, z_2) &= \ln\left(\frac{\mathrm{cosec}(\beta)+\cot(\beta)}{\mathrm{cosec}(\alpha)+\cot(\alpha)}\right) && (2.18)\\
&= \ln\left(\frac{\sin(\alpha)(1+\cos(\beta))}{\sin(\beta)(1+\cos(\alpha))}\right)\\
&= \ln\left(\frac{1+\cos(\beta)-\cos(\alpha)+\cos(\alpha)\cos(\beta)}{\sin(\beta)\sin(\alpha)}\right)\\
&= \ln\left(\frac{(A+B)^2}{B^2-A^2}\right)\\
&= \ln\left(\frac{|z_1-z_2|+|z_1-\overline{z_2}|}{|z_1-\overline{z_2}|-|z_1-z_2|}\right) && (2.19)\\
&= 2\tanh^{-1}\left(\frac{|z_1-z_2|}{|z_1-\overline{z_2}|}\right) && (2.20)\\
&= \cosh^{-1}\left(1+\frac{|z_1-z_2|^2}{2y_1y_2}\right). && (2.21)
\end{aligned}$$

Thus points on the real axis are infinitely far from all other distinct points, as is the point at complex infinity.

Here we use primarily the half-plane model due to the simplicity in this geometry of the billiard systems to be considered later. The group of transformations which map the half-plane to itself and preserve lengths while doing so are the fractional linear transformations or Möbius transformations

$$\mathfrak{h} = z \mapsto z' = \frac{az+b}{cz+d}; a, b, c, d \in \mathbb{R}, \tag{2.22}$$

with the condition $ad - bc > 0$ to ensure that the mapping has an inverse. These are the isometries of the half-plane and will play an important role in the quantum theory of billiard systems on this space, when those systems possess corresponding symmetries. Combinations of these transformations have the same properties as matrix multiplication so it is useful to use a matrix representation

$$\mathfrak{h} = \begin{pmatrix} a & b \\ c & d \end{pmatrix} \tag{2.23}$$

whence it is apparent that that multiplication of $\mathfrak{h}$ by any real number produces the same transformation, so it is appropriate to normalise $ad - bc = 1$ (which corresponds to only considering matrices with unit determinant). This means a matrix representation is unambiguous up to a sign (both $\pm\mathbb{I}$ correspond to the identity transformation). Hence the required matrix group of transformations is $\mathrm{PSL}(2,\mathbb{R}) = \mathrm{SL}(2,\mathbb{R})/\pm\mathbb{I}$. That is the Projective Special Linear group, the quotient group of the Special Linear group modulo a sign (the Special Linear group $\mathrm{SL}(2,\mathbb{R})$ is the group of all real fractional linear transformations with unit determinant defined above). From here on matrix notation is used for convenience and this remaining ambiguity kept in mind. The group $\mathrm{PSL}(2,\mathbb{R})$ is generated by the elements

$$S = \begin{pmatrix} 0 & -1 \\ 1 & 0 \end{pmatrix} \quad T = \begin{pmatrix} 1 & t \\ 0 & 1 \end{pmatrix}, \tag{2.24}$$

where $t \in \mathbb{R}$, which correspond to the transformations

$$S(z) = -1/z \quad \{T_t(z)\} = \{z + t\}, \tag{2.25}$$

that is the simple operations of inversion across the unit circle and translation in the x direction by t. It is easy to show that under these transformations the metric (2.4) is invariant, thus this invariance extends to all members of the group and it is isomorphic to the group of isometries discussed above.

2.2 Classical mechanics on the half-plane

An unconstrained particle moving on the half-plane follows the geodesics given by (2.12). The canonical choice of parameterisation used in that pair of equations corresponds to constant unit velocity

$$v = \sqrt{g_{ij}\frac{\mathrm{d}x^i}{\mathrm{d}t}\frac{\mathrm{d}x^j}{\mathrm{d}t}} = 1. \tag{2.26}$$

The kinetic energy is the usual $\frac{1}{2}mv^2$, where the mass of the particle is m (taken as 1 from here on) thus giving a free Lagrangian

$$L = \frac{1}{2y^2}(\dot{x}^2 + \dot{y}^2), \tag{2.27}$$

with the dot notation indicating differentiation with respect to time (not necessarily the canonical choice). Since this Lagrangian has no explicit dependence on time or the x coordinate, obvious conserved quantities are the energy

$$E = \frac{1}{2y^2}(\dot{x}^2 + \dot{y}^2) \tag{2.28}$$

and the momentum in the x direction

$$p_x = \frac{\partial L}{\partial \dot{x}} = \frac{\dot{x}}{y^2}. \tag{2.29}$$

The momentum in the y direction

$$p_y = \frac{\partial L}{\partial \dot{y}} = \frac{\dot{y}}{y^2} \tag{2.30}$$

is not conserved.

The Hamiltonian is

$$H = \frac{1}{2}g^{ij}p_i p_j = \frac{y^2}{2}(p_x^2 + p_y^2). \tag{2.31}$$

A third conserved quantity associated with the free motion can be found by analogy with the motion on a regular sphere; the angular momentum,

$$M = xp_x + yp_y. \tag{2.32}$$

The existence of these independent constants of motion implies complete integrability of the system, unsurprisingly for this free motion. The principle of least action allows us to find again the geodesics described above by (2.6). Important now however, is the fact that the distance between neighbouring trajectories increases exponentially with time, a typical characteristic of chaotic systems. This behaviour is the result of the equation governing geodesic deviation [Sch80b],

$$\frac{\partial^2 \xi(s)}{\partial s^2} = -R(s)\xi(s). \tag{2.33}$$

Here ξ measures the non-Euclidean distance between two points on separate geodesics, a distance s along each from some initial conditions. These initial conditions determine the first derivative of ξ, and the equation (2.33) shows how the curvature of the underlying space affects the second derivative (the rate of change of velocity of separation). Here the value -1 for R, the Gaussian curvature, leads to an exponential divergence, and the Lyapunov exponent for the trajectories is the square root of $-R$, here equal to 1.

Later we shall consider systems where the motion is restricted. Then this divergence of trajectories will lead to the properties of strong chaos for those systems such as ergodic exploration of phase space and the existence of a symbolic dynamics for the motion [Art24].

2.3 Quantum mechanics on the half-plane

In the Schrödinger picture of quantum mechanics, the fundamental equation is

$$\hat{H}(t)|\Psi(t)\rangle = \imath\hbar\frac{\partial}{\partial t}|\Psi(t)\rangle \tag{2.34}$$

where t is the time, $\hbar$ is Planck's constant divided by 2π and $\hat{H}(t)$ is a self-adjoint operator acting on the Hilbert space of vectors $|\Psi(t)\rangle$. Here potentials varying in time are not considered so this equation separates out into two pieces and the general time-independent Schrödinger equation is

$$\hat{H}|\Psi(t)\rangle = E|\Psi(t)\rangle = E|\psi\rangle\exp(-\imath Et/\hbar), \tag{2.35}$$

where E is a constant corresponding to the energy of the particle considered.

Since the metric in the Poincaré half-plane is given by (2.4), the appropriate time-independent Schrödinger equation for quantum systems in this geometry's coordinate basis is

$$\hat{H}\psi(x,y) = -\Delta_{LB}\psi(x,y) = -(g^{ij}\psi(x,y)_{,i})_{;j} = -y^2(\frac{\partial^2}{\partial x^2}+\frac{\partial^2}{\partial y^2})\psi(x,y) = \lambda\psi(x,y), \tag{2.36}$$

where $\lambda = 2mE/\hbar^2 + \frac{1}{4}$, E is the energy of a particle of mass m [Gut90; WJ89] and the ',' and ';' symbols mean partial and covariant differentiation respectively. The Laplace-Beltrami operator Δ_{LB} is the generalisation of the Laplacian to Riemannian manifolds and is defined as written in the third equality of (2.36).

That this is the correct analogue of the Euclidean equation can be justified firstly by identification of the operator Δ_{LB} as the unique covariant second-order differential operator on the space [BV86], obtainable by careful quantization of the variables in (2.31), and further by semiclassical considerations, whence arises the curious term 1/4 added to the scaled energy. Its similarity to the Helmholtz equation and other second-order partial differential equations allows various analogies with physical systems to be made when looking at the rather abstract problems considered here, including [Stö99; ALST05] optically inhomogeneous media, shallow water surface waves and even the curved space of the early universe.

2.3.1 Free particle Green's function

A fundamental object of interest in any quantum system is the Green's function. This obeys the inhomogeneous equation

$$(-\hat{H} + \lambda)G(z, z'; \lambda) = \delta(z - z'), \tag{2.37}$$

with appropriate boundary conditions for the system under consideration, where the function on the right hand side is the two dimensional Dirac delta function. As such the Green's function gives the response of a system at energy λ to a delta-impulse at z'.

We derive here the free particle Green's function G_0, with outgoing wave boundary conditions, as this plays a vital role in the connection between classical and quantum theory via the Selberg trace formula which we describe later in section 3.3.1.1.

Since all points on the half-plane are equivalent, G_0 should only depend on the hyperbolic distance ρ between z and z'. Using the distance formula (2.21) and changing to the variable

$$\xi = \cosh\rho(z, z') = 1 + \frac{(x - x')^2 + (y - y')^2}{2yy'} \tag{2.38}$$

in (2.37), we obtain

$$(1-\xi^2)\frac{\mathrm{d}G_0}{\mathrm{d}\xi^2} - 2\xi\frac{\mathrm{d}G_0}{\mathrm{d}\xi} + l(l+1)G_0 = 0, \quad \xi \neq 0, \tag{2.39}$$

which is Legendre's equation with $l = -1/2 - \imath k$, where $k = \sqrt{\lambda - 1/4} = \sqrt{2mE}/\hbar$, which is the scaled momentum. The details of the change of variables can be found in appendix A. Hence $G_0(\rho, \lambda)$ for $\rho \neq 0$ is a Legendre function. Considering the required boundary conditions [Bog06], that is

$$\lim_{\rho\to\infty} G_0(\rho) \propto \mathrm{e}^{\imath k\rho} \tag{2.40}$$

for an outgoing wave at infinity and

$$\lim_{\rho\to 0} G_0(\rho) = \frac{\ln(\rho)}{2\pi}, \tag{2.41}$$

to produce the delta function in (2.37), we identify the required solution to be

$$G_0(z, z'; \lambda) = -\frac{1}{2\pi} Q_{-1/2-\imath k}(\cosh\rho(z, z')), \tag{2.42}$$

where $Q_n(s)$ is the Legendre function of the second kind. This has asymptotic behaviour as ρ tends to infinity [EMOT53]

$$\lim_{\rho\to\infty} Q_{-1/2-\imath k}(\cosh\rho(z, z')) = \sqrt{\frac{\pi}{2k\sinh\rho}}\mathrm{e}^{\imath(k\rho-\pi/4)}. \tag{2.43}$$

This Green's function will be most useful when considering the semiclassical theory of billiards later (see section 3.3). Using the method of images with G_0 one readily obtains the Green's function for bound systems in terms of their classical periodic orbits and thus detailed information about their spectra.

2.3.2 Scattering theory

In the case of free motion in the half-plane, solutions to (2.36) separate into a simple product form, $\psi(k; x, y) \propto X(k; x)Y(k; y)$. Performing this separation of variables, with separation constant ϕ, we get the two equations

$$\frac{\partial^2 X(k; x)}{\partial x^2} + \phi^2 X(k; x) = 0 \tag{2.44}$$

with solution (using a standing wave form of the solution for X, in anticipation that the motion in the x-direction will be bounded) $X(k;x) \propto \cos(\phi x + \theta)$, with some arbitrary constant θ, and

$$\frac{\partial^2 Y(k;y)}{\partial y^2} + \frac{\lambda}{y^2} Y(k;y) - \phi^2 Y(k;y) = 0. \tag{2.45}$$

This equation for Y, on substituting $Y = \sqrt{y}\mathcal{Y}(k;y)$, becomes

$$\frac{\partial^2 \mathcal{Y}(k;y)}{\partial y^2} + \frac{1}{y}\frac{\partial \mathcal{Y}(k;y)}{\partial y} + \frac{(\lambda - 1/4)}{y^2}\mathcal{Y}(k;y) - \phi^2 \mathcal{Y}(k;y) = 0, \tag{2.46}$$

which is the equation for the modified Bessel functions, only with a plus sign in front of the term $\frac{(\lambda-1/4)}{y^2}$. This thus has solutions, for $\phi \neq 0$, $I_{\imath k}(\phi y)$ and $K_{\imath k}(\phi y)$, which are the modified Bessel functions of the first and second kind respectively, with imaginary order $k = \sqrt{\lambda - 1/4}$, which is again the scaled momentum. The final form of the free solutions to Schrödinger's equation, for $\phi \neq 0$, is thus

$$\psi(k;x,y) \propto \cos(\phi x + \theta)\sqrt{y}\left(AI_{\imath k}(\phi y) + BK_{\imath k}(\phi y)\right). \tag{2.47}$$

with arbitrary constants A and B. ϕ is a separation constant thus solutions with different values of ϕ can be superimposed to yield solutions obeying specific boundary conditions as required. In general the Bessel functions are aperiodically oscillatory in y up until $y > \frac{\lambda}{\phi^2}$, whereupon they start to grow or decay exponentially. Since here we shall only consider scattering at large y, the physically relevant Bessel function is $K_{\imath k}(\phi y)$, which decays at infinity. $I_{\imath k}(\phi y)$ grows exponentially for large y, so we take $A = 0$. More details and precise expressions for the behaviour of these functions are given in appendix D or the interested reader can consult such classic monographs as Watson or Abramowitz [Wat66; AS65].

If $\phi = 0$ then in this special case $X(k;x) = Cx + D$. Again we require states that remain finite as x grows, so we put $C = 0$ and there is a constant x dependence. The solutions in y for this case are oscillatory all the way to infinity;

$$\psi(k;x,y) = \frac{1}{\sqrt{2\pi}} y^{1/2 \pm \imath k} \tag{2.48}$$

which are normalised to the Dirac delta function as is usual for such unbound states. From hereon we shall neglect to write the x explicitly in $\psi(k;x,y)$, since

it is not present in the expression for the scattering wavefunction. Considering the time-dependence of the Schrödinger equation (2.34) these can be thought of as plane waves coming from or going to infinity. As such they have constant probability current $\Im(\psi^* \text{grad}\psi)$.

Systems which admit such states have very different properties to closed systems. Classically they correspond to scattering systems, where a particle approaches some area (called the scattering centre) of interest from infinity and is either captured by system if it has a strong enough attractive potential, or it escapes again. In more than one dimension, the relative probability for the particle scattering into a solid angle $\mathrm{d}\Omega$ is measured by a quantity called the differential cross section,

$$\frac{\mathrm{d}\sigma}{\mathrm{d}\Omega} = \frac{\text{scatteredflux/solidangle}}{\text{incidentflux/area}}. \tag{2.49}$$

As in the Euclidean case, in quantum mechanics this can be expressed in terms of the S matrix, which maps incoming asymptotic scattering states to outgoing ones, that is

$$\psi_{\text{out}}(\mathbf{p}) = \int \mathrm{d}^2 p' \langle \mathbf{p}|S|\mathbf{p}'\rangle \psi_{\text{in}}(\mathbf{p}'). \tag{2.50}$$

$\mathbf{p}$ is the vector momentum. This property implies the unitarity of S since it must be linear and norm-preserving. Ignoring states that don't scatter ($\mathbf{p}' = \mathbf{p}$) and at constant energy (elastic scattering) so that $S = \delta(E_p - E_{p'}) f(p, p')$ where E and p are the energy and momentum of the particle respectively [Tay72],

$$\frac{\mathrm{d}\sigma}{\mathrm{d}\Omega}(p, p') = \left| f(p, p') \right|^2. \tag{2.51}$$

Here $\frac{\mathrm{d}\sigma}{\mathrm{d}\Omega}(p, p')$ measures the differential cross section for incoming states with momentum p scattering into solid angle $\mathrm{d}\Omega$ around the direction defined by p'.

A careful analysis [LP76] reveals that we can define improper scattering states with asymptotic form as above (2.48) for any system open at infinity and that the amplitude $f(p, p')$ gives the relative phase of the incoming and outgoing waves. Here the unitarity of S corresponds to the fact that particles cannot be created or destroyed in the scattering process. These scattering states thus have the asymptotic form

$$\psi(k;y) \simeq \frac{1}{\sqrt{2\pi}}(y^{1/2-\imath k} + f(p,p')y^{1/2+\imath k}). \tag{2.52}$$

Obviously here $p' = -p = k$. In general one would consider scattered waves in all directions but due to the unusual form of (2.47), states with non-constant x-dependence do not escape to infinity but decay exponentially. This is analogous to the situation in Euclidean scattering systems where a particle with sufficiently low energy will not be able to scatter in states with high angular momentum. Considering each quantised value of angular momentum as a different class of scattering state, or channel, the inaccessible channels are said to be closed to scattering. Here due to the geometry of the half-plane, all the channels with variable x-dependence are closed. This is also reminiscent of the theory of evanescent electromagnetic waves which occur when the size of one component of the wavevector exceeds the absolute magnitude of the wavevector, leading to other components being imaginary and thus an exponentially decaying state. Hence although one has a multichannel scattering system, only one channel is open at all energies.

Since there is only one channel open at any energy, the term S matrix is somewhat a misnomer. It is in fact a scalar since there is only one mapping, $k \mapsto -k$. Due to the particularly simple form of $f(p,p')$ in this situation we shall henceforth use the terms S, S matrix and $f(p,p')$ interchangeably. The unitarity of S restricts it to being a simple phase factor defined as

$$S = \mathrm{e}^{2\imath\delta(k)}, \tag{2.53}$$

where $\delta(k)$ is called the phase shift and is unambiguous up to addition of a multiple of π. Due to the restricted nature of this problem, the cross section as defined in (2.51) is identically unity (whatever goes in must come out!). Any interesting features of a particular potential or domain will only be seen in the phase shift.

Despite the rather unusual features of the half-plane in the general context of scattering theory, it is clear that in seeking numerical solutions to the Schrödinger equation in open systems that the most general solution must contain a term proportional to (2.52) and thus we can simply define δ as half of the measured

difference in phase between the incoming and outgoing terms. The asymptotic solution will then have form

$$\psi(k;y) \simeq \sqrt{\frac{2}{\pi}}\sqrt{y}\mathrm{e}^{\imath\delta}(\cos(k\ln y+\delta)), \tag{2.54}$$

where the meaning of the name phase shift is made clear by its shifting of the phase of the stationary wave. Further discussion of the scattering and a more careful mathematical presentation is given in [WJ89] where the phase shift is introduced in terms of well-defined wave packets.

The most dramatic features in most scattering systems are the resonances. These are regions of momentum where the phase shift rapidly increases by π. Almost all resonances are caused by the vicinity of a pole in the complex momentum plane of S being close to the real axis [Tay72] and we here consider that the poles of S define the resonances of a particular system. Near such a pole, S will have the limiting unitary form

$$S(k) = \mathrm{e}^{2\imath\delta(k)} \approx \mathrm{e}^{2\imath\delta_{bg}}\frac{k-k_0^*}{k-k_0}. \tag{2.55}$$

δ_{bg} is some slowly varying background phase shift upon which the resonance is superimposed and it is the rapid change of the phase of $k-k_0$ if the pole k_0 is near the real axis that is of interest. One also sees from (2.55) that at such a pole of S the coefficient multiplying the outgoing, scattered wave becomes infinite, which corresponds to the vanishing of the incoming wave. In the upper half of the momentum plane the positive imaginary part of k leads to exponentially bound states and it can be shown that k must be pure imaginary (from the hermitian property of the Hamiltonian [Tay72]). In general there are tricky questions to answer regarding the analyticity of the scattering matrix in the lower half of the momentum plane, but for the simple billiard systems considered here which are potential-free, this is not an issue. The wavefunction at these poles is an improper, exponentially growing state. Approximating the phase shift as $\delta(k) \approx \delta(k_0) + \delta'(k_0)(k-k_0)$ and neglecting the approximately constant background factors, we see that the outgoing wave near a resonance has the form $\exp(\imath k(\ln y + 2\delta'(k_0)))$ and thus lags the incoming wave by a distance $2\delta'$ (distance in the y-direction is given as $\ln y$ by (2.21)) or as is more often expressed, a time delay

$$\tau = \frac{1}{k} 2\delta'(k) = \frac{\mathrm{d}\delta}{\mathrm{d}\lambda}. \tag{2.56}$$

Having introduced the free classical and quantum mechanics on the half-plane, we now move on to consider what adjustments must be made to accommodate systems with restricted motion. The next chapter introduces the concept of a billiard system and presents a detailed calculation for the system at the centre of our investigation - Artin's billiard.

Chapter 3

Billiard systems on the Poincaré half-plane

3.1 Billiard systems

As hinted at in the previous chapter, the mechanics in hyperbolic geometry, described in section 2.2, become vastly more interesting when we constrain the motion to some smaller region of the half-plane. This can be done either by introducing sets of hard reflecting walls that fence off some area, or by *compactification* of some region. Then the divergence of trajectories leads to ergodic exploration of the energy shell and even harder forms of chaos for particular choices of region [BV86]. Compactification is achieved by identification of points on paired boundary segments and by this process many interesting surfaces can be formed. Constraining the motion in this way makes the study of the classical motion akin to the study of the motion of a ball on a billiard table, albeit a strangely shaped and curved one! This is where the name of these 'billiard' systems arises [Had98].

Compactification in this space can be understood by analogy with the Euclidean case, where for example identification of opposite sides of a quadrilateral leads to the formation of a torus. Here we actually consider mostly noncompact surfaces, which are open to the outside world at infinity so as to allow for scattering of particles. The class of domains considered all have finite area though, so contact with infinity is made via a thin horn and the rest of the

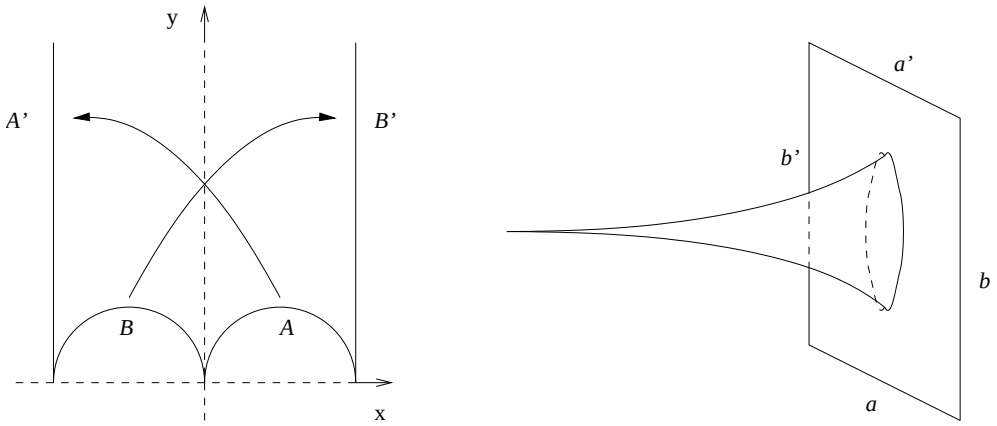

Figure 3.1: The singular square on the Poincaré half-plane (left), and an analagous system in Euclidean geometry (right).

billiard is constrained similarly to closed systems. A simple example is the singular square described in [Gut90] and illustrated to the left of figure 3.1, which is the region in the half-plane bounded by the two lines $x = \pm 1$ and the circles $(x \pm 1/2)^2 + y^2 = 1/4$. One identifies the right hand circle, A, with the vertical line on the left, A', and similarly for B and B', as indicated in the figure by the arrows. This leads to a torus as for a Euclidean square, except that one point on its surface is at infinity. This can be visualised by cutting a circular hole in a Euclidean square in the xy plane and attaching an exponentially curved horn shape to the hole, specifically the surface of revolution generated by rotating the tractrix about the z-axis. The tractrix has equation

$$x = 1/\cosh(\rho), \quad z = \rho - \tanh(\rho), \tag{3.1}$$

and Gaussian curvature -1 as required. The rest of the square curves round on itself to form the usual torus when the sides are identified. This analogous system is shown on the right of figure 3.1, where the sides of the square are to be identified according to $a \to a'$ and $b \to b'$.

It is of particular interest to choose as a region the fundamental region of some discontinuous group. Then the identification mentioned above can be made by the group elements and the mechanics can be described mathematically by using

the group laws. Particularly, and importantly for semiclassical considerations (see section 3.3), there is a one-to-one correspondence between *conjugacy classes* of group elements and periodic orbits in the system (two elements p and p' are conjugate to each other if there is some third group element g, such that $p' = gpg^{-1}$).

A fundamental region for any group is the set of all points closer to an arbitrary point, z_0, than any other of the orbit $\{\Gamma z_0\}$ (that is, the set of all images of z_0 under transformation by each of the group Γ's elements). Equivalently it is a region, no two of whose points are identified by a group transformation other than the identity, and such that the neighbourhood of any point on the boundary contains points congruent to points in the region. As such, copies of the fundamental region can be used to tile the plane. This symmetry is responsible for many of the special properties of motion constrained to such areas. It is here that the wealth of variety displayed by hyperbolic geometry is particularly clear. In Euclidean geometry there are only 17 distinct tiling groups [Sch78], but on the Poincaré half-plane there are infinitely many [FK97]! This is partially due to the lack of a distance scale in the Euclidean plane, which means that tessalations there are invariant under uniform dilation.

A general method for finding a fundamental region for a properly discontinuous group Γ is given in [For29]. First remove from the half-plane the interior of all isometric circles, $|cz + d| = 1$, where c and d range over all possibilities for group elements $\begin{pmatrix} a & b \\ c & d \end{pmatrix}$ of the transformed group $G\Gamma G^{-1}$, G being the transformation in $\mathrm{SL}(2, \mathbb{C})$ mapping a point z_0 within the region to infinity. Transforming this region with the inverse mapping G^{-1} then gives a fundamental region for the group Γ. This works because the mapping determined by the matrix $\begin{pmatrix} a & b \\ c & d \end{pmatrix}$ takes the exterior of the isometric circle of that transformation to the interior of the inverse mapping's isometric circle, and vice-versa. Thus the region exterior to all isometric circles is mapped out of that region by any group transformation.

3.1.1 Quantum billiards

The systems we consider here are quantum analogues of the classical billiard tables described above. Though due to the wave-particle duality of quantum

mechanics the author finds comparisons to swimming pools or baths more pertinent in general if looking to explain matters in laymen's terms. It soon becomes apparent that there are many quantum systems which share the same classical limit. This is a general feature of the quantization problem and to be expected since the classical limit 'washes out' some of the quantum fine-scale structure. In fact there are also quantum systems with several classical limits, though this is less intuitively apparent [Cre95].

When considering domains which can be the fundamental region for some discontinuous group, again the option of identifying sides of the billiard pairwise becomes tempting and then the boundary conditions on the wavefunction (2.47) become periodic with periodicity determined by the group elements generating the identifications. In this case the eigenfunction spectrum can be broken down into even and odd functions with respect to this periodicity. The class of odd functions correspond to the solutions of the Dirichlet problem (with the wavefunction set to zero at the boundaries) and the even solutions to the Neumann problem (with the normal derivative of the wavefunction set to zero at the boundaries). Within each of these classes there may of course be further symmetries and it is important when examining the statistics of spectra especially to identify these, since superposition of independent sequences of eigenvalues which may obey one set of statistics on their own can produce very different results when taken together. In particular superposition of independent random spectra can lead to far more near-degeneracy than expected in an arbitrary desymmetrised chaotic system. It was presumed that some kind of hidden symmetry was responsible for the Poissonian level spacing statistics of certain groups on the half-plane that will be investigated here (see section 5.3.2), though this was found to be wrong at least in the sense initially thought.

It is clear that the plane-wave solutions (2.48), and thus scattering states, only occur in billiards with Neumann boundary conditions on at least any vertical walls in the half plane, due to their constant x dependence. We shall focus on such systems. The next section describes the billiard shape which forms the reference point for our research. A derivation of the scattering coefficient in this case is given as an example of what behaviour to expect for generic open systems, which

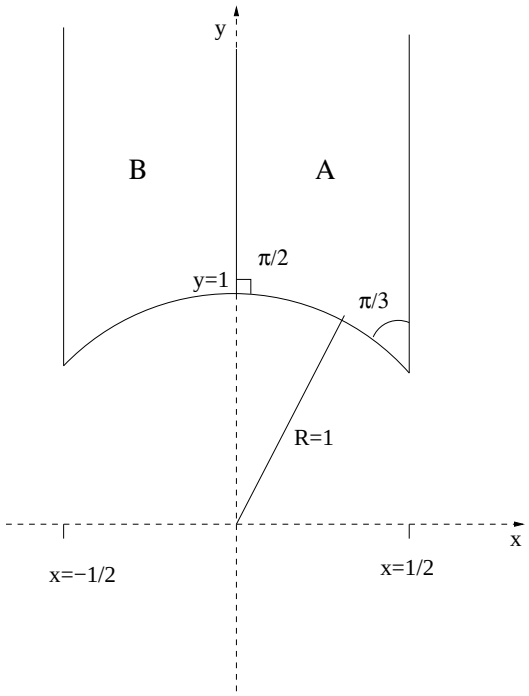

Figure 3.2: The modular domain and Artin's billiard on the Poincaré half-plane. Artin's billiard is the region A, to the right of the imaginary axis.

remarkably can be done analytically for this two-dimensional chaotic scattering system, though it will turn out to have several non-universal features.

3.2 Artin's billiard

Artin's billiard is the infinite triangle in the Poincaré half-plane representation of hyperbolic geometry with angles $\pi/2$, $\pi/3$ and 0. This is the triangle bounded by the unit circle and the lines $x = 1/2$ and $x = 0$, or using a complex plane notation it is the right hand half of the modular domain, defined by the lines $z = \pm 1/2 + \imath y$ and the inequality $|z| \geq 1$. It is the region A, bordered by solid lines in figure 3.2. The modular domain is the union of regions A and B, which is the reflection of A in the imaginary axis.

The modular domain is a fundamental region for the modular group, $\mathrm{PSL}(2, \mathbb{Z})$. This subgroup of $\mathrm{PSL}(2, \mathbb{R})$ (which was introduced earlier in the discussion of the

transformations of the half-plane (2.22)) is represented by the group of all rank two matrices with integer entries and unit determinant. It is the integer propery of the matrix elements that has made this group an object of close study for number-theorists. Due to the simple relationship of its canonical fundamental domain and Artin's billiard, we see that when calculating the solutions of Schrödinger's equation (2.36) in Artin's billiard, our choice of Neumann boundary condition on the line $x = 0$ is equivalent to looking at the even part of the spectrum for the modular group. Thus in particular, the scattering solutions defined by (2.48) which have constant x-dependence are shared between the two systems. Referring back to section 2.3.2 we see that the general quantum-mechanical solution for Artin's billiard can be written as

$$\psi(k;x,y) = \frac{1}{\sqrt{2\pi}}(y^{1/2-\imath k} + S(k)y^{1/2+\imath k}) + \sum_{n=1}^{\infty} b_n(k)\cos(2n\pi x)\sqrt{y}K_{\imath k}(2n\pi y), \tag{3.2}$$

with the coefficients $b_n(k)$ to be determined and the $2n\pi$ in the argument of the cosine and Bessel functions determined by imposing the Neumann boundary condition on the vertical walls of Artin's billiard at $x = 0$ and $x = 1/2$. We recall that the functions $K_{\imath k}(2n\pi y)$ decay exponentially as y grows, having the form. $K_{\imath k}(2n\pi y) \simeq \frac{1}{\sqrt{4ny}}\exp(-2n\pi y)$. The next section details the calculation of $S(k)$, (2.53), for the modular group and thus gives the resonances of Artin's billiard, as the poles of S in the complex momentum plane.

3.2.1 Explicit calculation of S for arithmetic systems

Since we will extend the derivation given here to the Hecke groups to be considered later (see section 5.4), at first a general discontinuous subgroup of $\mathrm{PSL}(2,\mathbb{R})$, Γ, is considered. Following Gutzwiller's derivation [Gut83] we sum the image of an incoming free plane wave $y^{1/2-\imath k}$ over all images of the fundamental domain of the group Γ. This group can have its elements represented by matrices

$$\sigma = \begin{pmatrix} a & b \\ c & d \end{pmatrix}, \tag{3.3}$$

so that the action of σ on a point in the half-plane, z, generates a transformed y-coordinate ($y = \Im(z)$) and thus plane wave according to

$$\Im(\sigma(z)) = \Im\left(\frac{az+b}{cz+d}\right) = \frac{y}{|cz+d|^2}. \tag{3.4}$$

We thus obtain a general expression for the scattered wavefunction

$$\psi(x,y) = \psi(z) = \sum_{\sigma\in\Gamma} \Im(\sigma(z))^{1/2-\imath k} = \sum_{\sigma\in\Gamma} \frac{y^{1/2-\imath k}}{|cz+d|^{1-2\imath k}}, \tag{3.5}$$

where only unique images under the mapping σ are summed over. The symmetry of this sum enforces the desired periodic boundary conditions on ψ since

$$\psi(x,y) = \psi(z) = \psi(\sigma(z)) \tag{3.6}$$

by construction.

It is also obviously a solution to the Schrödinger equation (2.36) since the Laplacian commutes with all the mappings $g_\sigma = z \mapsto \sigma(z)$. This technique of enforcing boundary conditions by linearly superposing solutions to a differential equation is familiar to physicists as the method of images. It is equivalent to the intuitive method of multiple scattering used for example in [GR89] to calculate the resonance spectrum of a three-disc scattering system.

It turns out that the expression (3.5) is well-known to number theorists as the definition of the Eisenstein series $E(z,s)$ for the group Γ, with parameter $s = 1/2 - \imath k$. These are objects from the theory of automorphic forms (essentially generalised periodic functions under the operations of some group) so perhaps it should not be surprising that they occur here. In the instance of the modular group, this object has been well studied and what follows is an expansion of the presentation in [Kub73]. There a great deal of attention is paid to the analytic continuation of the sum to cases when $\Re(s) < 1$, a degree of technicality we do not wish to pursue here. The results are assumed valid for $s = 1/2 - \imath k$ and the interested reader is referred to the literature on the subject [Kub73; LP76].

3.2.2 Modular group

We now wish to extract S from the general expression (3.5) in the particular case of the modular domain. For the modular group the matrix representations of the group elements are of the form

$$\sigma = \begin{pmatrix} a & b \\ c & d \end{pmatrix}; \{a, b, c, d \in \mathbb{Z} | ad - bc = 1\} \tag{3.7}$$

We first consider which elements will generate duplicate images of the incoming wave, and thus need to be left out of the sum (3.5). Only one representative of each left coset $\Gamma_0\sigma$ is included in the sum (3.5) since (using the notation $\{\}$ to indicate a set of elements, often with some parameter which distinguishes between different elements in the set, such as b' below)

$$\Gamma_0 = \left\{ \begin{pmatrix} 1 & b' \\ & 1 \end{pmatrix} \right\}; b' \in \mathbb{Z} \tag{3.8}$$

and thus

$$\Gamma_0\sigma = \left\{ \begin{pmatrix} a + b'c & b + b'd \\ c & d \end{pmatrix} \right\}, \tag{3.9}$$

which all produce the same $y(z)' = y(\sigma z) = y/\left|cz + d\right|^2$.

Now we consider the Fourier decomposition $\psi = \sum_m a_m(y)\exp(-2\pi\imath m x)$. We focus on $a_0(y)$ since it is the term constant in x, $m = 0$, which asymptotically gives the S-matrix (3.2). ψ for the modular domain is periodic with period 1 in x (see figure 3.2) so

$$a_0(y) = \int_0^1 \sum_{\sigma \in \Gamma_0 \backslash \Gamma} \frac{y^{1/2-\imath k}}{\left|cz + d\right|^{1-2\imath k}} \mathrm{d}x. \tag{3.10}$$

The identity term in the sum gives a contribution $y^{1/2-\imath k}$ but the rest of the sum is more tricky.

Considering now the right cosets

$$\sigma\Gamma_0 = \left\{ \begin{pmatrix} a & b + ab' \\ c & d + cb' \end{pmatrix} \right\}, \tag{3.11}$$

we see these are equal (as far as their role in (3.5) is concerned) only for any σ and σ' with $c' = c$ and $d' \equiv d (\mathrm{mod}\, c)$. Thus for any $c > 0$ (c and $-c$ give identical sets of images) we have to consider only $d < c$ with the determinant constraint $ad - bc = 1$ or here $(c, d) = 1$ where $(,)$ signifies the greatest common divisor (c and d are coprime). The remainder of the cosets can be taken account of in the integral by seeing that if $\sigma = \begin{pmatrix} a & b + ab' \\ c & d + cb' \end{pmatrix}$ then

$$y(\sigma z) = y/\left|cz + d + cb'\right|^2 = y/\left|c(z + b') + d\right|^2 \tag{3.12}$$

so that

$$\int_0^1 y(\sigma(z))^{1-2\imath k} \mathrm{d}x = \int_{b'}^{b'+1} y(z')^{1-2\imath k} \mathrm{d}x' \tag{3.13}$$

by the simple substitution $x' = x + b'$.

Now we are left with

$$a_0(y) = y^{1/2-\imath k} + \int_{-\infty}^{\infty} \sum_{0<c, 0\le d<c\in\mathbb{Z}|(c,d)=1} \frac{y^{1/2-\imath k}}{|cz + d|^{1-2\imath k}} \mathrm{d}x. \tag{3.14}$$

Substituting $\rho = x + d/c$ this becomes

$$\begin{aligned} a_0(y) &= y^{1/2-\imath k} + \sum_{c>0} \frac{1}{|c|^{1-2\imath k}} \int_{-\infty}^{\infty} \sum_{0\le d<c|(c,d)=1} \frac{y^{1/2-\imath k}}{|\rho + \imath y|^{1-2\imath k}} \mathrm{d}\rho \\ &= y^{1/2-\imath k} + \sum_{c>0} \frac{1}{|c|^{1-2\imath k}} \sum_{0\le d<c|(c,d)=1} \int_{-\infty}^{\infty} \frac{y^{1/2-\imath k}}{(\rho^2 + y^2)^{1/2-\imath k}} \mathrm{d}\rho. \end{aligned} \tag{3.15}$$

Considering first the arithmetic factor

$$\sum_{c>0} \frac{1}{|c|^{1-2\imath k}} \sum_{0\le d<c|(c,d)=1} , \tag{3.16}$$

we see that the sum over d is Euler's totient function $\phi(c)$, the number of integers up to c which are coprime to c. If $c = p_1^{m_1} p_2^{m_2} \ldots p_r^{m_r}$ as a product of primes, then

$$\phi(c) = c\left(1 - \frac{1}{p_1}\right)\left(1 - \frac{1}{p_2}\right)\ldots\left(1 - \frac{1}{p_r}\right). \tag{3.17}$$

So

$$\sum_{n=1}^{\infty} \frac{\phi(n)}{n^s} = \sum_{n=1}^{\infty} \frac{n}{n^s} \left(1 - \frac{1}{p_1}\right) \dots \left(1 - \frac{1}{p_n}\right), \tag{3.18}$$

where p_n is the largest prime factor of n and the product contains its other prime factors as required by (3.17).

Expanding this via the unique representation of integers by primes (cf. the Euler product form for the Riemann zeta function - see [Tit51] for this and many other useful identities), we obtain.

$$\begin{aligned}
\sum_{n=1}^{\infty} \frac{\phi(n)}{n^s} &= \prod_p \left\{ 1 + \frac{p\left(1 - \frac{1}{p}\right)}{p^s} + \frac{p^2\left(1 - \frac{1}{p}\right)}{p^{2s}} + \dots \right\} \\
&= \prod_p \left\{ 1 + \left(1 - \frac{1}{p}\right) \left(\frac{1}{p^{(s-1)}} + \frac{1}{p^{2(s-1)}} + \dots \right) \right\} \\
&= \prod_p \left\{ 1 + \frac{\left(1 - \frac{1}{p}\right)}{p^{(s-1)}} \left(1 + \frac{1}{p^{(s-1)}} + \dots \right) \right\} \\
&= \prod_p \left\{ \frac{\left(1 - \frac{1}{p^{(s-1)}}\right) + \left(\frac{1}{p^{(s-1)}} - \frac{1}{p^s}\right)}{\left(1 - \frac{1}{p^{(s-1)}}\right)} \right\} \qquad (3.19) \\
&= \frac{\zeta(s-1)}{\zeta(s)}. \qquad (3.20)
\end{aligned}$$

Substituting this back into (3.15) we get

$$a_0(y) = y^{1/2-\imath k} + \frac{\zeta(-2\imath k)}{\zeta(1-2\imath k)} \int_{-\infty}^{\infty} \frac{y^{1/2-\imath k}}{(\rho^2 + y^2)^{1/2-\imath k}} \mathrm{d}\rho. \tag{3.21}$$

The integral can be rewritten (putting $t = \rho/y$) as

$$\int_{-\infty}^{\infty} \frac{y^{1/2-\imath k}}{(\rho^2 + y^2)^{1/2-\imath k}} \mathrm{d}\rho = y^{1-(1/2-\imath k)} \int_{-\infty}^{\infty} \frac{1}{(1+t^2)^{1/2-\imath k}} \mathrm{d}t. \tag{3.22}$$

Substituting $u = t^2$ we obtain

$$y^{1-(1/2-\imath k)} \int_0^{\infty} \frac{u^{1/2-1}}{(1+u)^{1/2-\imath k-1/2+1/2}} \mathrm{d}t, \tag{3.23}$$

which equals

$$y^{1-(1/2-\imath k)}\int_0^1 q^{1/2-1}(1-q)^{1/2-\imath k-1/2-1}\mathrm{d}q \tag{3.24}$$

on the further substitution $u = q/(1-q)$. The integral remaining is a representation of the Beta function [Arf85],

$$B(1/2,-\imath k) = \frac{\Gamma(1/2)\Gamma(-\imath k)}{\Gamma(1/2-\imath k)}. \tag{3.25}$$

Finally putting this into (3.21) we get

$$a_0(y) = y^{1/2-\imath k} + y^{1/2+\imath k}\frac{\zeta(-2\imath k)}{\zeta(1-2\imath k)}\frac{\Gamma(1/2)\Gamma(-\imath k)}{\Gamma(1/2-\imath k)} \tag{3.26}$$

and using the functional equation for the zeta function

$$Z(w) = \pi^{-w/2}\Gamma(w/2)\zeta(w) = Z(1-w), \tag{3.27}$$

this rearranges to

$$a_0(y) = y^{1/2-\imath k} + \frac{\pi^{-\imath k}\Gamma(1/2+\imath k)\zeta(1+2\imath k)}{\pi^{\imath k}\Gamma(1/2-\imath k)\zeta(1-2\imath k)}y^{1/2+\imath k}. \tag{3.28}$$

$$S(k) = \frac{Z(1+2\imath k)}{Z(1-2\imath k)} \tag{3.29}$$

is therefore the S-matrix, the fundamental object of scattering theory discussed in section 2.3.2 and in particular the scalar amplitude in (3.2). It was shown that the poles of S in the lower half of the complex momentum plane correspond to resonances of the system, so in this case they are given by the poles of $\frac{Z(1+2\imath k)}{Z(1-2\imath k)}$. The Γ function has no zeros and poles at zero and the negative integers. The zeta function has a single pole at $w = 1$ and so-called 'trivial' zeros at the negative even integers. An examination of the form of S shows that the poles of the zeta functions both occur at $k = 0$ and thus cancel. The same happens for the trivial zeros of $\zeta(1 \pm 2\imath k)$ and the poles of $\Gamma((1 \pm 2\imath k)/2)$, both occurring at $k = \pm\imath(n + 1/2)$, $n \in \mathbb{Z}$. Thus the only poles which manifest themselves in the scattering matrix are at the nontrivial zeros of the zeta function in the denominator. Assuming the Riemann hypothesis to hold (a huge volume of numerical

results support this, see for example [Odl]), these all lie on the 'critical' line $\Re(w) = 1/2$. This results in poles of S at

$$k = \frac{k_n}{2} - \frac{\imath}{4}, \tag{3.30}$$

where k_n are the Riemann zeros. This quite remarkable formula states that for Artin's billiard *all* the resonances have width exactly $1/4$, at least in momentum space. In fact this system is even more special, for complementary to the Eisenstein series (3.5) a discrete set of bound eigenfunctions of the Laplacian are found too, that is states with vanishing first Fourier coefficient. These are the automorphic functions or *cusp forms* that the mathematicians are generally interested in. What is unusual about them from the point of view of a physicist is that they have real momentum and thus positive energy and lie superimposed upon the continuum scattering spectrum. Such states in atomic phyiscs are called *bound states in the continuum*. These are not conventional bound states in that the only bound state comes from substituting the particular value $k = \frac{\imath}{2}$ into (3.29). They arise due to particular coincidences of coupling between scattering channels being exactly zero and are extremely sensitive to perturbation of the parameters which determine the coupling strength. A discussion of such states and the conditions required for their existence is given in [Fri98] and a simple example of how such situations can arise was presented in [Rob86]. It is expected that under arbitrary perturbations of the system all the cusp forms will acquire negative imaginary parts and become proper resonances. Such behaviour is seen here under the two deformations of Artin's billiard considered in this thesis and results are presented in chapter 5.

The availability of explicit expressions for the positions of the resonances, for certain choices of the parameters which describe the billiard systems investigated here, is invaluable in keeping tabs on the numerical investigation performed later when the parameters are allowed to run freely over a range (see chapter 4). Of course, there are ways of explicitly writing down a solution of some sort in most cases, but ultimately numerical investigation will be required to treat all choices of variables, particularly far from situations where we have explicit expressions. The next chapter introduces these deformations and looks at how far we can get without numerics, before we present the details of our calculations in chapter 5.

Next however, having derived an analytic expression for the scattering matrix in Artin's billiard, we look at what can be said analytically about the bound states. For the cusp forms in billiards which have some underlying group structure, there is an explicit formula for the density of states, known as Selberg's trace formula. For general billiards there is a corresponding formula which is only valid semiclassically. Thus we first present a more general discussion of the semiclassical connection between quantum and chaotic mechanics.

3.3 Semiclassical mechanics

Semiclassically quantum mechanics is linked to classical mechanics via Feynman's path integral formulation of quantum mechanics and the Gutzwiller trace formula relating the quantum propagator to the classical periodic orbits.

The propagator $K(z, z', t, t')$, is a fundamental object for any quantum system and relates the state of that system in one place at one time to that elsewhere at a later time. Formally

$$\Psi(z', t') = \int K(z, z', t, t')\Psi(z, t)\mathrm{d}z. \tag{3.31}$$

For time independent systems, K only depends on the difference in time, $\tau = t' - t$ and is also related to the Green's function for the system (2.37) via a Laplace transform.

$$G(z, z'; \lambda) = -\imath \int_0^\infty K(z, z', \tau) \exp(\imath\lambda\tau)\mathrm{d}\tau. \tag{3.32}$$

By considering how the propagator for arbitrary time differences could be built up from propagators for infinitesimal time steps, Feynman [FH65] showed that it could be written as a certain sum over all possible paths connecting the initial and final points in space and time. Each possible path contributes with a phase determined by the classical action of that path,

$$S(z, \dot{z}, t_2 - t_1) = \int_{t_1}^{t_2} L(z, \dot{z}, t)\mathrm{d}t, \tag{3.33}$$

where L is the Lagrangian (2.27), so that

$$K(z, z', \tau) = \int \mathcal{D}z(t) \exp^{\frac{\imath}{\hbar} S[z(t)]} . \tag{3.34}$$

Here $\int \mathcal{D}z(t)$ notationally stands for a precise definition of the sum over all paths $z(t)$ joining the initial and final points z and z' in time τ (in terms of discretisation of the paths into finite time steps, in the limit of that step size going to zero) [FH65]. van Vleck [vV28] proposed that semiclassically only the possible classical path(s) would contribute to the sum in (3.34) so that

$$K(z, z', \tau) = A \exp^{\frac{\imath}{\hbar} S_{\mathrm{cl}}[z(t)]}, \tag{3.35}$$

where A is some calculable amplitude and S_{cl} is the action computed along the classical path(s). This formula, and corrections to it, can be derived in the stationary phase approximation from (3.34) as shown by Gutzwiller [Gut67] and others. It is also reminiscent of the WKB ansatz (which obtains the action in the exponent as the solution of the Hamilton-Jacobi equation for the system) and is an approximate solution to the Schrödinger equation in the semiclassical limit $\hbar \to 0$.

Taking the semiclassical approach further, Gutzwiller showed that very generally the classical and quantum pictures of a system are connected by his famous trace formula. With repeated application of the stationary phase method for evaluating semiclassical integrals in a path integral such as above, an expression for the trace of the Green's function can be developed in terms of a sum over all classical periodic orbits for the system, the restriction to periodic orbits coming from the stationary phase conditions. From the trace of the Green's function all desired information about the quantum spectrum can be extracted, though there can be serious difficulties in dealing with the convergence of the sums that arise. The result is [Gut90]

$$g(E) = \int G(z, z, E) \mathrm{d}z = g_0(E) - \frac{\imath}{\hbar} \sum_{p,n} \frac{T_p}{|\det(M_p^n - 1)|^{1/2}} \exp\left[\frac{\imath}{\hbar} n S_p(E) - \imath \frac{n\pi\mu_p}{2}\right] . \tag{3.36}$$

Here p labels each *primitive* periodic orbit (that is, a distinct single cycle) and n counts repeated traversals of that orbit, which has primitive period T_p, action

integral around the primitive orbit $S_p(E)$ (this energy-dependent action is related to the time-dependent action (3.33), sometimes called the *principal function*, by $S(E) = S(t) + Et$), monodromy matrix (which measures the stablity of the orbit) M_p and Maslov index (discussed in the next section) μ_p. The sum is applicable to isolated periodic orbits. Continuous families of orbits such as the 'bouncing ball' orbits in some billiard systems [SSCL93] have to be treated separately, as does the contribution from orbits of zero length, which is addressed in the next section 3.3.1. These typically smooth contributions to $g(E)$ are lumped into the term $g_0(E)$ on the right hand side of (3.36). The crucial point is that this formula is applicable to all systems, no matter how chaotic, at least in the limit $\hbar \to 0$. If we have knowledge of the classical periodic orbits, we have knowledge of the quantum spectrum, and similarly possesion of the full quantum energy spectrum allows reconstruction of the classical periodic orbit length spectrum.

Information about the quantum spectrum is extracted from the trace (3.36) in a quantity known as the density of states. Consider the important identity

$$d(E) = -\frac{1}{\pi}\Im\left(\int G(z,z,E+\imath\epsilon)\mathrm{d}z\right) \quad (\epsilon > 0), \tag{3.37}$$

where the limit $\epsilon \to 0$ is understood and where

$$d(E) = \frac{\mathrm{d}N}{\mathrm{d}E} = \sum_n \delta(E - E_n) \tag{3.38}$$

is the density of states of a system, this being the derivative of its staircase function $N(E)$, which counts the number of individual quantum energy levels, E_n, found up to a certain energy E. This identity is shown by writing the integrand in the right hand-side of (3.37) in the form

$$\begin{aligned} G(z_A, z_B, E+\imath\epsilon) &= \langle z_A | \frac{1}{E+\imath\epsilon-\hat{H}} | z_B \rangle \\ &= \int \delta(z_A - z) \frac{1}{E+\imath\epsilon-\hat{H}} \delta(z - z_B)\mathrm{d}z \\ &= \int \sum_n \psi_n^*(z_A)\psi_n(z) \frac{1}{E+\imath\epsilon-\hat{H}} \sum_m \psi_m^*(z)\psi_m(z_B),\ \mathrm{d}z \end{aligned}$$

$$= \sum_n \psi_n^*(z_A)\frac{1}{E+\imath\epsilon-\hat{H}}\psi_n(z_B)$$
$$= \sum_n \frac{\psi_n^*(z_A)\psi_n(z_B)}{E+\imath\epsilon-E_n}, \tag{3.39}$$

using the eigenfunction expansion of the delta functions. Setting $A = B$ and taking the trace, which means integration over the spacial coordinates, is merely the normalization condition on the eigenfunctions ψ_A. Finally recognising an expression for the delta function in what remains gives

$$\lim_{\epsilon\to 0}\left(-\frac{1}{\pi}\Im\left(\int G(z,z,E+\imath\epsilon)\mathrm{d}z\right)\right) = \lim_{\epsilon\to 0}\left(-\frac{1}{\pi}\Im\left(\sum_n \frac{1}{E+\imath\epsilon-E_n}\right)\right)$$
$$= \sum_n \delta(E-E_n) = d(E), \tag{3.40}$$

as required.

Applying (3.37) to (3.36) thus gives for the density of states of a generic system

$$d(E) = d_0(E) - \frac{1}{\pi\hbar}\sum_{p,n}\frac{T_p}{|\det(M_p^n-1)|^{1/2}}\cos\left[\frac{1}{\hbar}nS_p(E)-\frac{n\pi\mu_p}{2}\right], \tag{3.41}$$

yielding the quantum spectrum in terms of purely classical quantities. Here $d_0(E)$ represents the smooth contribution to the density of states coming from $g_0(E)$ in (3.36).

3.3.1 Semiclassics for billiards

A most useful extension of the methods leading to the trace formula (3.41) is in the asymptotic evaluation of the function $d(E)$. In particular the zero-length orbits mentioned before generate a smooth contribution to this density, superimposed on which the oscillatory terms produce the familiar quantum step structure for N.

This smooth contribution, $\bar{N}$, is equivalent to what is known as Weyl's law [Wey11], derived before the invention of quantum theory through a consideration

of diffusive behaviour in a fixed domain. In its simplest form it says the number of states up to a given energy is proportional to the available phase-space at that energy. Corrections to this leading-order approximation have been worked out in detail for billiard systems [BB70; BH76] and the result is, specialising now to billiard systems on the Poincaré half-plane with scaled energy λ,

$$4\pi\bar{N}(\lambda) \simeq A\lambda + \epsilon L\sqrt{\lambda} + 4\pi \sum_r \frac{1}{24}\left(\frac{\pi}{\alpha_r} - \frac{\alpha_r}{\pi}\right) + \frac{RA}{6} - \frac{1}{6}\oint \mathrm{d}s k(s) + O(\lambda^{-1/2}). \tag{3.42}$$

Here A is the hyperbolic area of the billiard considered, and L its perimeter. R is the scalar Riemannian curvature, here equal to the constant value -2, $k(s)$ is the curvature of the boundary, defined in [GHSV91] and α_r are the angles of any corners in the system. ϵ is equal to plus or minus 1 for walls with Neumann and Dirichlet boundary conditions respectively, thus systems with Neumann boundary conditions tend to have larger numbers of energy levels than corresponding systems with the Dirichlet constraint.

For open systems there seems as yet to be no general consensus as to what the appropriate generalisation of Weyl's law is. Physical considerations suggest taking a closed system with its boundary sufficiently far from the scattering region should behave like the corresponding scattering system asymptotically [CAM+04], and elsewhere it has been proposed that there should be a Weyl-like growth condition using the volume of the classical repeller in place of the full phase-space in (3.42) [LSZ03]. The systems considered here are unusual in that they are open in such a way that their area remains finite. Thus the first Weyl term is still relevant, though the perimeter still causes divergence of the series. Systematic corrections due to this unique property are presented in [Ven78], the result being the appearance of a term proportional to $\ln\lambda$.

The effects of the choice of constraints on the wavefunction at boundaries are seen in the details picked out by Gutzwiller's trace formula, as well as in the bulk behaviour of the quantum spectrum. Applying (3.41) now gives a semiclassical expression for the oscilitary correction terms to the smooth density of states (3.42) in billiard systems

$$d_{\rm osc}(k) = 2kd_{\rm osc}(\lambda) = \frac{k\hbar^2}{m}\left(-\frac{1}{\pi}\Im\left(\int G(z,z,E)\frac{{\rm d}x{\rm d}y}{y^2}\right) - \frac{{\rm d}\bar{N}(E)}{{\rm d}E}\right)$$
$$= \frac{1}{\pi}\sum_{p,n}{}' \frac{l_p}{|\det(M_p^n - 1)|^{1/2}}\cos\left[n\left(kl_p - \frac{\mu_p\pi}{2}\right)\right]. \qquad (3.43)$$

Here we have changed to k rather than λ as the more appropriate parameter for these systems with no internal potential function. This allows the substitution of for orbit lengths $l_p = \frac{k\hbar}{m}T_p$ for orbit periods T_p. The prime on the sum indicates that the sum over orbits of zero length, responsible for the smooth Weyl terms, has been left out.

In principle this sum should allow calculation of the full quantum step function $N(k)$ for billiards on the half-plane. Sadly in practice the sum is highly divergent, due to the exponential proliferation of periodic orbits as orbit length increases. Powerful techniques have been developed to tackle such difficulties, for instance the use of dynamical zeta functions and spectral determinants [Kea92] (techniques inspired by the connection with number theory via Riemann's zeta function, as mentioned in the Introduction, chapter 1), or cycle expansions in systems which are sufficiently chaotic so as to admit a symbolic description [CE89; THM96]. Still, it is not always possible to make use of the formula (3.43).

Examining the terms in the trace formula (3.43), for billiard systems in particular the Maslov index is crucial to a full appreciation of the quantum spectrum. When semiclassically evaluating the integral for each orbit in (3.34), the configuration space approximation to the wavefunction becomes invalid at classical turning points in the trajectory (specifically, the amplitude A in (3.35) has a singularity). Shifting to momentum space eliminates this problem, but a phase lag of $\pi/2$, or equivalently an increase in the Maslov index by one, is picked up for every turning point passed, due to quantum tunnelling into the classically forbidden region. Moreover, in the case of billiard systems the hard reflections are more pathological and the phase picked up varies.

The Dirichlet constraint sets the wavefunction ψ to zero on the boundary and can be simulated via the introduction of an infinitely high and deep potential wall along the boundary of the domain considered. This introduces an phase lag of π for each reflection rather than $\pi/2$. Though there is no analogue of the wall for

Neumann boundary conditions the classical limit is nonetheless the same. This constraint involves setting the normal derivative $\frac{\partial}{\partial \hat{\mathbf{n}}}$ of the wavefunction along the boundary to zero. In this case there is no phase change on a reflection.

Combining these contributions, that is the Maslov index μ_p and additional phases picked up from reflections, for each particular orbit in the sum gives the total phase factor occurring in (3.43).

3.3.1.1 Selberg trace formula

Surprisingly, when applied to a periodic system such as the modular domain which is the fundamental domain of some discontinuous group acting on the half-plane (see section 3.1), the asymptotic relation (i.e. it is only valid in the semiclassical limit $k \to \infty$) (3.43) becomes exact and corresponds to Selberg's trace formula [Sel56]. This is an application of the method of images to the general case of tiling by group transformations, similarly to that used in the derivation of S for the modular group (see section 3.2.2). Selberg's formula was constructed in the realm of number theory and has been intensely studied by mathematicians for years. This furnishes yet another reason why investigation of systems in this abstract space can be so profitable, the interaction between different approaches and interests in those studying these problems has borne much fruit.

Although mathematically there are many intricacies involved in deriving Selberg's formula, for the simple case of a compact, or closed billiard whose group's elements are all hyperbolic (which is always the case for compact billiards with geodetic walls in hyperbolic geometry and implies that all periodic orbits are unstable - see section 3.1), it can be written down quite simply.

Again we work from the identity (3.37) but use the explicit free Green's function (2.42) and apply the method of images used in section 3.2.1 for a plane wave. That is, the full Green's function G is written in terms of the free particle Green's function G_0 as

$$G(z, z', k) = \sum_{\sigma \in \Gamma} G_0(z, \sigma(z'), k), \tag{3.44}$$

where the sum is over elements σ of the group Γ which generate non-repeated images of the fundamental domain. The explicit form of G_0 was derived in section

2.3.1. For groups with only hyperbolic elements, the sum can be performed analytically [Bog06] and we move straight to the striking result

$$d(k) = \frac{A}{2\pi} k \tanh(k) + \frac{1}{2\pi} \sum_{\{p\},n} \frac{l_p}{\sinh \frac{nl_p}{2}} \cos\left(nkl_p\right). \tag{3.45}$$

The sum here is over *conjugacy classes* of primitive elements, labelled by $\{p\}$, and their repetitions n. As described in section 3.1, these are in one-to-one correspondence with the primitive periodic orbits labeled by l_p in (3.45). Here A is the area of the fundamental domain of the group. The first term is the Selberg equivalent of the smooth density of states, the Weyl term $\bar{d}$, which is obtained from the term involving the identity element in (3.44), just as the Weyl term was obtained from the term in (3.36) involving orbits of zero length. The form is identical to the Gutzwiller trace formula (3.43), and yet this is an exact quantum mechanical result, where as the former was asymptotic. The reasons for this curious coincidence are not yet fully understood. Useful forms of (3.45) can be obtained by convolving it with a smoothing function $h(k)$, to assist convergence of the sums.

In the more general case of an arbitrary discontinous group acting on the half-plane, Selberg's trace formula contains several extra terms contributed by the elliptic and parabolic group elements. Though too technical to warrant a full description here, we quote the final result for the full spectrum of the modular group, which is the one of direct relevance to our research. For further details, one is referred to the literature [BV86; Ven78]. The trace formula is

$$\begin{aligned}
\sum_i h(k_i) \quad = \quad & \frac{A}{2\pi} \int_{-\infty}^{\infty} k \tanh(\pi k h(k) \mathrm{d}k + \sum_{\{r\}} \sum_{j=1}^{m-1} \frac{1}{m \sin(\frac{j\pi}{m})} \int_{-\infty}^{\infty} \frac{\mathrm{e}^{-2\pi k j/m}}{1+\mathrm{e}^{-2\pi k}} h(k) \mathrm{d}k \\
& + \sum_{\{p\}} \sum_{j=1}^{\infty} \frac{l_p}{\sinh \frac{jl_p}{2}} \tilde{h}(jk) \\
& + \frac{1}{2\pi} \int_{-\infty}^{\infty} h(k) \frac{S'}{S} \left(\frac{1}{2} + \imath k\right) \mathrm{d}k - \frac{1}{\pi} \int_{-\infty}^{\infty} h(k) \frac{\Gamma'}{\Gamma} \left(1 + \imath k\right) \mathrm{d}k \\
& - 2\ln(2) \tilde{h}(0) + \frac{1}{2} \left(1 - S(\frac{1}{2})\right) \tilde{h}(0).
\end{aligned} \tag{3.46}$$

In the above, h is a smoothing function which, subject to certain restrictions, ensures convergence of the various sums on the right hand side. The left hand side is thus a function of the bound state eigenvalues k_i. A is the hyperbolic area of the modular domain, the k_i are the momentum eigenvalues of the cusp forms. k is the momentum, though this is always integrated over. $\{r\}$ and $\{p\}$ are the sets of conjugacy classes of primitive elliptic and hyperbolic elements respectively, the latter corresponding to primitive periodic orbits of length l_p. $\tilde{h}$ is the Fourier transform of h. S is the scattering matrix calculated earlier as (3.29) and Γ here is Euler's gamma function. The eigenvalues for the cusp forms and the resonance positions are thus encoded in the periodic orbits of the modular billiard. Venkov showed in [Ven78] how it is possible to extract a trace formula for the separate odd and even spectra from (3.46), the even spectrum being the one of relevance in this thesis.

Chapter 4

Deformations of Artin's billiard

In this chapter we define the deformations of Artin's billiard that we will use to study how the bound states and resonances evolve under those deformations. We also describe some general methods applicable to studying how the resonances move under deformation.

4.1 Parametrisation of a transition from an integrable to chaotic billiard

We recall that Artin's billiard, introduced in the last chapter 3.1, is the infinite triangle in the Poincaré half plane representation of hyperbolic geometry with angles $\pi/2$, $\pi/3$ and 0. It is the region A, bordered by solid lines in figure 4.1, with the particular values $\mathcal{L} = C_p = 1$.

In the scheme of Csordás et al. [CGS91], $\mathcal{L}$ is held constant at 1 and the lower boundary of the domain is parameterised by a real number, the 'control parameter' $0 \leq C_p \leq 2$. C_p is the inverse radius of the circle passing through $z = \imath$ which has its centre on the imaginary axis in $\mathrm{Im}(z) \leq 0$. Thus on the lower boundary

$$y = 1 - \frac{C_p x^2}{1 + \sqrt{1 - C_p^2 x^2}}. \tag{4.1}$$

The integrable case corresponds to $C_p = 0$, i.e. the boundary lies at $y = 1$ and the domain is rectangular, and Artin's billiard has $C_p = 1$. For $C_p > 2$ the

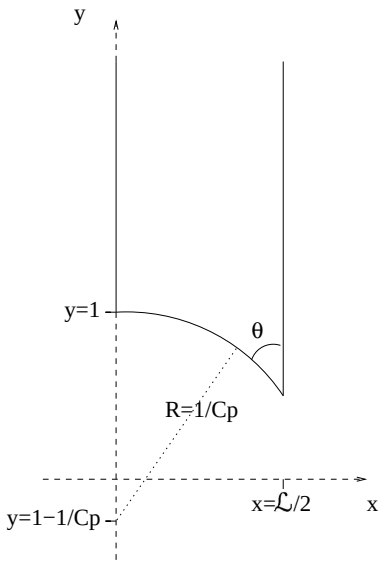

Figure 4.1: The billiards considered on the Poincaré half-plane.

lower part of the billiard becomes open as well as the top. Here we study how the system evolves as C_p varies continuously in the range $0 \leq C_p < 2$. Classically this corresponds to a transition from integrable to chaotic dynamics and we describe this transition in terms of a Poincaré surface of section in section 5.1.1. Quantum mechanically, in section 5.3 we map the variation of the spectra as a function of C_p, using as reference the known limits at $C_p = 0$ and $C_p = 1$.

In fact in the integrable case, $C_p = 0$, there are no resonances. This can easily be seen by considering the Neumann condition on the lower boundary for just the continuum part of the solution in (3.2), since all of the channels are decoupled in this case. This gives

$$S(k) = -\frac{1/2 - \imath k}{1/2 + \imath k}, \tag{4.2}$$

which would have a single pole at $k = \imath/2$ except that corresponds to a constant eigenfunction solution of (2.36) with $\lambda = 0$, not a scattering state. (In the general case, for $C_p \neq 0$, in order to satisfy the boundary condition on the lower curve, no such simple relation exists between incoming and outgoing waves and a non-trivial numerical method must be used to investigate the behaviour of the spectrum.)

This integrable system is central to our investigations, as the simple calculation of its purely real spectrum provides good estimates for the location of resonances of billiards under small perturbations to the lower boundary. We also find good agreement with the theoretical predictions for what happens to the resonance spectrum when we perform the deformation under C_p, as will be shown in the chapter on numerical results 5. A typical transition from integrability to chaos is seen in both the classical and quantum dynamics. This is in marked contrast to what happens near $C_p = 1$, where radical departures from standard theory are seen which must be reinterpreted in light of the unusual arithmetic properties of the system at that particular value [Bog06].

4.2 Hecke groups and parametrisation of the transition between their corresponding billiard systems

A second deformation consists in translating the vertical boundary $x = \mathcal{L}/2$, with $\mathcal{L}$ varying between $\mathcal{L} = 1$ and $\mathcal{L} = 2$. The case $\mathcal{L} = 1$ corresponds to Artin's billiard and as we change $\mathcal{L}$ we encounter several other billiards which are a fundamental region for some discontinuous group, in particular the Hecke triangle groups, which include arithmetic and non-arithmetic cases. By keeping the lower boundary fixed on the unit circle centred at the origin, we ensure all the walls are geodetic, and thus they provide no focussing or defocussing of trajectories. The classical dynamics are ergodic for the whole parameter range and this is due solely to the exponential divergence of trajectories caused by the negative curvature of the Poincaré half-plane.

Hecke groups $\Gamma(2, n)$ for the Poincaré half-plane, $\mathbb{H}$, are generated by the two matrices S and T,

$$S = \begin{pmatrix} 0 & -1 \\ 1 & 0 \end{pmatrix} \quad T = \begin{pmatrix} 1 & \mathcal{L} \\ 0 & 1 \end{pmatrix}, \tag{4.3}$$

where

$$\mathcal{L} = 2\cos(\pi/n),\ n \in \mathbb{Z} | n > 2. \tag{4.4}$$

Using S and T it is easy to show that a fundamental domain for each group can be taken as the region in $\mathbb{H}$ defined by

$$|\Re(z)| \leq \mathcal{L}/2, \quad |z| \geq 1,\ z \in \mathbb{H} \tag{4.5}$$

with coordinates x and y defined as

$$x = \Re(z),\ y = \Im(z). \tag{4.6}$$

For the groups considered here, a simpler construction is convenient than that given in section 2.1. Considering the elliptic transformation

$$z' = \frac{-1}{z + \mathcal{L}}, \tag{4.7}$$

represented by the matrix $ST = \begin{pmatrix} 0 & -1 \\ 1 & \mathcal{L} \end{pmatrix}$, we see that it represents rotation about the fixed point $(-\mathcal{L}/2, \imath\sqrt{1-(\mathcal{L}/2)^2})$ by an angle 2θ given by $\mathcal{L}^2 = 2 + 2\cos(2\theta)$ or $\mathcal{L} = 2\cos(\theta)$. It is a necessary condition on the group generated by S and T to be properly discontinuous that θ be commensurable with π, or more precisely that $r\theta = s\pi$ for some $r, s \in \mathbb{Z}$. To avoid overlap of copies of the fundamental region touching the fixed point under multiple rotations this condition is further restricted by $s = 1$. Hence the Hecke groups described above are the only properly discontinuous groups in $0 < \mathcal{L} < 2$. That the region proposed as a fundamental region above maps back onto itself exactly after r rotations is simply extended to show its tiling property using S and T as suggested and thus completing the argument for its admissibility as such.

In figure 4.1 the fundamental domains for the Hecke groups correspond to $C_p = 1$, $\mathcal{L}/2 = \cos(\pi/n) = \cos(\theta)$, $n \in \mathbb{Z} | n > 2$. In fact they are the region A at those values of the parameters, in union with its reflection in the imaginary axis. By considering only the Neumann boundary condition on that line we restrict ourselves to one symmetry class of the full group, as we did for the modular group in section 3.2.2. However it is this class which contains the resonances and it is those which we are interested in studying. Several studies have been done

on the bound spectra in this and other symmetry classes, good starting points for the interested reader are [Hej92a] and [BV86].

Here we follow the behaviour of the spectrum as $\mathfrak{L}$ varies continuously in the range $1 \leq \mathfrak{L} \leq 2$. We expect to see generic behaviour for chaotic systems in the cases where $\mathfrak{L}$ does not happen to make the region a fundamental domain of a Hecke group as described above. Contact is made with the perturbation made by parameter C_p at $\mathfrak{L} = 1$, where $\Gamma(2,3)$ coincides with Artin's billiard, thus we study the transition to that special case in yet another way. In fact one might expect non-generic behaviour for all the cases where there is a group underlying the triangle ($\theta = \pi/n$) but it has been shown [Bog06] that similar behaviour to that in Artin's billiard is only found for the cases $n \in \{3, 4, 6\}$ (that is, not at $n = 5$, which is the other case studied here). In these cases $\mathfrak{L}^2$ is an integer and the matrix elements of the group can be expressed simply. In general they are shown to belong to the broader class of arithmetic groups and the important distinguishing criterion is in properties of the trace of the matrix groups. These are particularly simple examples. These 'nice' features also enable an explicit construction of S, which gives useful data to check our numerical results against (3.2.1).

The next two sections describe theoretical approaches to calculating how some of the quantities of interest in these systems vary in general as the two deformations just described are applied to Artin's billiard. First we look at perturbation theory for how the resonant energies change under small shifts in the billiard shape. Then a method for directly obtaining S at any value of the pair $\{C_p, \mathfrak{L}\}$ from the Green's function for a simpler, closed system is presented. Our full results on the numerical solutions of the classical and quantum mechanics of these billiard systems are presented in chapter 5.

4.3 Perturbation theory for resonances

The diagram 4.2 shows Artin's billiard, or one of its deformations under $\mathfrak{L}$ or C_p, with a slightly modified version which has width $(\mathfrak{L} + \mathrm{D}\mathfrak{L})/2$ rather than $\mathfrak{L}/2$. The m^{th} resonant wavefunction, ψ_m, of the billiard obeys the Schrödinger equation

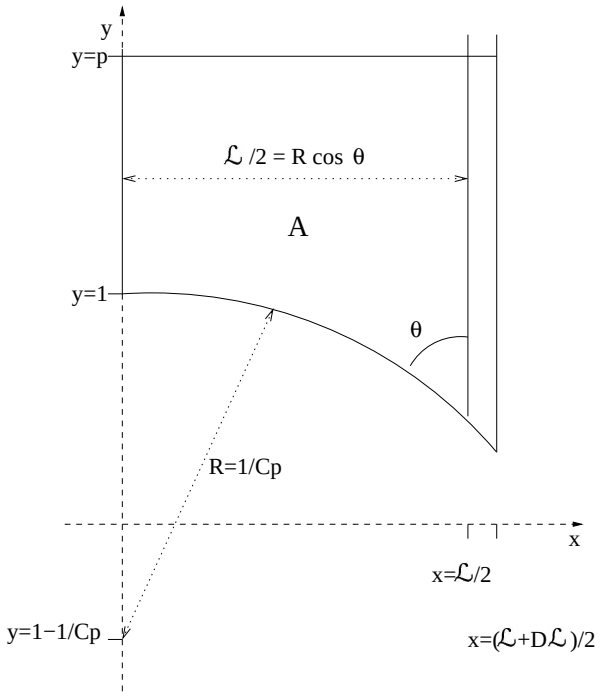

Figure 4.2: Perturbation to Artin's billiard.

$$-\Delta_{LB}\psi_m = \lambda_m \psi_m, \tag{4.8}$$

obeying Neumann boundary conditions on all walls and with the outgoing boundary condition $\psi_m(k;y) = \frac{1}{\sqrt{2\pi}} y^{1/2+\imath k}$ at $y = \infty$.

The perturbation considered here is to extend the long edge by $\mathrm{D}\mathcal{L}/2$, as shown by the furthest-right line in figure 4.2. If the original billiard had area and perimeter A and P respectively, this extended billiard has increased area and perimeter A^1 and P^1. The new resonant energies and wavefunctions obey the Schrödinger equation with modified (complex) energy λ_n^1

$$-\Delta_{LB}\psi_n^1 = \lambda_n^1 \psi_n^1, \tag{4.9}$$

with Neumann boundary conditions now on the modified boundary, P^1. Multiplying the Schrödinger equation for ψ_n^1 by ψ_m and that for ψ_m by ψ_n^1, then taking the difference, we obtain

$$(\lambda_n^1 - \lambda_m)\psi_n^1 \psi_m = \nabla \cdot (\psi_n^1 \nabla \psi_m - \psi_m \nabla \psi_n^1). \tag{4.10}$$

Integrating over A, a finite version of the billiard cut off at p in the y-direction, and applying Gauss's theorem twice (see appendix B for a derivation in the Poincaré half-plane), this becomes

$$\begin{aligned}
(\lambda_n^1 - \lambda_m) \int_A \psi_n^1 \psi_m \mathrm{d}A = & \\
& \int_P (\psi_n^1 \nabla_\perp \psi_m - \psi_m \nabla_\perp \psi_n^1) \mathrm{d}P \\
= & \int_0^{\mathcal{L}/2} \left(\psi_n^1(x,p) \frac{\partial \psi_m(x,p)}{\partial y} - \psi_m(x,p) \frac{\partial \psi_n^1(x,p)}{\partial y} \right) \mathrm{d}x \\
& - \int_{\sqrt{1-(\frac{\mathcal{L}}{2})^2}}^{p} \psi_m(\mathcal{L}/2, y) \frac{\partial \psi_n^1(\mathcal{L}/2, y)}{\partial x} \mathrm{d}y,
\end{aligned} \tag{4.11}$$

since the normal derivative, $\nabla_\perp$, vanishes on all walls for ψ_m, and on all walls excepting the vertical line $x = \mathcal{L}/2$ for ψ_n^1. Letting p be large enough that only the exponentially-growing outbound wave survives in a Fourier decomposition of the resonant wavefunction,

$$\psi_m(k;x,y) = \frac{1}{2\pi} y^{1/2+\imath k_m} + \sum_j a_j \cos(2\pi j x/\mathcal{L})\sqrt{y} K_{\imath k_m}(2\pi j y/\mathcal{L}), \tag{4.12}$$

this simplifies to

$$\begin{aligned}(\lambda_n^1 - \lambda_m)\int_A \psi_n^1 \psi_m \mathrm{d}A &= \frac{\mathcal{L}}{8\imath\pi^2} p^{\imath(k_m+k_n^1)}(k_m - k_n^1) \\ &\quad - \int_{\sqrt{1-(\frac{\mathcal{L}}{2})^2}}^{p} \psi_m(\mathcal{L}/2, y)\frac{\partial \psi_n^1(\mathcal{L}/2,y)}{\partial x}\mathrm{d}y. \end{aligned} \tag{4.13}$$

If we let the perturbation length, $\mathrm{D}\mathcal{L}/2$, tend to zero, the term $\frac{\partial \psi_n^1(\mathcal{L}/2,y)}{\partial x}$ is of first order in that small parameter;

$$\begin{aligned} 0 &= \frac{\partial \psi_n^1((\mathcal{L}+\mathrm{D}\mathcal{L})/2, y)}{\partial x} \\ &= \frac{\partial \psi_n^1(\mathcal{L}/2,y)}{\partial x} + \mathrm{D}\mathcal{L}/2 \frac{\partial^2 \psi_n^1(\mathcal{L}/2,y)}{\partial x^2} + \mathcal{O}(\mathrm{D}\mathcal{L}/2)^2. \end{aligned} \tag{4.14}$$

Inserting this first-order approximation into (4.11), we obtain

$$\begin{aligned}&(\lambda_n^1 - \lambda_m)\int_A \psi_n^1 \psi_m \mathrm{d}A \simeq \\ &\quad \frac{\mathcal{L}}{8\imath\pi^2} p^{\imath(k_m+k_n^1)}(k_m - k_n^1) \\ &\quad + \mathrm{D}\mathcal{L}/2 \int_{\sqrt{1-(\frac{\mathcal{L}}{2})^2}}^{p} \psi_m(\mathcal{L}/2,y)\frac{\partial^2 \psi_n^1(\mathcal{L}/2,y)}{\partial x^2}\mathrm{d}y. \end{aligned} \tag{4.15}$$

Using (4.9) this becomes

$$\begin{aligned}&(\lambda_n^1 - \lambda_m)\int_A \psi_n^1 \psi_m \mathrm{d}A \simeq \\ &\quad \frac{\mathcal{L}}{8\imath\pi^2} p^{\imath(k_m+k_n^1)}(k_m - k_n^1) \\ &- \frac{\mathrm{D}\mathcal{L}}{2} \int_{\sqrt{1-(\frac{\mathcal{L}}{2})^2}}^{p} \psi_m(\mathcal{L}/2,y)\left(\lambda_n^1 \psi_n^1(\mathcal{L}/2,y) + \frac{\partial^2 \psi_n^1(\mathcal{L}/2,y)}{\partial y^2}\right)\mathrm{d}y \end{aligned}$$

$$
\begin{aligned}
= \quad & \frac{\mathcal{L}}{8\imath\pi^2} p^{\imath(k_m+k_n^1)}(k_m - k_n^1) \\
- \quad & \frac{\mathrm{D}\mathcal{L}}{2}\lambda_n^1 \int_{\sqrt{1-(\frac{\mathcal{L}}{2})^2}}^{p} \psi_m(\mathcal{L}/2,y)\psi_n^1(\mathcal{L}/2,y)\mathrm{d}y \\
+ \quad & \frac{\mathrm{D}\mathcal{L}}{2} \int_{\sqrt{1-(\frac{\mathcal{L}}{2})^2}}^{p} \frac{\partial\psi_m(\mathcal{L}/2,y)}{\partial y}\frac{\partial\psi_n^1(\mathcal{L}/2,y)}{\partial y}\mathrm{d}y. \qquad (4.16)
\end{aligned}
$$

after an integration by parts on the second term.

Setting $m = n$, the difference between $\psi_n(0,y)$ and $\psi_n^1(0,y)$ will also be first order in $\frac{\mathrm{D}\mathcal{L}}{2}$ so, taking the first term of the right-hand side over to the left and letting $\mathrm{D}\mathcal{L} \to 0$, we find for the velocity of the resonant momenta,

$$
\begin{aligned}
\dot{k_n} \quad = \quad & -\left(\lambda_n \int_{\sqrt{1-(\frac{\mathcal{L}}{2})^2}}^{p} (\psi_n(\mathcal{L}/2,y))^2 \right. \\
& \left. - \left(\frac{\partial\psi_n(\mathcal{L}/2,y)}{\partial y}\right)^2 \mathrm{d}y\right) \Big/ \left(2k_n \int_A (\psi_n)^2\,\mathrm{d}A - \frac{\mathcal{L}}{8\imath\pi^2}p^{\imath(2k_n)}\right), \qquad (4.17)
\end{aligned}
$$

where the dot means differentiation with respect to the billiard length. Thus the velocity is obtained in terms of the unperturbed solutions, which are quantities obtainable from, for example, the numerical methods employed in chapter 5.

This result shouldn't depend on p, if it is chosen high enough, since the cutoff height should be arbitrary. That the term in the denominator of the right hand side of (4.17) involving p is cancelled exactly by a term from the area integral is seen by considering again the Fourier decomposition (4.12) of the resonant wavefunction. The only part of $(\psi_n)^2$ which is not exponentially damped at large y is the square of the first fourier component, $\frac{1}{4\pi^2}y^{1+2\imath k_n}$. Performing the integral over A, we obtain for this contribution to the first term in the denominator of the right hand side of (4.17)

$$
\begin{aligned}
2k_n \int_A \frac{1}{4\pi^2} y^{1+2\imath k}\mathrm{d}A \quad &= \quad \frac{k_n}{2\pi^2}\int_0^{\mathcal{L}/2}\int_{\sqrt{1-(\frac{\mathcal{L}}{2})^2}}^{p} y^{1+2\imath k}\frac{\mathrm{d}y}{y^2}\mathrm{d}x \\
&= \quad \frac{\mathcal{L}}{8\imath\pi^2}p^{2\imath k_n} - \frac{\mathcal{L}}{8\imath\pi^2}\left(\sqrt{1-(\frac{\mathcal{L}}{2})^2}\right)^{2\imath k_n}. \qquad (4.18)
\end{aligned}
$$

Thus all terms involving p are seen to cancel, as expected.

4.4 Obtaining S by closing the system

Having considered how to obtain expressions for the resonance parameters in a system close to one where we have known analytic or numerical solutions, we now demonstrate a method that allows one to obtain this information for more general systems. The prerequisite for its application is an ability to calculate the Green's function for a suitable closed billiard system. Fortunately this is far easier in general than the calculation of resonances, due to bound states having real eigenvalues. A rough application to Artin's billiard produces good agreement with the first few resonances, which are known from our earlier calculations (see section 3.2.2).

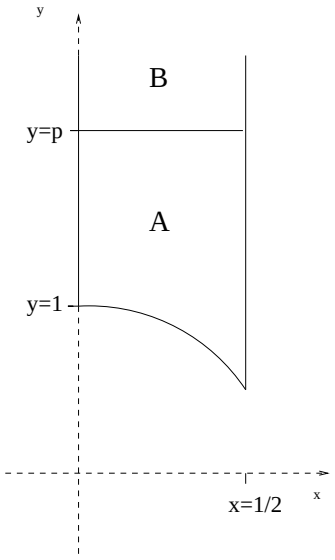

Figure 4.3: Artin's billiard on the Poincaré half-plane, cut off at $y = p$.

The diagram 4.3 shows Artin's billiard, split into two regions at $y = p$. If y is chosen large enough then the solution to the Schrödinger equation for the whole billiard,

$$-\Delta_{LB}\psi = \lambda\psi, \tag{4.19}$$

at energy $\lambda = k^2 + 1/4$ and with Neumann boundary conditions on all walls, will be of the form

$$\psi = y^{1/2}(ay^{-ik} + by^{ik}), \qquad y \gg 1, \tag{4.20}$$

since any oscillatory x-dependence will be exponentially damped by the dependence on y (see equation (3.2)).

This can be written as

$$\psi = y^{1/2}(a'e^{-ik\ln(y/p)} - b'e^{ik\ln(y/p)}), \tag{4.21}$$

so that

$$\psi(x,p) = p^{1/2}(a' - b') \tag{4.22}$$

and

$$\frac{\partial\psi(x,p)}{\partial y} = p^{-1/2}(\frac{1}{2}(a' - b') - ik(a' + b')). \tag{4.23}$$

Now consider the billiard defined by area A, again with Neumann boundary conditions on all walls, including on the line $y = p$. This has a complete set of normalized eigenfunctions of the Schrödinger equation (4.19), ϕ_n, with eigenvalues λ_n. We define Green's function for this billiard as

$$G(\underline{\mathbf{r}}, \underline{\mathbf{r}}', \lambda) = \sum_n \frac{\phi_n^*(\underline{\mathbf{r}})\phi_n(\underline{\mathbf{r}}')}{\lambda - \lambda_n}, \tag{4.24}$$

where $\underline{\mathbf{r}} = (x, y)$.

This Green's function is a solution of the inhomogeneous Schrödinger equation

$$(\Delta_{LB} + \lambda)G(\underline{\mathbf{r}}, \underline{\mathbf{r}}', \lambda) = \delta(\underline{\mathbf{r}} - \underline{\mathbf{r}}'), \tag{4.25}$$

so that, multiplying (4.19) by G, (4.25) by $\psi(\underline{\mathbf{r}})$ and taking the difference, we obtain

$$\psi(\underline{\mathbf{r}})\Delta_{LB}G(\underline{\mathbf{r}}, \underline{\mathbf{r}}', \lambda) - G(\underline{\mathbf{r}}, \underline{\mathbf{r}}', \lambda)\Delta_{LB}\psi(\underline{\mathbf{r}}) = \delta(\underline{\mathbf{r}} - \underline{\mathbf{r}}')\psi(\underline{\mathbf{r}}). \tag{4.26}$$

Taking the integral over A and applying Gauss's theorem twice (see appendix B), we end up with

$$\psi(\underline{\mathbf{r}}) = -\int_0^{1/2} G(\underline{\mathbf{r}}', (x,p), \lambda) \frac{\partial \psi(x,p)}{\partial y} \mathrm{d}x, \tag{4.27}$$

since the normal derivative of G vanishes on the entire boundary of A and that of ψ does so everywhere on the boundary except for the line $y = p$.

Substituting (4.23) into (4.27) and looking at a point $\underline{\mathbf{r}}' = (x', p)$, this becomes

$$p^{1/2}(a' - b') = -p^{-1/2}(\frac{1}{2}(a' - b') - ik(a' + b')) \int_0^{1/2} G(x', p, x, p, \lambda) \mathrm{d}x. \tag{4.28}$$

Now we assume G is constant in x and x' along $y = p$. This is approximately valid, provided that p is taken large enough. For a given value of λ, all terms in equation (4.24) with n larger than some particular $n_{\max}$ will be sufficiently suppressed, by the factor $\lambda - \lambda_n$ in the denominator of each term. The oscillatory part of what remains can be extracted by taking a Fourier-esque decomposition of G in the form (3.2). One thus chooses a large enough value of p, such that the Bessel function in the expression for the first expansion coefficient is close enough to zero. That is, such that

$$K_{i\sqrt{\lambda_{n_{\max}} - 1/4}}(2\pi p/\mathcal{L}) \ll 1, \tag{4.29}$$

so that exponential decay of the Bessel function suppresses all oscillatory contributions. All higher Fourier coefficients will decay faster, as will the coefficients for $\lambda_n < \lambda_{n_{\max}}$.

Performing the integral in (4.28) then gives

$$p^{1/2}(a' - b') = -p^{-1/2}(\frac{1}{2}(a' - b') - ik(a' + b'))\frac{1}{2}G(p, p, \lambda). \tag{4.30}$$

The scattering matrix, $S(\lambda)$, in this case a scalar, defined by

$$b' = Sa', \tag{4.31}$$

can be extracted from (4.30);

$$\begin{aligned} S &= \frac{p+\frac{1}{2}G(p,p,\lambda)(\frac{1}{2}-ik)}{p+\frac{1}{2}G(p,p,\lambda)(\frac{1}{2}+ik)} \\ &= 1-\frac{ikG}{p+\frac{1}{2}G(p,p,\lambda)(\frac{1}{2}+ik)}. \end{aligned} \tag{4.32}$$

This form of S is consistent with that obtained by another method in [SSS03]. An alternative approach to constructing S for billiards is given in [FS97]. They start by considering the whole system to have a state represented by

$$\mathbf{\Phi} = \begin{pmatrix} \underline{\mathbf{u}} \\ \Psi \end{pmatrix} \tag{4.33}$$

where $\underline{\mathbf{u}}$ represents the vector of amplitudes of the internal wavefunction (in A) expanded in some basis u_n and Ψ is the wavefunction in the region B, given by (4.20).

Then the Hamiltonian operates on the whole system as follows:

$$\mathcal{H}\begin{pmatrix} \underline{\mathbf{u}} \\ \Psi \end{pmatrix} = \begin{pmatrix} \hat{H}_A\underline{\mathbf{u}} + \underline{\mathbf{w}}\Psi\big|_{y=p} \\ -\Delta_{LB}\Psi \end{pmatrix}, \tag{4.34}$$

so that $\underline{\mathbf{w}}$ is a vector representing the coupling (assumed to be local to the joining point, p) of the continuum to the internal basis. $\hat{H}_A$ is the Hamiltonian matrix for the internal system A.

In order that this Hamiltonian operator be self-adjoint we have to impose some condition on the coupling. The suggested form is

$$\underline{\mathbf{w}}^\dagger\underline{\mathbf{u}} = \left(\frac{\partial}{\partial y}\Psi\right)\Big|_{y=p} \tag{4.35}$$

Together with the first row of (4.34) this gives

$$\underline{\mathbf{w}}^\dagger(E-\hat{H}_A)^{-1}\underline{\mathbf{w}}\Psi\Big|_{y=p} = \left(\frac{\partial}{\partial y}\Psi\right)\Big|_{y=p} \tag{4.36}$$

which leads straight to a value for S of

$$S = p^{-2\imath k}\frac{-\underline{\mathbf{w}}^\dagger(E-\hat{H}_A)^{-1}\underline{\mathbf{w}}p + (1/2-\imath k)}{\underline{\mathbf{w}}^\dagger(E-\hat{H}_A)^{-1}\underline{\mathbf{w}}p - (1/2+\imath k)}, \tag{4.37}$$

which has the resolvent operator displaced in both the numerator and denominator relative to (4.32), though this must be an effect of the coupling vector $\underline{\mathbf{w}}$.

What is harder to do is to cast this in the usual form,

$$S = 1 - 2\pi\imath\underline{\mathbf{w}}^\dagger \frac{1}{E - \mathcal{H}_{ef}}\underline{\mathbf{w}}, \tag{4.38}$$

where the poles of the S-matrix are given by eigenvalues of the non-Hermitian effective Hamiltonian $\mathcal{H}_{ef} = \hat{H}_A - \imath\pi\underline{\mathbf{w}}\underline{\mathbf{w}}^\dagger$, since the factors of $1/2$ that arise from the derivative of the external wavefunction preclude the use of the methods used in the above references.

However, starting from our expression (4.32) for S, we rewrite it as

$$S = 1 - 2ik\frac{G(p,p,\lambda)}{2p}\frac{1}{1 + \frac{G(p,p,\lambda)}{2p}(\frac{1}{2} + ik)}. \tag{4.39}$$

Then

$$S = 1 - 2i\mathbf{A}^\dagger G\mathbf{A}\frac{1}{1 + \mathbf{A}^\dagger G\mathbf{A}(\frac{1}{2k} + i)}, \tag{4.40}$$

with $A_i = \sqrt{\frac{k}{2p}}\phi_i(p)$ and $G = \frac{1}{E - \hat{H}_A}$. Here $\phi_i(p)$ means the i^{th} wavefunction of the closed billiard, A in figure 4.3, with the dependence on x integrated out, evaluated at $y = p$.

This in turn can be rewritten using the identity

$$\begin{aligned}
\mathbf{A}^\dagger G\mathbf{A}\left(1 + \mathbf{A}^\dagger G\mathbf{A}(\frac{1}{2k} + i)\right)^{-1} &= \Sigma_{j=0}^{\infty}(-(\imath + \frac{1}{2k}))^j(\mathbf{A}^\dagger G\mathbf{A})^{j+1} && (4.41)\\
&= \mathbf{A}^\dagger\left(1 + \mathbf{A}^\dagger G\mathbf{A}(\frac{1}{2k} + i)\right)^{-1} G\mathbf{A} && (4.42)\\
&= \mathbf{A}^\dagger\frac{1}{E - \hat{H}_A + (\frac{1}{2k} + i)\mathbf{A}\mathbf{A}^\dagger}\mathbf{A}, && (4.43)
\end{aligned}$$

which gives an S of the form (4.38) with $\mathcal{H}_{ef} = \hat{H}_A - (\frac{1}{2k} + i)\mathbf{A}\mathbf{A}^\dagger$.

Using a finite version of (4.24) with the sum truncated at 22 terms, we obtained an approximate Green's function for Artin's billiard cut off at $y = 10$.

For this we required numerical values for the energies λ_n and square modula of the wavefunctions $\phi_n(\underline{\mathbf{r}})$ evaluated on the line $y = 10$. These were obtained by a Finite Element Method (FEM) using the package FreeFem++ [PHH06]. This method is described in more detail in section 5.2.1.3. Once we have our approximate Green's function, the phase shift is extracted as half the phase of S, given by equation (4.32). The result for $k < 20$ is plotted in figure 4.4, covering the first six resonances of Artin's billiard. The smoother, dashed line is the theoretical curve obtained from (3.29). The resonances come at the points of rapidly varying δ, according to the general scattering theory presented in section 2.3.2. Given a slowly varying background phase shift, these are approximately at the points where the phase 'wraps round' from $\pi/2$ to $-\pi/2$, and a vertical line crosses the k-axis. Good agreement with the theoretical curve is obtained for low values of momentum, and the first few resonance positions can even be read off $(7.07, 10.5$ and $12.5)$, to three significant figures.

Methods for extracting the resonance parameters from phase shift data are discussed in section 5.2 and will unfortunately turn out to be not very effective for the billiard systems studied here, due to the large numbers of extremely narrow resonances which appear near the integrable and arithmetic cases investigated. The next chapter introduces the range of methods we applied to tackling the general problem of analyzing the resonance spectra of Artin's billiard, and its deformations introduced in the previous sections.

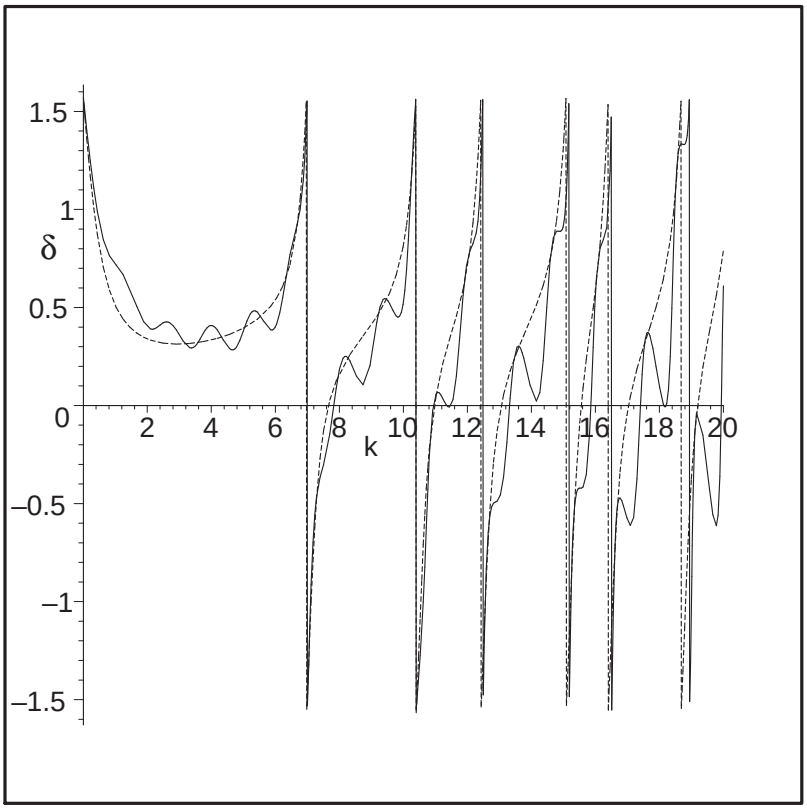

Figure 4.4: Plot of the variation of the phase shift with momentum for Artin's billiard, obtained from an approximation to the Green's function of the billiard closed at $y = 10$ (solid line), and from an exact form of δ, derived from (3.29).

Chapter 5

Results

5.1 Classical considerations

Before showing how the resonance spectrum evolves as the lower boundary of Artin's billiard is deformed, we numerically investigate how the underlying classical mechanics varies with C_p. This backs up our statements of integrability at $C_p = 0$ and ergodicity at $C_p = 1$, with phase space becoming progressively more chaotic as C_p increases. The effect the classical phase space has on the quantum spectrum will be illustrated in section 5.3

5.1.1 Classical phase-space

The classic tool for investigation of phase-space structure is a Poincaré surface of section. The idea is that by examining the points at which trajectories in the full phase-space cross some plane, we can still extract useful information about the stability of orbits and about bulk structures such as attractors. Although the systems considered here are only 2-dimensional, so that entire trajectories *could* be plotted, the idea of extracting the critical information by taking a section of phase-space is still useful. In particular, noticing that between bounces the dynamics are trivial, Csordás et al. [CGSV94] suggest a 'bounce mapping' where what are essentially the momenta are plotted immediately after every collision with a wall. In fact this idea is refined to consider only bounces from the lower wall, which is the curve parameterised by the control parameter C_p in (4.1).

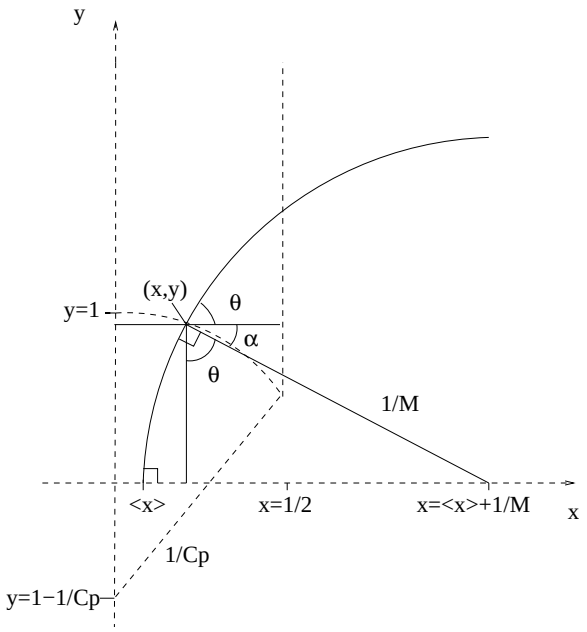

Figure 5.1: Geometry of the bounce mapping.

Additionally it is better to plot the variables $(\langle x\rangle, M)$, the 'footprint' (the point on the real axis where the trajectory ends infinitely far in the past) and inverse radius of the trajectory taken after each bounce, since these variables remain constant between bounces. Though other choices are equally justifiable, we make this selection for direct comparison with the results in [CGSV94]. Figure 5.1 shows the geometry of the situation.

The algorithmic procedure is as follows: A value of x is chosen at random from the range $(0, 1/2)$ and then a random angle of trajectory chosen from that point on the lower boundary (in the range $(\alpha, \pi + \alpha)$, where α is the angle the lower boundary makes with a horizontal line at x). The radius and footprint of the trajectory are calculated from these by the formulae

$$M = \cos(\theta)/y \tag{5.1}$$

and

$$\langle x\rangle = x + (\sin(\theta) - 1)/M. \tag{5.2}$$

Negative values of M are possible and correspond to trajectories moving to the left, otherwise trajectories move away from $\langle x \rangle$ to the right. Reflections off the vertical walls are trivial and the next contact with the lower boundary is calculated with the quadratic formula for the intersection of the two circles defined by the trajectory and the lower boundary. Then $\theta = \tan^{-1}(\mathrm{d}y/\mathrm{d}x)$ and after reflection it maps to

$$\theta \mapsto \pi + 2\alpha - \theta \tag{5.3}$$

for trajectories with positive gradient, or

$$\theta \mapsto 2\alpha - \theta \tag{5.4}$$

otherwise, according to the law of specular reflection at that point. This process is iterated over a suitable number of initial conditions and bounces of each random trajectory thus generated. Special care is needed if the angle of a trajectory happens to hit exactly $\theta = \pi/2$, when it would escape to infinity, but in practice this never happens.

Reproducing the three cases from [CGSV94] required only a single randomly chosen trajectory for the cases $C_p \in \{0.5, 1\}$, but when C_p is small the near-integrable nature of the motion means a single orbit tends to get stuck on a stable periodic orbit, so ten random trajectories were selected to give a fuller picture of the phase space. The progression of the phase space to more and more chaotic is clearly seen until the single trajectory ergodicly explores the whole available phase space at $C_p = 1$. In fact the islands of stability visible in figure 5.3 vanish by $C_p = 0.8$ and the phase space can be considered completely chaotic from that point on. Each graph contains 10^5 points in total.

The odd shape of the region explored is due to the choice of parameters. The near-symmetry under ($M \mapsto -M$, $\langle x \rangle \mapsto 1 - \langle x \rangle$) is in fact due to there being a forwards and reverse traversal of each orbit - an orbit characterised by the pair $(\langle x \rangle, M)$ has the pair $(\langle x \rangle + 2/M, -M)$ for a particle following it towards negative values of x. Additionaly the possible values of $(\langle x \rangle, M)$ are constrained by the requirement that the trajectory intersects the billiard system at some point. This means that for a given positive value of M, $\langle x \rangle$ can only lie in the range

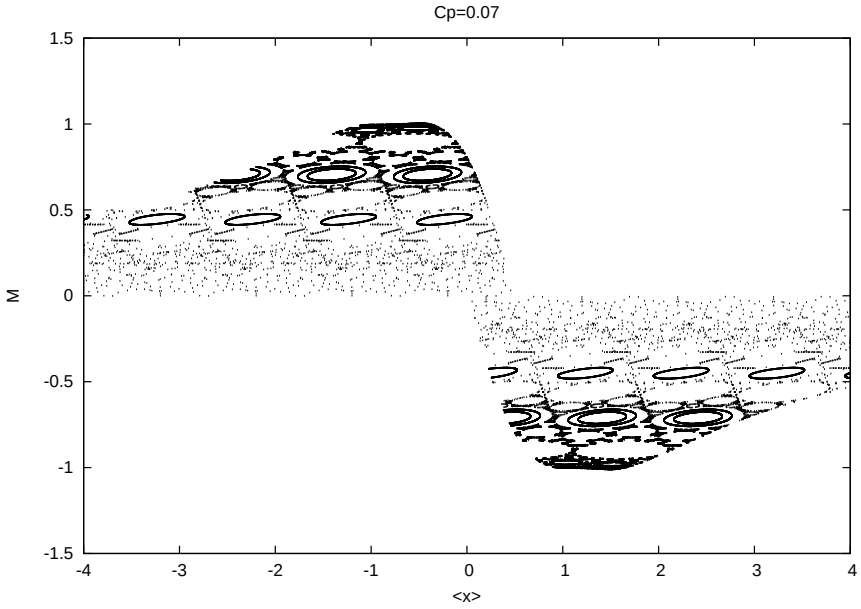

Figure 5.2: Bounce mapping for $C_p = 0.07$.

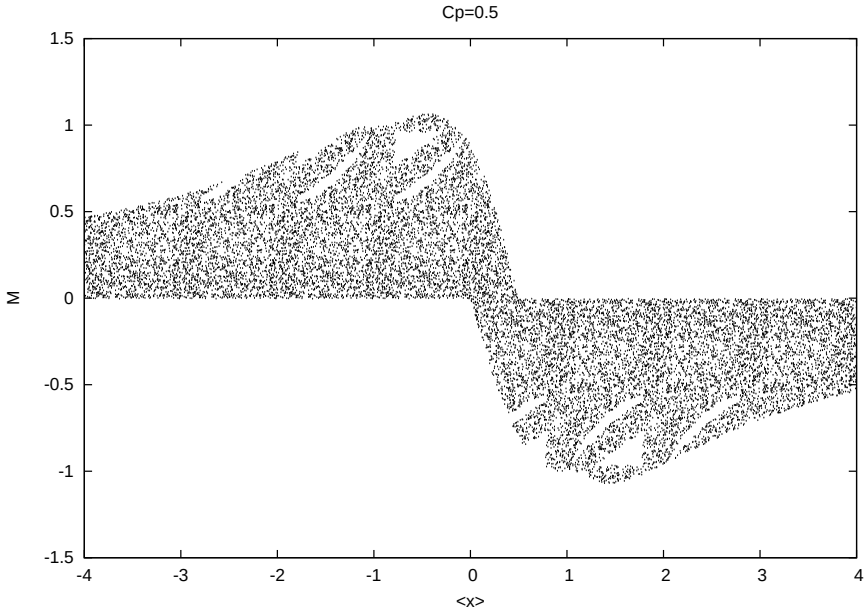

Figure 5.3: Bounce mapping for $C_p = 0.5$.

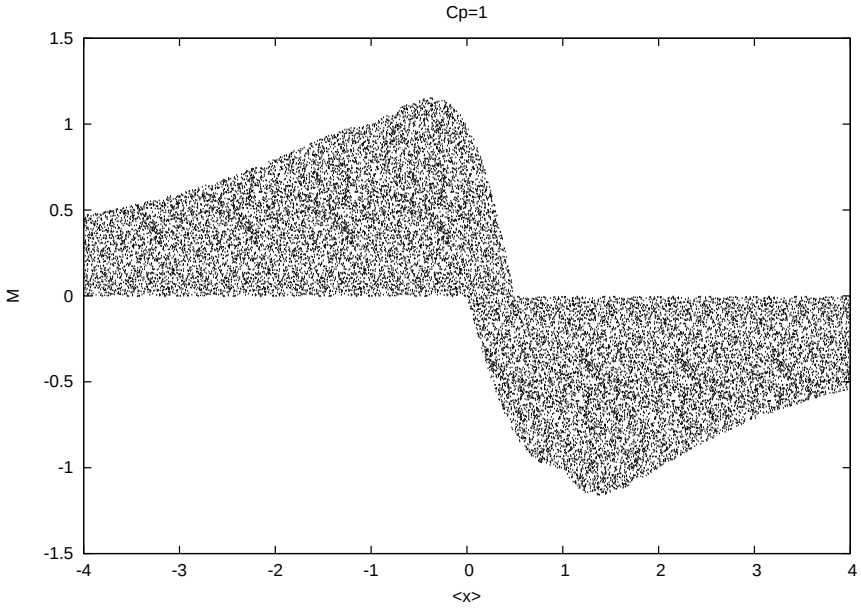

Figure 5.4: Bounce mapping for $C_p = 1$.

$$(-\frac{1}{M}(1+\sqrt{1-M^2}) \leq \langle x \rangle \leq \frac{1}{2} - \frac{1}{M}(1-\sqrt{1-(My_{\min})^2}), \qquad (5.5)$$

except when $M > 1$, which raises the left bound to $-\frac{1}{M}(1-\sqrt{(1-M^2)-\frac{2M}{C_p}(1-M)}$. $y_{\min} = (1-1/C_p) + \sqrt{1/C_p^2 - 1/4}$, the lowest point on the lower boundary, at $x = 1/2$. M, the inverse radius of the trajectory, must of course be less than the reciprocal of this number since trajectories must be circles which touch the real axis at right angles.

5.1.2 Stability of orbits

A more detailed analysis of the stability of some orbits is now conducted. Again we follow the methods from [CGSV94], but choose a different set of orbits to study. The curvature $\kappa(t)$ of a trajectory is the inverse radius of the circle defining the wave front of nearby trajectories coming from a point at $t = 0$. In Euclidean space this decreases as $1/t$ since the radius increases linearly for free motion, but here, due to the exponential divergence of neighbouring trajectories (2.33), it is described by the equation [CGSV94]

$$\dot{\kappa}(t) = -R - \kappa^2(t), \tag{5.6}$$

where the Gaussian curvature $R = -1$.

For a periodic orbit of period T, $\kappa(t+T) = \kappa(t)$ and the Lyapunov exponent is given by the average of κ over a period [CM03; BD95],

$$\lambda = \frac{1}{T}\int_0^T \kappa(t)\mathrm{d}t. \tag{5.7}$$

The solution of (5.6) between collisions with the lower boundary is (for $C_p \leq 1$)

$$\kappa(t) = \tanh(t - t_0), \tag{5.8}$$

where $t_0 = \tanh^{-1}(\kappa(0))$ will be determined by the periodicity condition. At a bounce from a geodetic wall there is no change in κ, but when the lower boundary is varied according to the parameter C_p it jumps by an amount [CM03]

$$Q = \frac{-2q}{\cos(\phi)}, \tag{5.9}$$

where ϕ is the angle the trajectory makes with the normal to the wall on collision and

$$q = \frac{-C_p(C_p - 1)}{\left(C_p - 1 + \sqrt{1 - C_p^2 x_0^2}\right)} \tag{5.10}$$

is the curvature of the lower boundary, given by

$$q = \frac{1}{r_g} - \frac{1}{r_{C_p}}, \tag{5.11}$$

with r_{C_p} being the radius of the boundary, $1/C_p$, and r_g being the radius of the tangent geodesic to that curve at the point of collision. Considering this and (5.6) we see that when $C_p > 1$, κ stays greater than 1 for all time and thus the Lyapunov exponent is greater than 1 due to (5.7).

Now the periodicity condition reads

$$\tanh(-t_0) = \tanh(T - t_0) - Q, \tag{5.12}$$

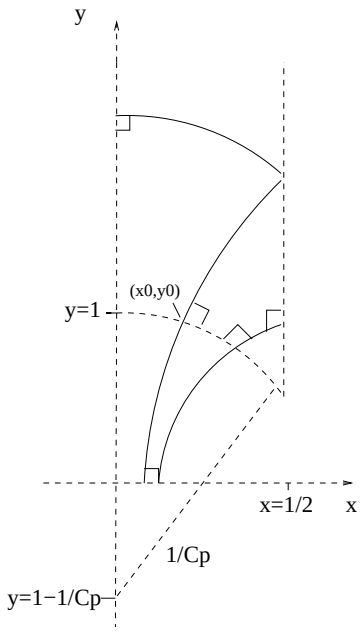

Figure 5.5: Geometry of the set of orbits considered.

an equation for t_0. Once this is solved for a particular orbit, its Lyapunov exponent, λ, can be found from (5.7) since

$$\begin{aligned}\lambda &= \frac{1}{T}\int_0^T \tanh(t-t_0)\mathrm{d}t \\ &= \frac{1}{T}\ln\left(\frac{\cosh(T-t_0)}{\cosh(t_0)}\right) \\ &= \frac{1}{T}\ln\left(\cosh(T)-\sinh(T)\tanh(t_0)\right). \end{aligned} \tag{5.13}$$

The class of orbits considered here is represented by figure 5.5 where orbits with one and two bounces off the vertical walls are shown. To satisfy the requirement of periodicity, the contact with the lower boundary defined by (4.1) and a particular value of C_p must be at right angles (represented by squares in figure 5.5), as must the final reflection from a vertical wall . Thus for any value of C_p there is a family of orbits labelled by the number of bounces, m, off the vertical walls.

It is clear that these curves are equivalent (when continued across the vertical walls by group transformations) to the set of trajectories perpendicular to the lower boundary and centred on the real axis at $x = m/2$. To satisfy orthogonality at a point x_0 on the lower boundary, the curve

$$(x - m/2)^2 + y^2 = a_m^2, \tag{5.14}$$

which has gradient

$$\frac{\mathrm{d}y}{\mathrm{d}x} = \frac{-(x - m/2)}{\sqrt{a_m^2 - (x - m/2)^2}}, \tag{5.15}$$

must firstly have this gradient at the point x_0 equal to that of the normal to the lower boundary given by (4.1)

$$x^2 + (y - (1 - C_p))^2 = 1/C_p^2, \tag{5.16}$$

that is

$$\frac{\mathrm{d}y}{\mathrm{d}x}(x_0) = \frac{\sqrt{1 - C_p^2 x_0^2}}{C_p x_0} = \frac{-(x_0 - m/2)}{\sqrt{a_m^2 - (x_0 - m/2)^2}}. \tag{5.17}$$

This yields the requirement on the radius of the trajectory

$$a_m^2 = \frac{(x_0 - m/2)^2}{1 - C_p^2 x_0^2} \tag{5.18}$$

which, substituted back into (5.14), gives a value of y for the trajectory at the point x_0,

$$y_0^2 = (x_0 - m/2)^2 \frac{C_p^2 x_0^2}{1 - C_p^2 x_0^2}. \tag{5.19}$$

For an orthogonal meeting of the lower boundary and trajectory this point must also be on the lower boundary, that is

$$y_0^2 = (x_0 - m/2)^2 \frac{C_p^2 x_0^2}{1 - C_p^2 x_0^2} = ((1 - 1/C_p) + \sqrt{(}1/C_p^2 - x_0^2))^2. \tag{5.20}$$

or

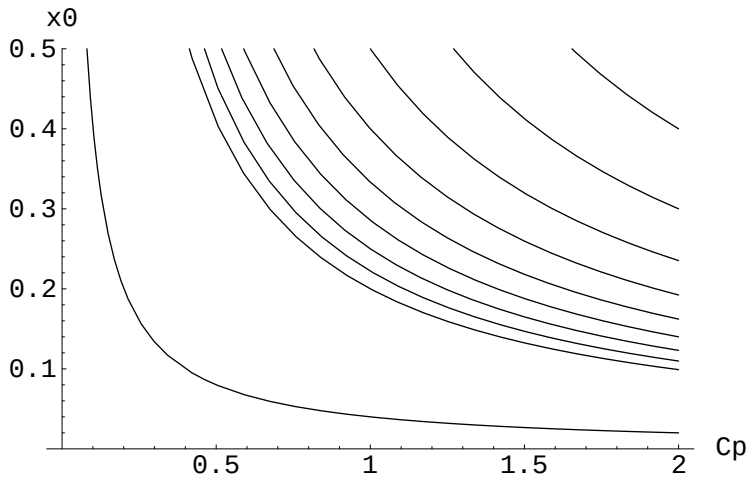

Figure 5.6: Variation of x_0 with C_p for orbits having differing values of m.

$$(\frac{m}{2}C_p^2x_0 - 1)^2 = (1 - C_p^2x_0^2)(1 - C_p)^2 \tag{5.21}$$

which, on solving for x_0, gives

$$x_0 = \frac{\frac{mC_p}{2} - (1 - C_p)\sqrt{(\frac{mC_p}{2})^2 - 1 + (1 - C_p)^2}}{C_p((\frac{mC_p}{2})^2 + (1 - C_p)^2)}. \tag{5.22}$$

x_0 and y_0 are written without explicitly displaying their dependence on m and C_p to ease the following expressions on the reader's eye.

Figure 5.6 shows how x_0 varies with C_p for values of m from 2 to 10 and for $m = 50$. Curves with higher values of m appear further to the left. It is apparent that in the restricted range considered, $0 < x < 1/2$, solutions do not exist for all values of C_p. In particular there is no periodic orbit of this form in this range with $m = 1$ and as m increases, the orbits exist at lower values of C_p, with correspondingly lower values of x_0 until $x_0 = 1/2$ is reached at some critical value of C_p.

Now we calculate a value of y_0 from (5.19) and using a formula for the distance between the two points, $\rho((x_0, y_0); (m/2, a_m))$ from (2.21), the period T_m drops out as the surprisingly simple expression

$$T_m = 2\cosh^{-1}(\frac{1}{c_p x_0}). \tag{5.23}$$

To determine the Lyapunov exponent from (5.7) it is still necessary to calculate t_0 from (5.12). Expanding the hyperbolic tangent and using the fact that $\phi = 0$ for this class of orbits we get

$$-\tanh(t_0^m) = \frac{\tanh(T_m) - \tanh(t_0^m)}{1 - \tanh(T_m)\tanh(t_0^m)} - 2q \tag{5.24}$$

and thus the relevant solution

$$\begin{aligned}
\tanh(t_0^m) &= q - \sqrt{q^2 + 1 - 2q/\tanh(T_m)} \\
&= \frac{-C_p(C_p-1)}{\left(C_p - 1 + \sqrt{1 - C_p^2 x_0^2}\right)} \\
&- \sqrt{\frac{C_p^2(C_p-1)^2}{\left(C_p - 1 + \sqrt{1 - C_p^2 x_0^2}\right)^2} + 1 + \frac{C_p(C_p-1)(2 - C_p^2 x_0^2)}{\left(C_p - 1 + \sqrt{1 - C_p^2 x_0^2}\right)\sqrt{1 - C_p^2 x_0^2}}}.
\end{aligned} \tag{5.25}$$

Substituting this into (5.13) and using simple hyperbolic trigonometrical identities to get explicit forms for expressions involving T_m, the final result is

$$\begin{aligned}
\lambda_m &= \frac{\ln\left(\frac{2}{C_p^2 x_0^2} - 1 + \frac{2\tanh(t_0^m)\sqrt{1 - C_p^2 x_0^2}}{C_p^2 x_0^2}\right)}{2\cosh^{-1}(\frac{1}{c_p x_0})} \\
&= \frac{\ln\left(1 + 2\tanh(t_0^m)\sqrt{1 - C_p^2 x_0^2} + (1 - C_p^2 x_0^2)\right) - \ln(C_p^2 x_0^2)}{\ln\left(1 + \sqrt{1 - C_p^2 x_0^2}\right)^2 - \ln(C_p^2 x_0^2)}.
\end{aligned} \tag{5.26}$$

Figure 5.7 shows this variation for periodic orbits with $m \in \{3, 4, 5, 9\}$. Higher values of m generate curves further to the left of the graph. However, this graph is slightly deceptive, since looking at figure 5.6 one sees that most of these curves don't exist with x_0 in the range $(0, 1/2)$. A slightly more realistic picture of the stability of this family of periodic orbits in this range is given by figure 5.8, which shows the variation of the Lyapunov exponent with C_p for imagined curves

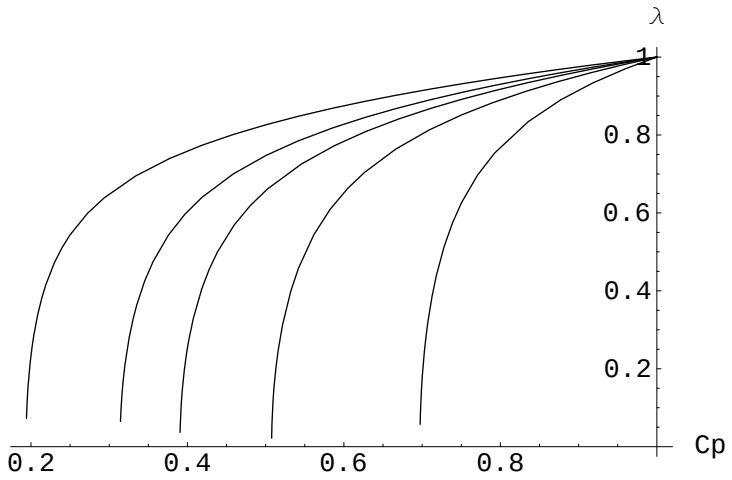

Figure 5.7: Variation of the Lyapunov exponent with C_p for orbits having differing values of m.

with fixed values of x_0 at $0.001, 0.01, 0.1$ and 0.5 respectively. Smaller values of x_0 generate the more unstable orbits (larger λ). The family of periodic orbits considered here exist at discrete points along these curves.

The family of orbits considered in [CGSV94] were all unstable for $C_p > 0.8$ and it is fair to say that the results here with the last stable orbit, even out of the domain considered, destabilising for $C_p > 0.7$, together with the phase portrait in section 5.1.1, support the conclusion drawn in [CGSV94] that the phase space is completely chaotic once the condition $C_p > 0.8$ holds. Note that for the whole family of orbits at $C_p = 1, \lambda = 1$, i.e. in the special case of Artin's billiard, all the Lyapunov exponents are 1.

We have explicitly mapped the phase space for deformation of the lower boundary, but it is clear that the classical motion is completely chaotic for the deformation parameterised by $\mathcal{L}$, since we keep C_p fixed at 1 while that varies. In that case all the walls are then geodetic, so there is no focussing or defocussing of trajectories, and all the orbits will have Lyapunov exponent 1.

We now go on to examine the behaviour of the quantum spectrum when the deformations are applied.

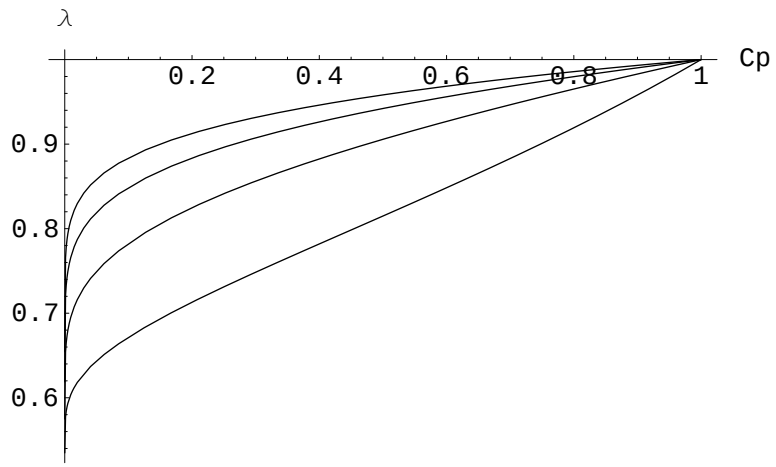

Figure 5.8: Variation of the Lyapunov exponent with C_p for orbits having differing values of x_0.

5.2 Quantum methods for locating resonances

Before embarking on a description of the methods used to obtain numerical approximations for the resonances of the billiard systems described in chapter 4, a brief review of the position we find ourselves in is appropriate. Since the metric in the Poincaré half-plane is (2.4), $g_{ij} = y^{-2}\delta_{ij}$, the Schrödinger equation for these billiards is (2.36)

$$y^2(\frac{\partial^2}{\partial x^2} + \frac{\partial^2}{\partial y^2})\psi = -\lambda\psi, \tag{5.27}$$

where $\lambda = 2mE/\hbar^2 + \frac{1}{4}$ and E is the energy of a particle of mass m.

The systems under consideration were described in sections 4.1 and 4.2, and were illustrated in figure 4.1. The first perturbation changes the shape of the lower boundary of Artin's billiard continuously, between a flat horizontal line and the circle of radius 1/2 passing through the points $z = 0$ and $z = \imath$. The second perturbation considered shifts the right hand vertical wall, while keeping the lower boundary fixed as the unit circle in the half-plane. Solutions of (5.27) are sought which obey Neumann boundary conditions on all walls. Considering first this boundary condition on $x = 0$ and $x = \mathcal{L}/2$, that is

$$\frac{\partial \psi}{\partial \hat{n}} = 0, \tag{5.28}$$

where $\frac{\partial}{\partial \hat{n}}$ is the normal derivative of the wavefunction on the boundary, one can write a set of solutions to (5.27) for fixed λ that are bounded (as y tends to infinity) in the form

$$\psi_m(k; x, y) = \cos(2\pi m x/\mathcal{L})\sqrt{y}K_{\imath k}(2\pi m y/\mathcal{L}), \quad m \in \mathbb{N} \tag{5.29}$$

where $k = \sqrt{2mE}/\hbar$ is the scaled momentum and $K_{\imath k}$ is the modified Bessel function of imaginary order. These Bessel functions are solutions of the second-order differential equation

$$y^2 \frac{\mathrm{d}^2}{\mathrm{d}y^2} K_{\imath k}(2\pi m y/\mathcal{L}) + y\frac{\mathrm{d}}{\mathrm{d}y} K_{\imath k}(2\pi m y/\mathcal{L}) + (k^2 - (2\pi m y/\mathcal{L})^2) = 0, \tag{5.30}$$

which is obtained from (5.27) by substituting $\psi = \cos(2\pi m x/\mathcal{L})\sqrt{y}K(y)$ therein, and the $K_{\imath k}$ decay exponentially as $y \to \infty$.

The continuum solution is of the form

$$\psi_0(k; y) = y^{1/2}(y^{-\imath k} + S(k)y^{\imath k}), \tag{5.31}$$

obtained by solution of (5.30) with $m = 0$. This solution represents incoming and outgoing waves at infinity. S is the S-matrix, here a scalar since there is only one scattering channel available as discussed earlier in section 2.3.2. Together with the bound solutions (5.29) this forms a complete set of solutions to the scattering problem. Satisfying the boundary condition (5.28) on the lower boundary in figure 4.1 is not straightforward. In general, a linear combination of the bound and continuum wavefunctions at a given energy must be taken. This will thus have the form

$$\psi(k; x, y) = b_0 y^{1/2}(y^{-\imath k} + S(k)y^{\imath k}) + \sum_{m=1}^{\infty} b_m(k)\cos(2\pi m x/\mathcal{L})\sqrt{y}K_{\imath k}(2\pi m y/\mathcal{L}). \tag{5.32}$$

Using the analysis of section 2.3.2, we know that these scattering solutions exist at all positive energies. It is not too hard, using analogous methods to those

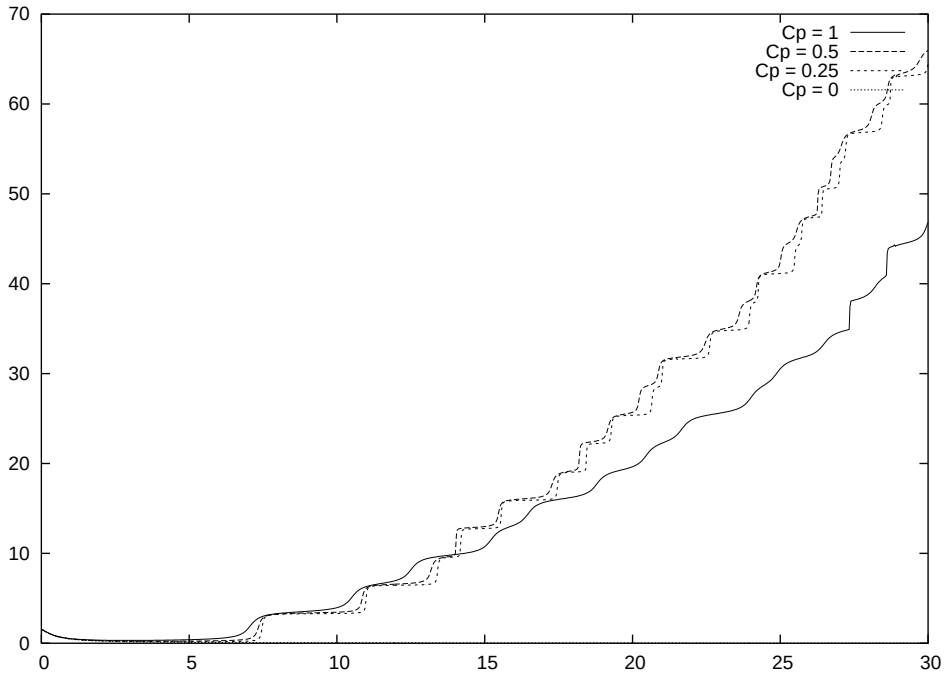

Figure 5.9: Variation of the phase shift (vertical axis) with momentum (horizontal axis), for differing values of C_p. The line for $C_p = 0$ is barely visible since in this case δ decays monotonically (see the text for an explanation).

described below or as in section 4.4, to follow the variation of S with increasing energy. In particular, the phase shift $\delta(k)$ is easily obtained and plots of this quantity against momentum for 4 values of C_p ($\mathcal{L} = 1$) are shown in figure 5.9. The line for $C_p = 0$ is barely visible since in this case $\delta = \frac{1}{2}\tan^{-1}\frac{k}{k^2-\frac{1}{4}}$ decays monotonically, as can be seen from the formula (4.2) for S at $C_p = 0$.

Though useful to get a qualitative idea of how these systems vary under perturbation, and though the rapid variation of δ at resonant momenta is clear, it is hard to extract quantitative information about the positions and widths of the resonances from these graphs. There are programs dedicated to exactly this task [BB86], but these fail for regions with strongly overlapping resonances. Though this is not the case for generic chaotic systems with only one scattering channel [FS97], here the special arithmetic cases cause the formation of arbitrarily narrow resonances in their vicinity. These narrow resonances are very hard to detect against a background of resonances with larger widths. In fact the line in

figure 5.9 for $C_p = 1$ is artificially lowered as k increases compared to that for the other values of C_p, due to the resonances having precisely zero width in that special case, thus not showing up under our crude investigation. It turns out, in these systems, to be more practical to use methods which allow calculation of the resonant positions and widths directly, instead of via the phase shift.

5.2.1 Finite elements and complex absorbing potentials

Because of the difficulties experienced when trying to extract the resonance parameters from phase shift data, as detailed in the previous section 5.2, we next considered methods commonly used in the literature which obtain that information directly. Particularly prevalent are methods involving complex rotation [Moi97] or complex absorbing potentials (CAPs) [SH00; RM93]. Both involve essentially the same idea: the major problem in applying standard techniques for finding eigenvalues of quantum Hamiltonians to the calculation of resonances is the non-L^2 nature of the resonant wavefunctions. That is they are not square-integrable on the relevant Hilbert space. By introducing the complex rotation or potential, the exponentially-growing resonant states are mapped to bound ones.

5.2.1.1 Complex rotation

The case of complex rotation, or complex scaling, is the more powerful of the methods and involves directly finding a transformation $\hat{S}$ which transforms the resonant states, ϕ_n^{res}, to square integrable ones. In our case $\phi_n^{\text{res}} = y^{1/2+\imath k^{\text{res}}}$ so that requires

$$\lim_{y\to\infty} \hat{S} y^{1/2+\imath k^{\text{res}}} = 0, \tag{5.33}$$

where k^{res} is the (complex) energy of the resonant state. These states obey a transformed Schrödinger equation with complex eigenvalue $\lambda^{\text{res}} = (k^{\text{res}})^2 + 1/4$;

$$(\hat{S}\hat{H}\hat{S}^{-1})\hat{S}\phi_n^{\text{res}} = \lambda^{\text{res}}\hat{S}\phi_n^{\text{res}}. \tag{5.34}$$

This new differential equation can then be solved, either exactly or by the usual numerical methods, for example the finite element techniques discussed later.

However, for our case of scattering in hyperbolic geometry the usual choices for the operator $\hat{S}$ do not have the desired effect. In one-dimensional Euclidean scattering, resonant states have the form $\mathrm{e}^{\imath k^{\mathrm{res}} y}$ and the operator

$$\hat{S} = \mathrm{e}^{\imath y \mathrm{e}^{\imath\theta} \frac{\partial}{\partial y}} \tag{5.35}$$

has the desired effect by substituting $y \to y\mathrm{e}^{\imath\theta}$ in ϕ_n^{res}. Due to the power-law dependence of the one-dimensional scattering in the Poincaré half-plane on y, such a replacement does not yield L^2 states and we have not pursued this line of enquiry. It is expected that such an approach would suffer the same difficulties as experienced for the CAP method, described below.

5.2.1.2 Complex Absorbing Potentials (CAPs)

In fact the CAP method is significantly simpler to implement than complex rotations, though for this ease of use a price must be paid. The resonance parameters are not found exactly but only in a certain limit - and one that is unattainable numerically. Still, useful information can be obtained and in fact decent agreement is obtained with the more detailed results we find in later sections.

The idea of the method is to add onto the Hamiltonian of the system an additional potential, with a scale factor η, and to take the limit of the solutions as $\eta \to 0$. This potential usually takes the form of a purely imaginary positive power law in the variable that the one-dimensional scattering is occurring in, which is only present after a certain cut-off in the variable, well away from the scattering centre of the system. That is

$$\hat{H}(r) \to \hat{H}(\eta, r) = \left\{ \begin{array}{ll} \hat{H}(r) + \imath\eta r^{\alpha} & r > p \\ \hat{H}(r) & r \leq p \end{array} \right\}, \tag{5.36}$$

for some $\{\eta, \alpha, p\} \in \mathbb{R}^+$. Riss and Meyer [RM93] have proved that for such a potential and indeed for a far larger class of complex potentials, the solutions form a discrete, bound set. Moreover, in the limit $\eta \to 0$, the logarithmic derivative of the solutions to the modified Schrödinger equation tends to that of the exponentially growing resonant scattering states of the unmodified version. Thus in the same limit, the resonance energies are recovered and in fact it was also

proved in the above that *all* the resonances have corresponding families of bound energies when the system is perturbed by η and so all resonances can be thus obtained. However, the continuous real spectrum of the unmodified Hamiltonian is also represented by the set of discrete solutions to the CAP-perturbed system. The limit of these states as η becomes small is not well-behaved as the discrete set must somehow revert to a continuum. These 'false resonances' must be isolated from the true ones, which is fortunately simple in practice since they lie (as proved in the above [RM93]) on a straight lines in the complex energy plane with an angle which varies with η.

The typical output of our numerical solution to Artin's billiard perturbed by such a CAP is shown in figure 5.10. This particular potential used the parameter values $\alpha = 4, p = 5$. The graph was obtained using a FEM method, as described in the next section 5.2.1.3, in an Artin's billiard cut off at $y = 10$. The set of states with linearly decreasing imaginary part and the straight lines branching off that are clearly identified as the discretised continuum. Actually, in this special case, the true resonances have linearly increasing imaginary parts too, since all have imaginary part $-\frac{1}{4}$ for the momentum according to the results of section 3.2.1. This is not the case in general, and the distinction is more clear.

The problem comes when trying to find solutions to the CAP-perturbed system numerically. If solutions are obtainable analytically, depending on the parameter η, then the limit as $\eta \to 0$ can be taken exactly. If however the solution to the problem is being approximated by a finite basis set, such as the earlier expansion method or the finite element routines used here, there is a fundamental limit on how small η can be taken. The very use of the CAP is in making the exponentially growing states map to bound ones when η is non-zero, but as it shrinks the perturbed states move closer to their free form, and in particular their decay to zero does not begin until values of the coordinates are reached which grow as η decreases. Thus any finite basis approximation to the resonance must fail in the limit $\eta \to 0$. Put another way: as the error due to a non-zero η shrinks, the error due to the incomplete expansion basis increases. Fortunately it is usually possible to find a saddle point in the parameter space where a reasonable compromise between these conflicting requirements is achieved.

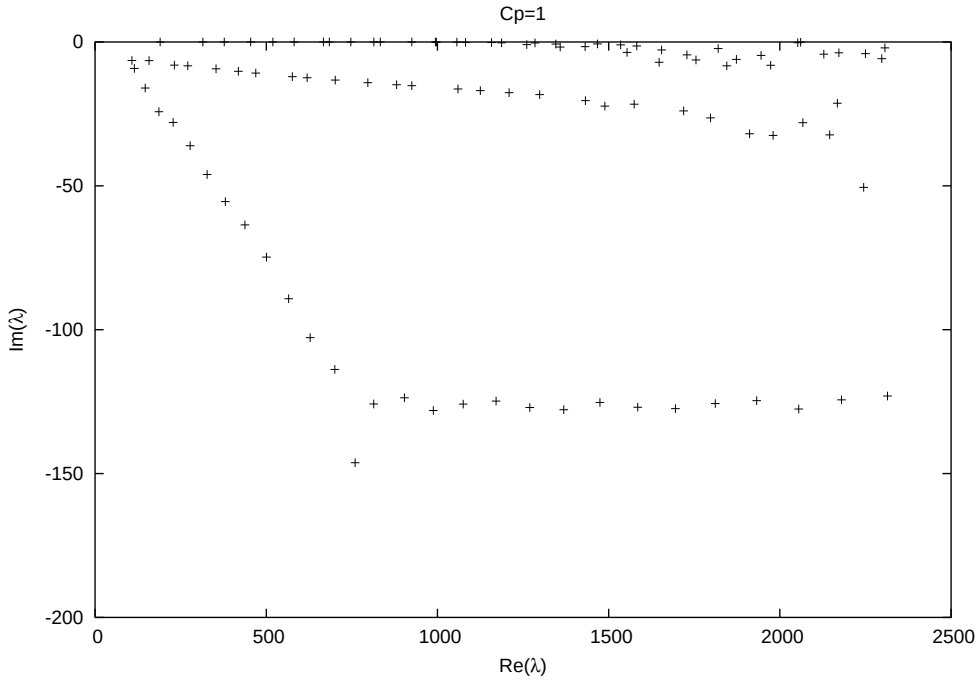

Figure 5.10: Typical distribution of solutions to a CAP-perturbed Artin's billiard. The horizontal and vertical axes show the real and imaginary parts of λ respectively.

5.2.1.3 Finite element method (FEM)

We use the finite element method because of the irregular shape of the lower boundary. This means it is not possible to find basis functions which satisfy particular boundary conditions on that wall. The FEM works by breaking the billiard down into many small polygonal elements, which taken together approximate the complete system.

The finite element approach to solving a partial differential equation in some domain starts by transforming the differential equation into an equivalent integral equation. This is then in a form suitable for discretisation, which here is done by triangulation of the domain then linear approximation of the wavefunction over each triangular element.

Because the bulk of numerical software available for tackling such a problem is designed for use in Euclidean space, we consider the equation

$$-\nabla^2\psi(x,y)+\imath\eta\frac{y^\alpha}{y^2}\psi(x,y)=\frac{\lambda}{y^2}\psi(x,y), \tag{5.37}$$

where α and η are suitable CAP parameters to be determined. Since the metric on the Poincaré half-plane is conformal, solutions ψ of this Euclidean partial differential equation with Neumann boundary conditions will also be the solutions we desire in hyperbolic geometry.

Premultiplying each side of (5.37) by a test function W, integrating over a Euclidean domain Ω (with boundary Γ) and using the usual Gauss's theorem we obtain the integral equation

$$\int_\Omega(\nabla W\cdot\nabla\psi(x,y)+\imath\eta W\frac{y^\alpha}{y^2}\psi(x,y))\mathrm{d}\Omega=\lambda\int_\Omega\frac{W\psi(x,y)}{y^2}\mathrm{d}\Omega, \tag{5.38}$$

where the boundary term obtained from use of Gauss's theorem is here identically zero due to the boundary conditions. Substituting a trial finite-basis solution for ψ,

$$\psi(x,y)\simeq\sum_{j=1}^{N}\psi_j\phi_j(x,y) \tag{5.39}$$

and replacing the test function W in (5.37) by each of the ϕ_i in turn, we obtain the linear system

$$\sum_{j=1}^{N} \psi_j \left(\int_\Omega (\nabla\phi_j(x,y) \cdot \nabla\phi_i(x,y) + \imath\eta\phi_j(x,y)\frac{y^\alpha}{y^2}\phi_i(x,y))\mathrm{d}\Omega \right) = \lambda \sum_{j=1}^{N} \psi_j \int_\Omega \frac{\phi_j(x,y)\phi_i(x,y)}{y^2}\mathrm{d}\Omega. \tag{5.40}$$

This is a generalised eigenvalue equation for λ :

$$\mathbf{A}\psi = \lambda\mathbf{B}\psi, \tag{5.41}$$

where

$$\psi = (\psi_1, \ldots, \psi_N)^T, \tag{5.42}$$

$$A_{ij} = \int_\Omega (\nabla\phi_j(x,y) \cdot \nabla\phi_i(x,y) + \imath\eta\phi_j(x,y)\frac{y^\alpha}{y^2}\phi_i(x,y))\mathrm{d}\Omega, \tag{5.43}$$

and

$$B_{ij} = \psi_j \int_\Omega \frac{\phi_j(x,y)\phi_i(x,y)}{y^2}\mathrm{d}\Omega. \tag{5.44}$$

Because (5.40) contains no higher than first derivatives of the basis functions, a particularly simple choice of basis can be made. The ϕ_i are defined piece-wise as interpolating linearly between different nodes of the triangulation of Ω. A node is a vertex of one or more triangles. A typical meshing is shown in figure 5.11 for $C_p = 0.7$. This meshing was performed by the software Elmer's Delaunay triangulation routine [LRP06].

If the N nodes of a mesh are labelled by their position vector $\mathbf{x}_j = (x_j, y_j)$ then the basis functions are defined by the condition

$$\phi_i(\mathbf{x}_j) = \delta_{ij} \tag{5.45}$$

where δ_{ij} is the Kronecker delta. The function $\psi(x,y)$ can thus be approximated as

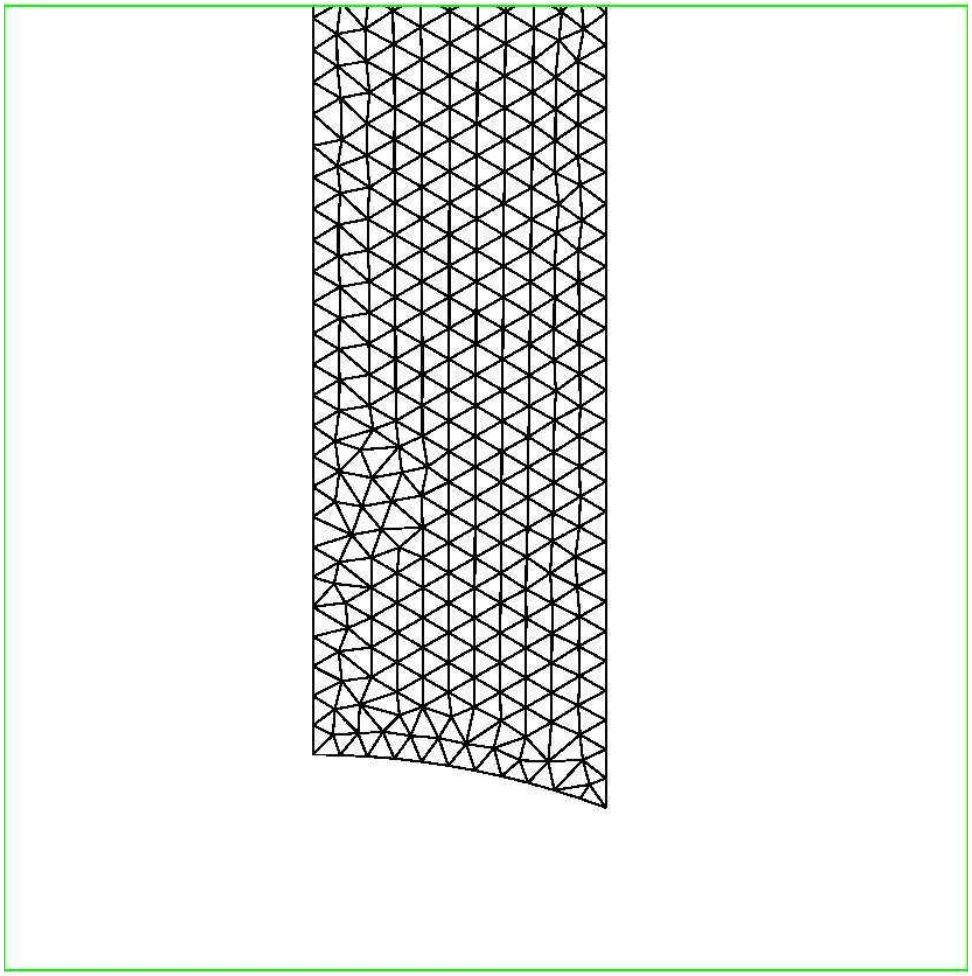

Figure 5.11: A triangulation of the lower part of Artin's billiard for $C_p = 0.7$.

$$\psi(x,y) \simeq \sum_{j=1}^{N} \psi(\mathbf{x}_j)\phi_j(x,y), \tag{5.46}$$

where $\psi(\mathbf{x}_j)$ is simply the value $\psi(\mathbf{x})$ takes at the node $\mathbf{x}_j$.

We chose coordinates (ρ,ξ) local to a particular element Ω_k, which includes nodes $\{\mathbf{x}_a,\mathbf{x}_b,\mathbf{x}_c\} = \{\mathbf{x}_i^k, i \in \{1,2,3\}\}$, such that the vertices of that element are the points $(0,0),(1,0)$ and $(0,1)$. Then the non-zero basis functions in this element will have the form

$$\begin{cases} N_1^k(\rho,\xi) &= 1-\rho-\xi \\ N_2^k(\rho,\xi) &= \rho \\ N_3^k(\rho,\xi) &= \xi, \end{cases} \tag{5.47}$$

where $N_1^k(\rho,\xi) = \phi_a(x,y)$ and so on. The coordinate transformation can also be expressed in terms of these basis functions, so that

$$\mathbf{x}^k(\rho,\xi) = \sum_{i=1}^{3} \mathbf{x}_i^k N_i^k(\rho,\xi). \tag{5.48}$$

Now the integrals in (5.40) can be performed over each element Ω_k in turn. For an arbitrary function $f(\mathbf{x})$,

$$\int_{\Omega_k} f(\mathbf{x})\mathrm{d}\Omega \simeq \sum_{i=1}^{3} f(\mathbf{x}_i^k) \int_{\Omega_k} N_i^k(\rho,\xi)\det(J)\mathrm{d}\rho\mathrm{d}\xi \tag{5.49}$$

with J being the Jacobian of the transformation from local coordinates (ρ,ξ) to global coordinates (x,y), that is

$$J = \begin{pmatrix} \frac{\partial x}{\partial \rho} & \frac{\partial y}{\partial \rho} \\ \frac{\partial x}{\partial \xi} & \frac{\partial y}{\partial \xi} \end{pmatrix}. \tag{5.50}$$

Since each basis function is identically zero in a large region of Ω, the matrices A and B are sparse and much of the calculation is trivial. Keeping track of the calculation is ably handled by software such as Elmer [LRP06] which we found particularly useful for dealing with CAP problems, since it allows all parameters to be complex. In section 4.4 we used the package FreeFem [PHH06], which was fast and effective to use for solving the closed billiard considered there, but wasn't flexible enough to deal with the complex potentials of this section. Further details

on the implementation of the finite element technique for instance about meshing or use of elements of a higher order than the simple linear triangles used here, can be found in the references [Bou01; RM02].

A typical output from Elmer was shown earlier (figure 5.10) and selected results are presented below (in table 5.1). Due to the infinite extent of the billiard systems we consider here, finite element methods turn out to be limited in their usefulness. As explained earlier, the CAP method requires finding solutions of the modified Schrödinger equation (5.36) in the limit $\eta \to 0$, and this produces eigenfunctions which are not L^2. To get good approximations to the resonant energies, wavefunctions that extend far in the y-coordinate must be used and it becomes impractical to mesh such long thin billiard shapes. It is possible that finite element methods could be used for the chaotic regions near the lower boundary of our billiard systems, and the solutions coupled somehow to otherwise derived solutions in the integrable large-y region, but such a technique has proved elusive so far.

One nice feature of the results from our finite element calculations is that the eigenfunctions (the resonant wavefunctions) are output directly with no extra effort required. Some of the low-lying states are displayed below (figure 5.12). Otherwise, the finite element and CAP methods have been mostly useful for solving closed billiards (used in the numerical approximation to the calculation of S in section 4.4 and for checking the reasonableness of our other results in the low-momentum regime).

5.2.2 Expansion method

To obtain large numbers of resonances, which are necessary for performing statistical analysis of the spectra, we finally struck on a method which has proved useful over a wide momentum and deformation parameter range. In essence it involves an expansion of the resonant wavefunction in the basis functions introduced at the start of this chapter (equations (5.29) and (5.31)) and then searching for the momenta at which the required boundary conditions are satisfied. What makes this tricky is that rather than finding a real parameter such as the phase shift tracked in section 5.2, or having to solve a complex eigenvalue equation

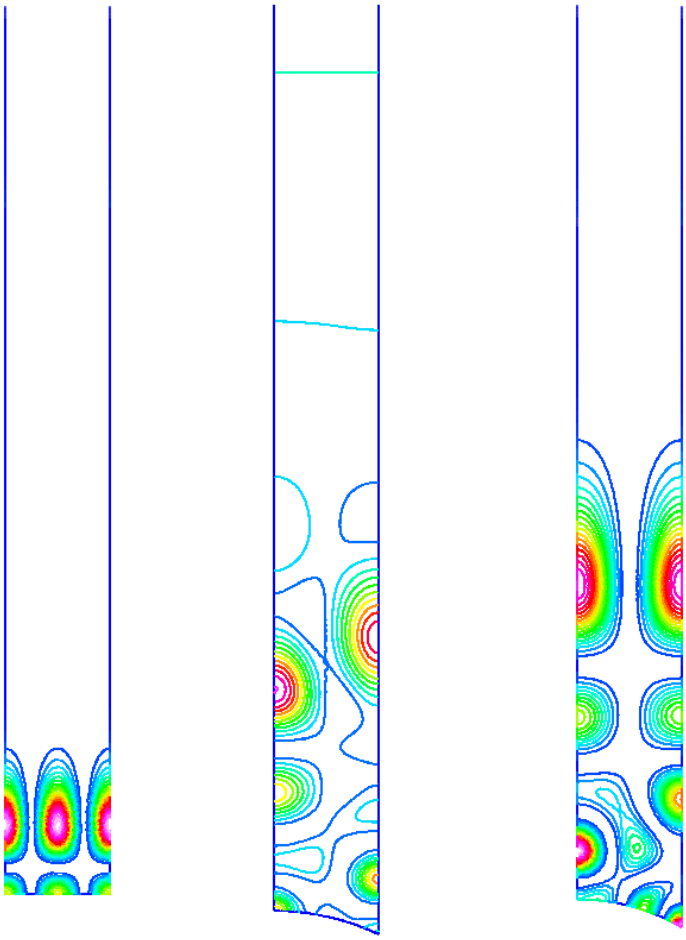

Figure 5.12: Left: Absolute value of the bound state ($C_p = 0$) at $k = 18.63$. Centre: Absolute value of the resonant wavefunction at $k = 15.32$. ($C_p = 0.85$). Right: Absolute value of the Cusp form at $k = 17.74$. ($C_p = 1$).

as in the finite element method, this requires a perilous and computationally expensive search in the complex plane for the complex zeros of a determinant defined in equation (5.53). Despite these challenges, the method has proved to be more efficient and scalable than the more direct methods of the previous sections. This section and the following sections on statistical properties of the resonances for Artin's billiard deformed by the parameter C_p, which were obtained using the method described here, are an expansion of results first published in [HMFOU05].

When considering an expansion of a resonant wavefunction into a basis set of the form (5.32), in order to directly calculate the resonance energies one must enforce the outgoing wave boundary condition at infinity (see section 2.3.2). That is, we require $\lim_{y\to\infty} \psi(k;x,y) = y^{1/2+\imath k}$. To do this we replace the continuum wavefunction by $\psi_0(k;x,y) = y^{1/2+\imath k}$ instead of the form given in (5.31). The full wavefunction is thus expanded in the form

$$\Psi_N(k;x,y) = \sum_{m=0}^{N-1} A_m \psi_m(k;x,y), \tag{5.51}$$

where the $\psi_m(k;x,y)$ were defined in equations (5.29) and above for $m = 0$.

This wavefunction by construction represents a resonance state and obeys the Neumann boundary condition at $x = 0$ and $x = \mathcal{L}/2$. To determine the coefficients A_m and the complex resonance eigenenergies or eigenmomenta k, one must enforce the Neumann boundary condition on the lower boundary in figure 4.1. Here this is done by using a modified collocation method, following the example of Csordás et. al. [GHSV91].

One calculates the normal derivative of (5.51) on the lower boundary and Fourier expands it into a set of N orthogonal functions $\sin(\frac{n\pi s}{L})$. As discussed in, e.g. [Sch80a; ADG+99], this modification of the method has several advantages. The original collocation method solves the equation $\frac{\partial \Psi_N}{\partial \hat{n}} = 0$ at M points on the lower boundary, giving a linear set of equations for the coefficients A_m. However the determinant of coefficients generated is in general poorly behaved and it is impossible to independently vary the number of points on the lower boundary M and the number of partial waves N. By instead taking a Fourier decomposition along the boundary of the normal derivative of the sum (5.51), and setting the first M Fourier coefficients to zero, a far more stable determinant is obtained, with

a near-diagonal form for a well-chosen expansion basis. Additionally, the number of points along the boundary used to evaluate the integrals for the coefficients is an independent parameter. Thus the shape can be well accounted for, even when only a small number of terms are used in the expansion (5.51).

The first N Fourier coefficients of this expansion D_n are given by

$$D_n = \sum_{m=0}^{N-1} C_{nm} A_m \tag{5.52}$$

where

$$C_{nm} = \oint \mathrm{d}s \sin(\frac{n\pi s}{L}) \frac{\partial \psi_m}{\partial \hat{n}}(k;s), \quad n = 1 \ldots N. \tag{5.53}$$

s is a parameterisation of the lower billiard boundary and L its length in that parameterisation. Here the simple relation

$$s = x \tag{5.54}$$

is taken on the lower boundary when $C_p \neq 1$. The integral (5.53) along the boundary will be evaluated numerically with evenly spaced steps in this parameter, so it is in fact more useful to choose a parameterisation which will increase this density in regions where the wavefunction varies more rapidly. For $C_p = 1$, this is easily accomplished by using the geodesic distance (2.20) along the curve instead of the x-coordinate. As y decreases, the density thus increases and this is particularly noticeable for larger values of $\mathcal{L}$, when the corner with angle $\arccos(\mathcal{L}/2)$ dips steeply down in y for growing $\mathcal{L}$. In (5.53), s ranges from 0 to $\mathcal{L}/2$ with the simple parameterisation (5.54) and from 0 to

$$s_{\max} = 2\tanh^{-1}\left(\sqrt{\frac{(\mathcal{L}/2)^2 + (1-\sqrt{1-(\mathcal{L}/2)^2})^2}{(\mathcal{L}/2)^2 + (1+\sqrt{1-(\mathcal{L}/2)^2})^2}}\right) \tag{5.55}$$

when the geodesic distance is used.

The normal derivative along the boundary parameterised by C_p is obtained in the following manner. It is defined as the scalar product of the vector gradient and the unit normal to the curve. The vector gradient of a function ϕ, $\underline{\nabla}\phi$ is given by $(y^2\frac{\partial\phi}{\partial x}, y^2\frac{\partial\phi}{\partial y}$ (so that $\underline{\nabla}\phi \cdot \underline{\mathrm{d}s} = \mathrm{d}\phi$). The tangent to the lower boundary (4.1) is

$$(1, \frac{\mathrm{d}y}{\mathrm{d}x}) = (1, \frac{-C_p x}{C_p y - (C_p - 1)}), \tag{5.56}$$

which leads to a normal $\underline{n} = (-\frac{\mathrm{d}y}{\mathrm{d}x}, 1)$ (Euclidean angles are preserved in the half-plane) with squared magnitude given by

$$|\underline{n}|^2 = \frac{(n^x)^2 + (n^y)^2}{y^2} = \frac{1}{y^2}\left(1 + \frac{C_p^2 x^2}{(C_p y - (C_p - 1))^2}\right) = \frac{1}{y^2(1 - C_p^2 x^2)}. \tag{5.57}$$

The final expression for the normal derivative is thus

$$\frac{\partial}{\partial \hat{n}}(\phi) = \underline{\nabla}\phi \cdot \underline{\hat{n}} = C_p y x \frac{\partial \phi}{\partial x} + y\sqrt{1 - C_p^2 x^2}\frac{\partial \phi}{\partial y}. \tag{5.58}$$

Applying this to the functions at hand, (5.29) gives the expression

$$\begin{aligned}\frac{\partial}{\partial \hat{n}}(\psi_m(k;s)) = \\ y^{3/2}\Bigg[\left(-2\pi m \frac{x}{\mathcal{L}} C_p \sin(2\pi m \frac{x}{\mathcal{L}}) + \frac{1}{2y}\sqrt{1 - C_p^2 x^2}\cos(2\pi m \frac{x}{\mathcal{L}})\right) K_{\imath k}(2\pi m \frac{y}{\mathcal{L}}) \\ - \frac{\pi m}{\mathcal{L}}\sqrt{1 - C_p^2 x^2}\cos(2\pi m \frac{x}{\mathcal{L}})\left(K_{1+\imath k}(2\pi m \frac{y}{\mathcal{L}}) + K_{-1+\imath k}(2\pi m \frac{y}{\mathcal{L}})\right)\Bigg],\end{aligned} \tag{5.59}$$

writing x and y here and in the following for $x(s)$ and $y(s)$. Using a recursion relation for the Bessel function ([AS65] 9.6.26)

$$K_{\imath k}(2\pi m \frac{y}{\mathcal{L}}) = \frac{\pi m y}{\imath k \mathcal{L}}\left(K_{1+\imath k}(2\pi m \frac{y}{\mathcal{L}}) - K_{-1+\imath k}(2\pi m \frac{y}{\mathcal{L}})\right), \tag{5.60}$$

this can be written in the form

$$\frac{\partial}{\partial \hat{n}}(\psi_m(k;s)) = \mathcal{K}(+) + \mathcal{K}(-), \tag{5.61}$$

where

$$\begin{aligned}\mathcal{K}(\pm) = \\ \frac{\pi m}{\mathcal{L}} y^{3/2} K_{\imath(k \pm \imath)}(2\pi m \frac{y}{\mathcal{L}})\Bigg[\sqrt{1 - C_p^2 x^2}\cos(2\pi m \frac{x}{\mathcal{L}})\left(\frac{\mp 1}{2\imath k} - 1\right) \\ \pm \frac{2\pi m C_p x y}{\imath k \mathcal{L}}\sin(2\pi m \frac{x}{\mathcal{L}})\Bigg].\end{aligned} \tag{5.62}$$

This form requires fewer evaluations of Bessel functions per matrix element, which is vital since this is the section of our code which takes most processor time.

The final ingredient in calculating the matrix elements (5.53) is the integral over s, for which an extended tenth-order quadrature formula is used (see appendix C for details).

The normal derivative is identically zero on the rest of the boundary by construction. The boundary condition on the lower boundary is now satisfied by setting the Fourier coefficients (5.52) equal to zero or equivalently by searching for the complex values k such that the determinant of the N by N complex matrix C_{nm} is zero. The summations are necessarily truncated at N, but N is chosen sufficiently large to achieve convergence of the eigenvalues. The higher the energy of the resonance the more values of n and m are required. A scaling with momentum of $N = \mathrm{int}(r_{\mathrm{scal}} + \alpha)$, where

$$r_{\mathrm{scal}} = \mathrm{Re}(k)\mathcal{L}/(2\pi\sqrt{1-(\mathcal{L}/2)^2}) \tag{5.63}$$

and int means taking the integer part of the expression, was found to yield zeros to the desired precision compared with the known cases $C_p = 0$ and $C_p = 1$. α is a small integer (good convergence was achieved for values of α between 2 and 6) which can be varied to help convergence for particular resonances. For higher values of N, the Bessel functions included become exponentially small and do not contribute significantly. This is due to the turning point in the differential equation (5.30) at $k = 2\pi my/\mathcal{L}$. Conservatively setting y to its lowest point in the billiard gives the scaling (5.63). In fact this is excessive and the parameter α can be lowered at large $\mathcal{L}$ to compensate.

In order to avoid overflowing the maximum computational precision available, each row of the matrix is scaled by its largest element, that is

$$C_{nm} \to C_{nm}/(\max_n(C_{nm})), \tag{5.64}$$

$\max_n$ indicating the maximum value of the operand when n takes all possible values. Then a singular-value decomposition is performed, using a standard LAPACK routine, to ease detection of the complex zeros of the determinant [Bac03; ABB+99]. This method produces results in agreement with those in

the literature [Ste94; HB82; Hej92b; Odl] for the known cases of $C_p = 1, \mathcal{L} \in \{1, \sqrt{2}, \sqrt{3}\}$ and with separately calculated values for $C_p = 0$, to the desired precision (6 figures).

In the integrable case ($C_p = 0$), the scattering has no resonances. All the eigenvalues are real and are given by the zeros of the derivatives at $y = 1$ of the functions (5.29) given above, that is they are determined by the condition

$$[\frac{\partial}{\partial y}(\sqrt{y}K_{ik}(2\pi m y))]_{y=1} = 0. \tag{5.65}$$

These corresponding eigenvalues, k_n, were calculated using Mathematica's [Wol05] FindRoot function. As shown in section 5.3.1, they can be well approximated for large k by standard semiclassical techniques. A comparison of eigenvalues obtained from the exact condition (5.65) and semiclassical methods is presented in table 5.3.1.

In order to calculate the widths and positions of the resonances at new values of the deformation parameters, first many eigenvalues for the integrable problem ($C_p = 0$) are calculated as described above. Using these values as seeds for the calculation, the parameter C_p or $\mathcal{L}$ can be varied a little, and a search in the complex plane for zeros of the least singular value of the matrix $\mathbf{C}$ near to the old values is performed. Then the parameters can be varied again, by larger amounts at each step, as information about the velocity of each resonance with each parameter allows better guesses as to the perturbed value.

Initially the search was performed by a simple taxicab routine, evaluating the function at the four points a small distance h from the seed in the positive and negative real and imaginary directions, and proceeding in the direction of the smallest value. With good estimates of the locations of the resonances, this proved reasonably reliable since the least singular value is fairly well behaved for the scaled matrix $\mathbf{C}$. However, it is hardly optimal in terms of function calls and a good improvement in speed was obtained by using instead two golden section searches [PTVF92] to bracket the minima with respect to the real and imaginary parts. Then the zero can be approximated by parabolic extrapolation and the minimum checked against the desired precision. If it has not yet been reached, the procedure repeats with the current minimum as seed and the starting step size decreased by a factor of 2.

Once the first values have been found at a value of C_p (or $\mathfrak{L}$ for the second deformation considered) close to the known case, the position of the zero at another, nearby value of the perturbation parameter is predicted again by parabolic extrapolation (linear if only two points are available). In general, with the position of a particular zero α_i a function of the parameter q, if we know its value at three points, $q_j, j \in 1, 2, 3$, then the quadratic form taking value $\alpha_i(q_j)$ at those points is given by

$$f(q) = aq^2 + bq + c \tag{5.66}$$

with

$$\begin{aligned} a &= \frac{\alpha_i(q_1)(q_2 - q_3) + \alpha_i(q_2)(q_3 - q_1) + \alpha_i(q_3)(q_1 - q_2)}{(q_1 - q_2)(q_1 - q_3)(q_2 - q_3)} \\ b &= \frac{\alpha_i(q_1)(q_3^2 - q_2^2) + \alpha_i(q_2)(q_1^2 - q_3^2) + \alpha_i(q_3)(q_2^2 - q_1^2)}{(q_1 - q_2)(q_1 - q_3)(q_2 - q_3)} \\ c &= \frac{\alpha_i(q_1)q_2q_3(q_2 - q_3) + \alpha_i(q_2)q_1q_3(q_3 - q_1) + \alpha_i(q_3)q_1q_2(q_1 - q_2)}{(q_1 - q_2)(q_1 - q_3)(q_2 - q_3)}. \end{aligned} \tag{5.67}$$

At first equally spaced steps in the perturbation parameter are taken, but if the zeros are being predicted well this is increased. If, on the other hand, a zero is found to be poorly predicted by (5.67), the step size can be temporarily decreased until the variation becomes more stable again. For equally spaced steps q_j, the next guess provided by (5.66) is given by the simple formula

$$\alpha_i(q_{j+3}) = \alpha_i(q_j) + 3(\alpha_i(q_{j+2}) - \alpha_i(q_{j+1})). \tag{5.68}$$

The most time consuming part of the routine, aside from the iterations required to reach any desired value of the perturbation parameter, is the setting up of the matrix (5.53) due to the many calculations of the Bessel functions (here involving complex values of k) required for each element. Powerful expansions similar to those in [GHSV91] are used taken mostly from [AS65] but largely based on routines used in [The05]. Details are given in appendix D.

The second case where there are results available [Ste94; HB82; Odl] to check against those obtained here is for Artin's billiard ($C_p = 1, \mathfrak{L} = 1$). The S-matrix, derived in section 3.2.2, is

$$S(k) = \frac{\pi^{-\imath k}\Gamma(\frac{1}{2} + \imath k)\zeta(1 + 2\imath k)}{\pi^{\imath k}\Gamma(\frac{1}{2} - \imath k)\zeta(1 - 2\imath k)}, \tag{5.69}$$

where $\Gamma(z)$ is Euler's gamma function and $\zeta(z)$ is Riemann's zeta function [Gut90; WJ89]. The resonances (poles of S) are given by the zeros of the denominator, which occur at $k = k_n/2 - \imath/4$, according to the Riemann Hypothesis, where the k_n are the Riemann zeros. The 'trivial' zeros are handily cancelled by the gamma functions. The k_n are well known [Odl89] to possess GUE level-spacing statistics. However, superimposed on this continuum are an infinite set of bound states (zero width) with Poissonian statistics due to arithmetic chaos [BSS92]. The numerical results presented here give both the resonances on the critical line and the cusp forms in one calculation. A similar situation occurs for the other arithmetic systems considered, at $\mathcal{L} = \sqrt{2}$ and $\mathcal{L} = \sqrt{3}$ [Hej92b], where three sets of resonances are found, categorised by their (fixed) widths.

Table 5.1 gives some of our results for the resonance spectra of the billiard systems parameterised by C_p and $\mathcal{L}$. The title 'exact' for the first column is somewhat inappropriate, since the values there are in fact numerical results calculated by other groups [HB82; Hej92a; Odl], accurate to at least five decimal places. In our calculations using the expansion method we worked to the fourth decimal place and one can see that good agreement is obtained at this level. The CAP method is not so accurate, but the results are supportive of at least the existence of solutions in that vicinity and are still good to a couple of significant figures. One might suggest using 'quick and dirty' CAP results to seed searches in the complex plane for resonances using the more accurate expansion method, since there is currently no other way to get results far away from known values using that method.

In the following sections, these results are presented, starting from the integrable case and initially deforming the lower boundary until Artin's billiard is reached, at which point we introduce the deformation of shifting the right-hand wall.

n,$\mathcal{L}$,C_p	Exact	CAP & finite element	Expansion method
2,1,0.1	n/a	11.0923 -0.00174236$\imath$	11.081125 -0.001625$\imath$
4,1,0.1	n/a	14.3147 -0.00057130$\imath$	14.302750 -0.000563$\imath$
10,1,0.1	n/a	21.0836 -0.00302566$\imath$	21.076750 -0.003001$\imath$
2,1,0.8	n/a	10.7259 -0.179477$\imath$	10.699250 -0.140070$\imath$
4,1,0.8	n/a	13.8847 -0.00219748$\imath$	13.874625 -0.001996$\imath$
10,1,0.8	n/a	20.6639 -0.166035$\imath$	20.658000 -0.168629$\imath$
2,1,1.0	10.511020 -0.25$\imath$	10.3803 - 0.310032$\imath$	10.511125 -0.250008$\imath$
4,1,1.0	13.779751 -0$\imath$	13.7874 - $3.3701 \times 10^{-9}\imath$	13.779625 0.000005$\imath$
10,1,1.0	20.459360 -0.25$\imath$	20.4666 - 0.249285$\imath$	20.459875 -0.250315$\imath$
50,1,1.0	40.688666 -0$\imath$	n/a	40.688500 -0.000000$\imath$
200,1,1.0	76.512345 -0.25$\imath$	n/a	76.512346 -0.250000$\imath$
1,$\sqrt{2}$,1.0	4.532360 -0.5$\imath$	n/a	4.532432 -0.499993$\imath$
4,$\sqrt{2}$,1.0	10.511020 -0.25$\imath$	n/a	10.511002 -0.249965$\imath$
10,$\sqrt{2}$,1.0	15.212438 -0.25$\imath$	n/a	15.212431 -0.250022$\imath$
25,$\sqrt{2}$,1.0	24.112353 -0$\imath$	n/a	24.112326 0.000040$\imath$
1,$\sqrt{3}$,1.0	2.859601 -0.5$\imath$	n/a	2.859602 -0.500005$\imath$
4,$\sqrt{3}$,1.0	8.038861 -0$\imath$	n/a	8.038862 0.000000$\imath$
10,$\sqrt{3}$,1.0	12.505428 -0.25$\imath$	n/a	12.505423 -0.249999$\imath$
25,$\sqrt{3}$,1.0	19.896104 -0$\imath$	n/a	19.896104 -0.000000$\imath$

Table 5.1: Comparison of methods for finding resonances of the billiard systems.

5.3 Deformation of the lower boundary

First we consider the behaviour of the resonances under the perturbation varying the lower boundary, parameterised by C_p. As detailed in section 5.1, as this parameter increases from 0 to 1 and beyond, the classical dynamics becomes progressively more chaotic until at $C_p = 1$ the system is hyperbolic and there are no longer any stable periodic orbits. Here we find both generic and non-generic behaviour for the resonance positions and widths in this range, including the remarkable reordering of the spectrum into two subspectra at $C_p = 1$.

5.3.1 Semiclassical spectrum for the integrable billiard

The seeds of our calculations are the eigenvalues determined for the system at $C_p = 0$. This corresponds to an integrable billiard with an exact quantization condition given by (5.65), solutions of which were found using Mathematica [Wol05]. A comparison of the exact and semiclassical eigenmomenta is given in table 5.3.1.

We start with an ansatz for the semiclassical wavefunction of

$$\psi_{\mathrm{sc}}(x, y, \lambda) = A(x, y, \lambda) \exp(\imath S(x, y, \lambda)). \tag{5.70}$$

We understand that the semiclassical limit corresponds to the limit $\lambda \to \infty$, since $\lambda \propto \frac{E}{\hbar^2}$. We know from earlier, e.g. equation (5.29), that we can separate out the x-dependence exactly with a sinusoidal behaviour. Thus our semiclassical approximation is only made on the y-dependence of the wavefunction (5.70). Preemptively we write $A(y)$ as $\sqrt{y}\exp(T(y))$, so (5.70) takes the form

$$\psi_{\mathrm{sc}}(x, y, \lambda) = \sqrt{y}\cos(2\pi m x) \exp(\imath S(y, \lambda) + T(y)). \tag{5.71}$$

m is the exact x-momentum quantum number. We substitute (5.71) into the equation (5.30), taking $\mathcal{L} = 1$ here. This leads, for the y-dependence, to the two equations

$$S'^2 - T'' - T'^2 - T'/y = \frac{\lambda - \frac{1}{4}}{y^2} - 4\pi^2 m^2 \tag{5.72}$$

and

$$S'/y + S'' + 2S'T' = 0, \tag{5.73}$$

for the real and imaginary parts respectively. Here primes denote the derivative with respect to y. Assuming the variation in T is much smaller than that in S, an approximation which is good in the semiclassical regime where wavefunctions are highly oscillatory, the first equation is just an expression of the Hamiltonian (2.31), identifying S' as the classical momentum in the y-direction, as expected [BB97]. Explicitly

$$\left(\frac{\mathrm{d}S}{\mathrm{d}y}\right)^2 = \frac{\lambda - \frac{1}{4}}{y^2} - 4\pi^2 m^2. \tag{5.74}$$

Solving this gives

$$S(y) = \pm k(\sqrt{1-u^2} + \ln(u) - \ln(1+\sqrt{1-u^2})), \tag{5.75}$$

with

$$u(y) = 2m\pi y/k \tag{5.76}$$

as a scaled y-variable and $k = \sqrt{\lambda - \frac{1}{4}}$ as before. Using this approximate solution in the second of the above equations yields for T

$$2T' = -\frac{1}{y} + \frac{1}{y}\left(\frac{1}{1-u^2}\right), \tag{5.77}$$

so that

$$T(y) = \frac{1}{2}\left(-\ln(y) + \ln(u) - \frac{1}{2}\ln(1-u^2)\right) \tag{5.78}$$

and thus a semiclassical wavefunction

$$\begin{aligned}\psi_{\mathrm{sc}}(x,u,k) &= \frac{\sqrt{u}}{(1-u^2)^{1/4}}\cos(2\pi m x) \\ &\quad \times \exp(\pm \imath k(\sqrt{1-u^2} + \ln(u) - \ln(1+\sqrt{1-u^2}))).\end{aligned} \tag{5.79}$$

That the phase varies much more quickly than the amplitude for large energies is now clear, as required.

This solution is singular at the classical turning point, $u = 1$. Linearising the Schrödinger equation in the vicinity of this point leads to Airy's differential equation and the semiclassical wavefunction obtained above can be matched to this known function either side of the pathological region [BB97]. Putting $q = y - \frac{k}{2\pi m}$ gives for small q

$$\frac{\partial^2 \psi_{\mathrm{sc}}}{\partial q^2} = q \frac{16\pi^3 m^3}{\sqrt{\lambda}} \psi_{\mathrm{sc}}. \tag{5.80}$$

In this region, for negative q, the WKB wavefunction (5.70) has q-dependence

$$\frac{1}{q^{1/4}} \exp(\pm \imath \frac{2}{3} q^{3/2} \pi^{3/2} n^{3/2} \frac{4}{\lambda^{1/4}}), \tag{5.81}$$

which must be compared to the explicit expression for the Airy function in the oscillatory region. This has asymptotic behaviour for negative q

$$\mathrm{Ai}(\alpha q) = \frac{1}{(\alpha q)^{1/4}} \sin(\frac{2}{3}(\alpha q)^{3/2} + \frac{\pi}{4}), \tag{5.82}$$

with $\alpha^3 = \frac{16\pi^3 m^3}{\sqrt{\lambda}}$. The semiclassical WKB wavefunction matches this if the positive and negative exponent solutions are combined with coefficients $\pm \frac{\alpha^{-1/4}}{2\imath} \exp(\pm \imath \frac{\pi}{4})$. Thus by a consideration of the behaviour in the vicinity of the classical turning point it is seen that the wave acquires an additional phase of $\pi/4$. The origin of this phase was discussed in the beginning of section 3.1, the number of turning points or 'caustics' on a trajectory being labelled by the Maslov index. As mentioned in the previous discussion, the type of boundary condition specified on a wall also can generate a phase difference, but for the Neumann boundary condition chosen here this is precisely zero. The final form is

$$\begin{aligned} \psi_{\mathrm{sc}}(x, u, k) &= \cos(2\pi m x) \\ &\times \left(\frac{\sqrt{u}}{(1-u^2)^{1/4}} \sin(-k(\sqrt{1-u^2} + \ln(u) - \ln(1+\sqrt{1-u^2})) + \frac{\pi}{4}) \right), \\ &|u-1| \gg 1. \end{aligned} \tag{5.83}$$

In order to satisfy the Neumann boundary condition on the lower boundary, a superposition of these solutions must in general be taken. In the simple, integrable

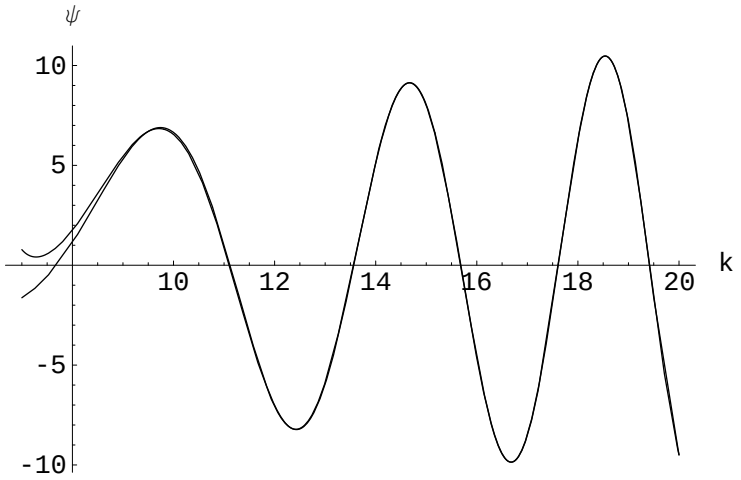

Figure 5.13: Comparison of exact (lower curve) and semiclassical solutions to the Schrödinger equation for the integrable billiard.

case with $C_p = 0$ however, the sinusoidal WKB waves have many zeros and zeros of the derivative on the line $y = 1$. This generates families of solutions with differing values of n. It is the superposition of these independent families that results in the Poissonian level-spacing statistics expected for generic integrable systems as described in section 5.3.2. Figure 5.13 shows the k-dependence of the derivative of ψ_{sc} for $7 < k < 20$ at $y = 1$ with $n = 1$, as well as the same for $\sqrt{y}K_{ik}(2\pi ny)$, the exact solution. Convergence is quickly achieved, provided the correct scaling $\sqrt{n}\exp(k\pi/2)$ is observed for the Bessel function. All but the first eigenvalue in any one subspectrum are reproduced remarkably closely.

From (5.79) and the following discussion we thus obtain a semiclassical quantization condition for the system with quantum numbers (l, n)

$$\frac{\mathrm{d}}{\mathrm{d}u}\left(\frac{\sqrt{u}}{(1-u^2)^{1/4}}\sin(-k(\sqrt{1-u^2}+\ln(u)-\ln(1+\sqrt{1-u^2}))+\frac{\pi}{4})\right)=0. \quad (5.84)$$

Which for very large k (ignoring the variation in the amplitude) on the line $y = 1$ gives simply the condition

n,l	exact	semiclassical a	semiclassical b
1,0	7.684571120	7.281845528	7.930736456
1,1	11.12375546	11.10598303	11.17419661
1,2	13.56605571	13.55759406	13.59527903
1,10	27.34383367	27.34217290	27.35139655
1,100	119.3755852	119.3753916	119.3765481
2,0	14.37489766	13.82251536	14.63578083
2,1	18.62765652	18.60678663	18.67738758
2,10	38.41997052	38.41829594	38.42694541
5,10	65.70610273	65.70426372	65.71247254

Table 5.2: Comparison of methods for finding eigenvalues of the integrable billiard. (a) and (b) are two semiclassical quantization conditions described in the text.

$$-(2n\pi)\sqrt{\left(\frac{k}{2n\pi}\right)^2-1}+k(\ln\left(\frac{k}{(2n\pi)}+\sqrt{\left(\frac{k}{2n\pi}\right)^2-1}\right)\simeq l\pi+\frac{\pi}{4},\ l,n\in\mathbb{Z}. \tag{5.85}$$

Table 5.3.1 compares the exact eigenvalues with the semiclassical approximations in a: (5.84) and b: (5.85). Other than the first eigenvalue in any subspectrum, agreement is good at both levels of approximation.

5.3.2 Random Matrix Theory

Having seeded our search for resonances with the eigenvalues of the integral billiard at $C_p = 0$, we proceed to obtain sets of resonances at several values of increasing C_p. Since we are interested in questions of quantum chaos, we will analyse the spectra in terms of the predictions of Random Matrix Theory (RMT), which is perhaps the most widely successful tool for investigating quantum systems with chaotic classical limits. It is the dramatic failure of Artin's billiard to comply with the RMT predictions that initially attracted the author to the area of quantum billiards in hyperbolic geometry. Here we introduce the predictions

for generic systems that RMT makes for the bulk properties of the spectra that we look at in the following sections.

Since the derivation of Gutzwiller's trace formula (3.36), which showed in particular how to semiclassically treat systems that are classically chaotic, a lot of work has been done theoretically and experimentally to study how traces of chaos manifest themselves in quantum systems. Classical measures of chaos such as Lyapunov exponents or ergodicity are trajectory based concepts yet in the quantum world trajectories simply don't exist.

Analogues of some of these properties have been suggested but particularly successful has been a conjecture of Bohigas, Giannoni and Schmit (BGS) [BGS84] stating that the spectra of systems with chaotic classical limits should have certain statistical properties. To be precise they conjectured that the eigenvalues of such systems should behave as though they had been randomly picked eigenvalues from an ensemble of random matrices with certain symmetry properties corresponding to the problem at hand. The ensembles are known as the Gaussian unitary (GUE), orthogonal (GOE) and symplectic (GSE) ensembles for the cases of systems without time reversal symmetry, with time reversal symmetry but no spin interactions, and those with time reversal symmetry and half-integer spins respectively. Parallel to this hypothesis is a similar statement concerning generic integrable systems derivable from semiclassical considerations and exposed by Berry [BT77]. These are conjectured to hold to a Poisson distribution.

Each of the symmetry classes generates certain constraints on the possible elements of a (large) matrix supposed to represent that system's Hamiltonian. From the derived distributions of elements, eigenvalue distributions and correlation functions can be obtained, much progress in this direction being made after introduction of the supersymmetry technique for evaluating the complex integrals involved. Great success has been found in application of these results to a vast range of physical systems [FS97; Stö99] ranging from the acoustics of concert halls, to fluctuations in the cosmic microwave background, to resonances in nuclear particles and microwave cavities and even to the statistical distribution of zeros of the Riemann zeta function [BK99]. The applicability of the ideas has proved far broader than the initial conjecturers could have expected.

A simple, yet seemingly effective, statistic for determining which class a system under investigation comes from is the nearest-neighbour distribution of eigenvalues. These are particularly simple to calculate for a give spectrum and yield significantly different short-range behaviour so making the differences easily distinguishable. The so-called Wigner surmise for each class is presented below. These are results for the distribution of eigenvalues in two-by-two matrices only, yet the functional forms differ from those for the full ensembles never by more than two percent and mostly far less.

$$p(s) = \frac{\pi}{2} s \exp^{-\pi s^2/4}, \tag{5.86}$$

is the Wigner surmise for the GOE (Gaussian Orthogonal Ensemble),

$$p(s) = \frac{32}{\pi^2} s^2 \exp^{-\frac{4}{\pi} s^2} \tag{5.87}$$

for the GUE (Gaussian Unitary Ensemble) and

$$p(s) = \frac{2^{18}}{3^6 \pi^3} s^4 \exp^{-\frac{64}{9\pi} s^2} \tag{5.88}$$

for the GSE (Gaussian Symplectic Ensemble).

$$p(s) = \exp^{-s} \tag{5.89}$$

is the Poisson distribution for comparison.

In random matrix models of quantum scattering, two limiting regimes can be considered, that in which the system is only 'weakly' open and resonances do not overlap much (their widths are small compared to their spacing on the real axis) and that in which there is strong coupling of the system to the continuum, where resonances may be broad and generally overlap.

The systems considered here are relatively simple in that there is only one channel open for scattering (only one state which corresponds to a particle escaping to infinity). In general, in the case of weak coupling to continua, first order perturbation theory is adequate to calculate the resonance widths in terms of eigenfunctions of a suitable closed system (this can be done here by closing the billiard at some sufficiently high value of y). In this case, RMT predicts that the

width distribution for a chaotic system with M weakly open channels is given by the χ^2 distribution [FS97],

$$\rho(w_n) = \frac{(\nu/2)^{(\nu/2)}}{\Gamma(\nu/2)} w_n^{(\nu/2-1)} \exp\left(-\frac{\nu}{2} w_n\right) \tag{5.90}$$

where w_n is the resonance width normalized to its mean value, the parameter $\nu = M$ or $\nu = 2M$ for systems with time-reversal invariance or broken time-reversal invariance respectively, and $\Gamma(x)$ is Euler's gamma function again. For the systems considered here, $\nu = 1$ and the corresponding distribution is known as the Porter-Thomas distribution, first derived in [PT56] where it provided a good fit to neutron-nuclei resonances.

Returning to the suggestion that the application of RMT in hyperbolic geometry was problematic, it was found for the billiard systems first studied [Sch80a] that the BGS conjecture did not hold. Specifically systems which display the strongest forms of classical chaos were found to possess Poissonian level-spacing statistics. This was a cause of great concern, since as mentioned earlier, the vast wealth of analysis by mathematicians on the half-plane meant that the classical mechanics of these systems was very well understood and pointed to them as being paradigms of at least classical chaos. However it was quickly realised that this unexpected result only held for one particular class of billiard system, though it took far longer to isolate exactly what property was unique to that class. The majority of problems investigated in hyperbolic geometry have proved to be fine examples of expected quantum behaviour. However, the existence of certain special cases is of particular interest and one hopes to gain insight into the precise nature of quantum manifestations of classical chaos by studying the way in which our general predictions break down.

5.3.3 The widths

The width of a resonance is taken here to be the absolute value of its imaginary part. In atomic physics, resonances correspond to meta-stable states of a compound system, and the lifetime of a state is directly related to its width (see section 2.3.2 for a brief introduction). Here the widths of the eigenmomenta, not eigenenergies are studied, since the interesting behaviour is more apparent in

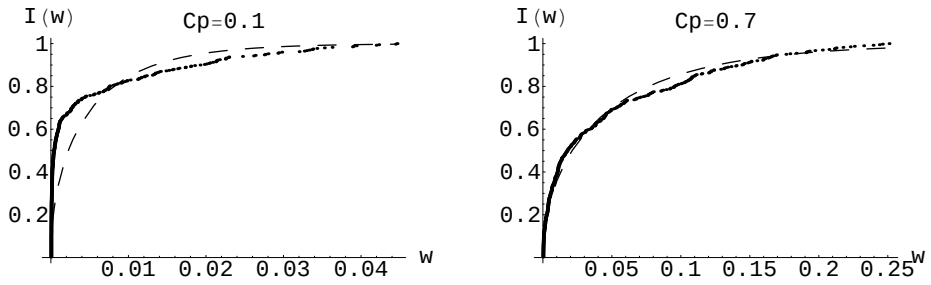

Figure 5.14: Integrated width density of 400 resonances for $C_p = 0.1$ and for $C_p = 0.7$ The dashed curve is the integrated Porter-Thomas distribution.

the momentum plane and since the two are simply related in a billiard system. Behaviour seen generically in atomic and other scattering problems is also seen here.

Figure 5.14 shows the numerical integrated width density $I(w)$ for $C_p = 0.1$ and $C_p = 0.7$. The case $C_p = 0.1$ is very close to the integrable system with no resonances at all and the resonances are only just starting to move off the real axis. The dashed line is the integrated Porter-Thomas distribution

$$I(w) = \mathrm{erf}(\sqrt{w_n/2}), \tag{5.91}$$

where $\mathrm{erf}(x)$ is the error function, which for $C_p = 0.7$ is a reasonable fit.

Figures 5.15 to 5.17 show the transition to arithmetic chaos in Artin's billiard as we vary C_p near $C_p = 1$. The width distribution initially separates into two classes which at $C_p = 1$ become concentrated exactly at $w = 0$ and $w = \frac{1}{4}$. This separation is reminiscent of the so-called 'trapping phenomenon', which occurs generically when the coupling to continua exceeds some critical value. M very unstable states (broad resonances) are formed, while the remainder of the spectrum moves back to the real axis [SZ89; PRSB00; HIL$^+$92]. However, this 'spectral reorganisation' usually only generates a number of broad states equal to the number of channels M which is not the case here since $M = 1$ and an infinite set of broad states are found. As C_p is increased further the two groups merge again and the χ^2 distribution is again recovered at $C_p \approx 1.2$ (see figure 5.17). The phenomenon seen here is attributed purely to the arithmetic chaos at $C_p = 1$.

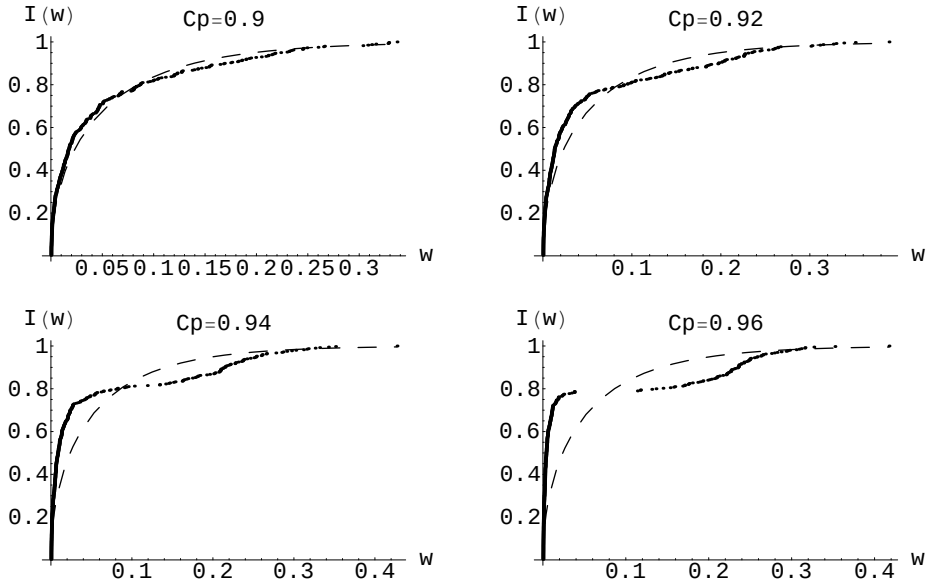

Figure 5.15: Integrated width densities of 400 resonances for $0.90 < C_p < 0.96$. The dashed curve is the integrated Porter-Thomas distribution.

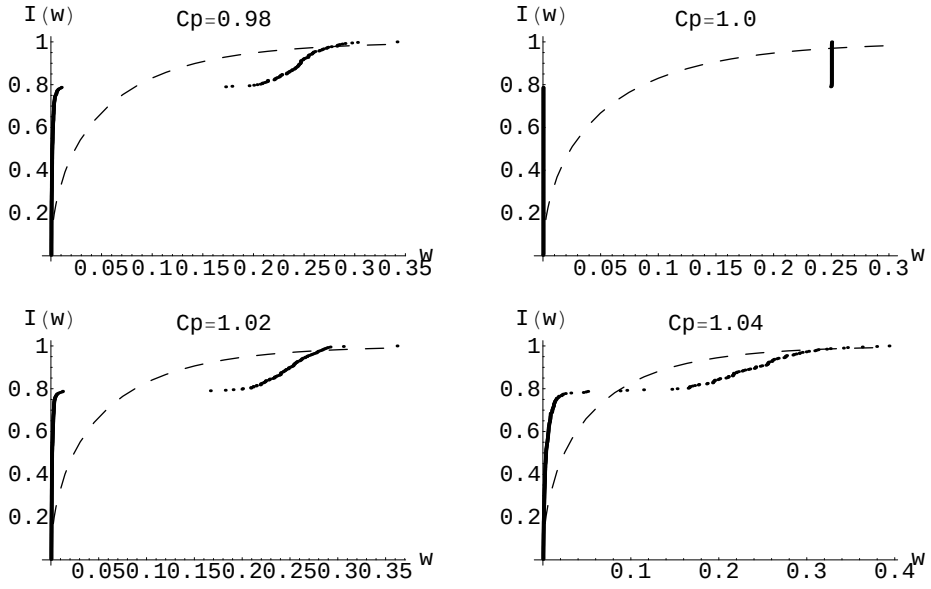

Figure 5.16: Integrated width densities of 400 resonances for $0.98 < C_p < 1.04$. The dashed curve is the integrated Porter-Thomas distribution.

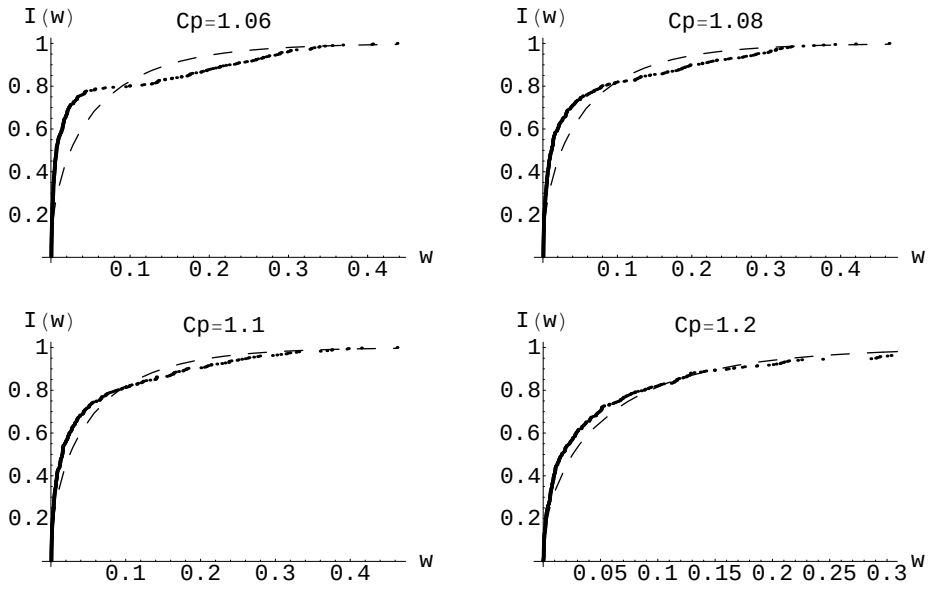

Figure 5.17: Integrated width densities of 400 resonances for $1.04 < C_p < 1.2$. The dashed curve is the integrated Porter-Thomas distribution.

5.3.4 Level-spacing statistics

The statistics of the real parts of the resonances were also investigated. Unlike the situation for the eigenvalues of closed billiards [GHSV91], there is no formula corresponding to Weyl's law (3.42) for the asymptotic density of resonance states. Instead a numerical fit to the data is first done, to allow the 'unfolding' of the spectrum to one with unit mean level density, via the transformation

$$x_i = \bar{N}(k_i), \tag{5.92}$$

where $\bar{N}(k)$ is the fitted integrated density of states for the particular billiard considered.

In terms of statistics of the unfolded eigenmomenta, the nearest-neighbour distribution is considered. The graph on the left of figure 5.18 shows the integrated distribution $I(s)$ of spacings between neighbouring unfolded levels ($s = x_{i+1} - x_i$) for the case $C_p = 0$, where the classical phase-space is completely integrable [CGSV94]. The distribution follows the Poissonian (dashed line) distribution

$$I(s) = 1 - \mathrm{e}^{-s}, \tag{5.93}$$

which is predicted for generic integrable systems [BT77; RV98]. Also shown are the integrated Wigner surmise for both the GOE (Gaussian Orthogonal Ensemble) (finely dashed line)

$$I(s) = 1 - \mathrm{e}^{-\pi s^2/4}, \tag{5.94}$$

and the GUE (Gaussian Unitary Ensemble) (solid line)

$$I(s) = -\frac{4}{\pi} s \mathrm{e}^{-\frac{4}{\pi}s^2} + \mathrm{erf}(2s/\sqrt{\pi}), \tag{5.95}$$

which are very close to the distributions predicted for fully chaotic systems with time-reversal invariance and broken time-reversal invariance respectively [Stö99].

In the graph on the right of figure 5.18 the same information is shown for $C_p = 0.7$ (where, as shown in section 5.1, the classical phase-space has become almost completely chaotic). The distribution seems to be well described by the GOE curve. In the graph on the left of figure 5.19 the distribution is shown for $C_p = 1$. As expected, it doesn't fit any of the distributions. The group of resonances with width $\frac{1}{4}$ are known to follow GUE statistics [Odl89] whereas the cusp forms obey the Poisson distribution. However in the graph on the left of figure 5.19 a fourth curve (thick line) is plotted which is a sum of (5.93) and (5.95) weighted by the percentage of resonances from each class (approximately in the ratio 3:1 of cusps to resonances). It gives a far better fit to the data than any one of the single distributions. Finally as C_p is increased further to $C_p \approx 1.2$ the GOE behaviour is recovered for the resonance positions (see the graph on the right of figure 5.19).

A method for parameterising the variation between these distributions was proposed by Brody [Bro73]. Although it has no sound theoretical basis such as is the case for those methods that base the parameterisation on the percentage of classical phase space which is completely chaotic, it is simple and may be applied to the situation near $C_p = 1$ where the change in statistics is due to arithmetic chaos, not a change in the classical phase-space. This is also the parameterisation used in [CGSV94].

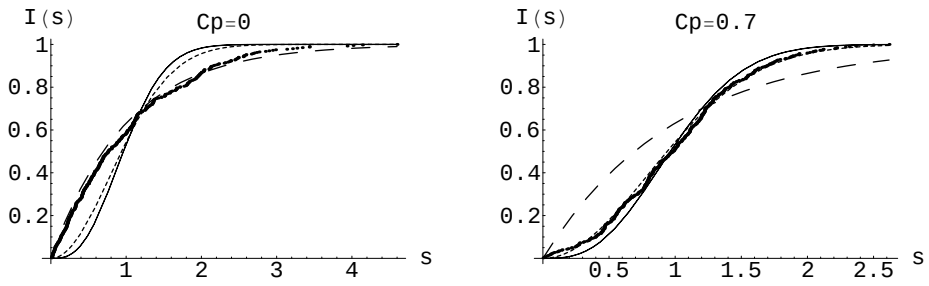

Figure 5.18: Integrated level-spacing distribution of 400 resonances for $C_p = 0$ and for $C_p = 0.7$. The dashed line is the integrated Poisson distribution, the finely dashed line is the GOE prediction and the solid line is the GUE prediction.

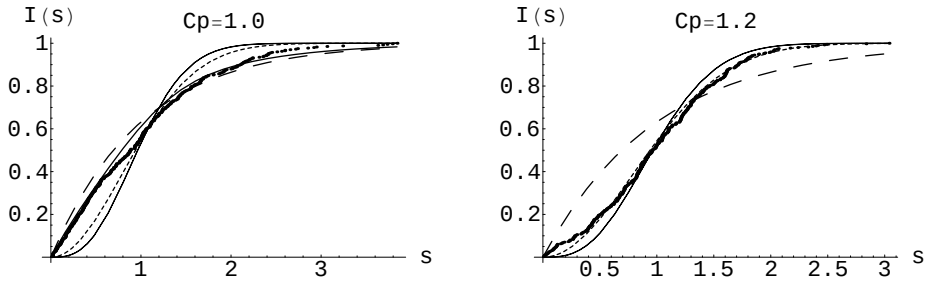

Figure 5.19: As figure 5.18 for 400 resonances at $C_p = 1$ and for $C_p = 1.2$. The thick curve in the $C_p = 1$ graph is a weighted average of the integrated Poisson and GUE densities.

The Brody distribution, normalised to unit mean and total probability, is given by [Stö99]

$$p(s,\nu) = a(\nu)(\nu+1)s^{\nu}\exp(-a(\nu)s^{\nu+1}), \tag{5.96}$$

where

$$a(\nu) = \left(\Gamma\left(\frac{\nu+2}{\nu+1}\right)\right)^{\nu+1} \tag{5.97}$$

and $\Gamma(x)$ is Euler's gamma function. For $\nu = 0$ this gives (5.93) and for $\nu = 1$ (5.94) is obtained.

The integrated level density of the Brody distribution is

$$I(s,\nu) = \int_0^s p(x,\nu)dx = 1 - \exp(-a(\nu)s^{\nu+1}). \tag{5.98}$$

Brody distributions were fitted to the numerical integrated density functions obtained (the error on the fit is much lower than for fitting to the density itself), using the method of least squares. The calculated values of ν give a useful measure of how close the distribution is to (5.93) or (5.94). Figure 5.20 shows the variation of the derived ν with C_p in the range $0 \leq C_p \leq 1.2$. A similar result was obtained by Csordás et al. in [CGSV94], for the bound states of billiards with Dirichlet boundary conditions. The distribution moves from Poissonian in the case where the classical dynamics are fully integrable up to GOE when they are completely chaotic. The sharp transition to near-Poissonian statistics at $C_p = 1$, in the sense that there are many more cusp forms than resonances with width $\frac{1}{4}$ in a given energy range, is shown in more detail. The value of ν obtained here for $C_p = 1$ agrees well with the scaling behaviour with N, the number of eigenvalues found, which was seen in [CGSV94]. The transition to arithmetic chaos at $C_p = 1$ is clearly defined.

5.3.5 Fourier transform of the spectra

To check on higher order correlation functions, e.g. two point correlations, and to compare further with RMT predictions the Fourier transform of the positions

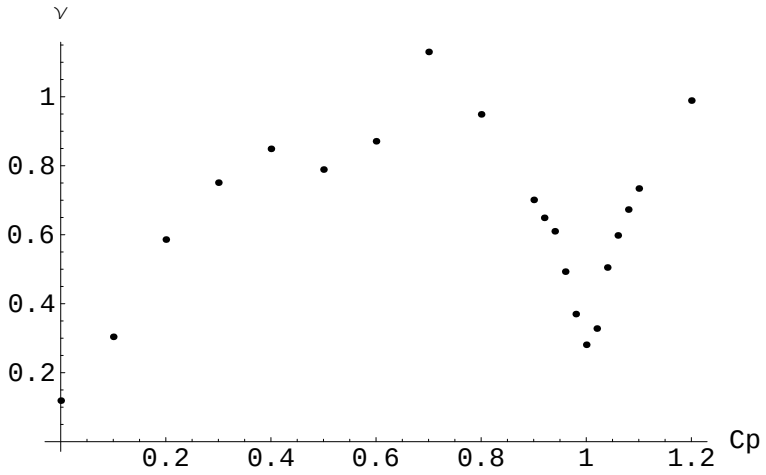

Figure 5.20: Variation of the Brody parameter ν with C_p.

of the resonances have been calculated [LLJP86]. Figure 5.21 shows the modulus squared of the direct Fourier transform,

$$C(t) = \int_{-\infty}^{\infty} \sum_{i=1}^{N} \delta(k_i - k) \mathrm{e}^{-2\pi\imath kt} \mathrm{d}k \tag{5.99}$$

of the real parts of the resonance positions for the values of C_p shown, after a Gaussian smoothing has been applied with width $\sigma = t/10$, following Alt et al. [AGG+97] who give a recent review of the method in the context of superconducting microwave billiards. In addition the ensemble averaged curve predicted by RMT for the GOE is plotted.

$$|C(t)_{GOE}|^2 = |b(t) - 1|^2 \,, \tag{5.100}$$

where

$$b(t) = \begin{cases} 1 - 2t + t\ln(1+2t) & 0 < t < 1 \\ -1 + t\ln((2t+1)/(2t-1)) & t > 1 \end{cases}$$

The Fourier transforms were performed on 400 levels. The correlation hole predicted by RMT for GOE systems for small t is present in the case $C_p = 0.7$ and is filled for $C_p = 0$, consistent with RMT predictions for a system obeying

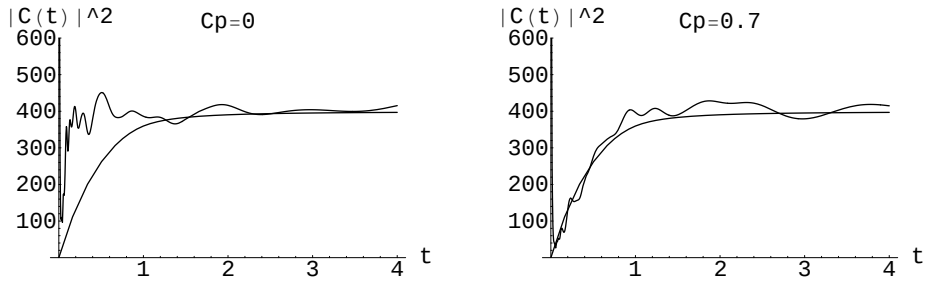

Figure 5.21: Gaussian smoothed absolute square of the Fourier transform of the spectrum at $C_p = 0$ and for $C_p = 0.7$. The smooth line is the GOE prediction.

Poissonian statistics. In the case $C_p = 1$ it is well known that the Fourier transform for the spectrum defined by the Riemann zeros follows the GUE prediction remarkably closely [Odl89]. The same behaviour is seen in the Fourier transform for $C_p = 1.2$ as for $C_p = 0.7$.

5.3.6 Correlations between widths and positions

It is also of interest in scattering systems to examine if there is any correlation between the positions and widths of the resonances. RMT predicts that there should be no correlation for weakly open systems with isolated resonances. This can be tested for, again using Fourier transforms, but now applied to a spectrum weighted by the widths [LS93]:

$$C(t) = \int_{-\infty}^{\infty} \sum_{i=1}^{N} w_i \delta(k_i - k) \mathrm{e}^{-2\pi\imath kt} \mathrm{d}k \tag{5.101}$$

The prediction of RMT for the GOE case is that the correlation hole is filled by two thirds [LS93], as is seen in figure 5.22 for $C_p = 1.2$.

However for $C_p = 0.7$, as seen on the left of figure 5.23 there is a dip in the Fourier transform for very short times which is at odds with RMT predictions eventhough the widths are well described by the Porter-Thomas distribution and the resonance positions by GOE and the RMT two point correlation function. The figure on the right of 5.23 demonstrates that the correlations are destroyed if the widths are assigned randomly to positions. This indicates the existence of

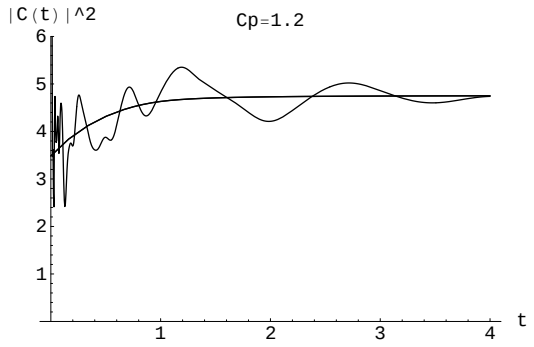

Figure 5.22: Gaussian smoothed absolute square of the Fourier transform of the width-weighted spectrum at $C_p = 1.2$. The smooth line is the GOE prediction.

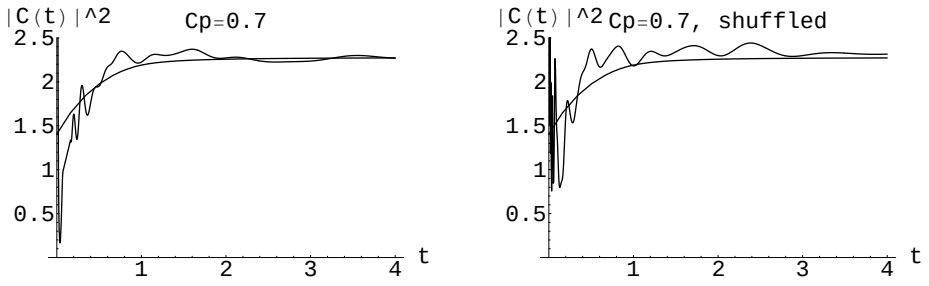

Figure 5.23: Gaussian smoothed absolute square of the Fourier transform of the width-weighted spectrum at $C_p = 0.7$ (left) and the same for the widths distributed randomly rather than on their corresponding positions (right). The smooth line is the GOE prediction.

long range non-universal correlation between the positions and widths. A similar correlation between positions and intensities was found in a study of chaotic Rydberg molecules [LS93]. It would be interesting to make a further investigation of the origin of the above correlations.

5.4 Deformation of the vertical boundary

Having introduced the methods used to analyse the spectra in the previous section 5.3, now a similar procedure is applied to the data obtained when Artin's billiard is perturbed by varying $\mathcal{L}$. In this case, the classical dynamics are always hyperbolic (the Lyapunov exponents are 1 due to the geodetic walls) but for the special cases when $\mathcal{L}$ is the square root of an integer, transitions to arithmetic chaos are seen with spectral reorderings similar to those seen in section 5.3.3. The following two sections present our derivations of the scattering matrix S in the two special arithmetic cases encountered here, $\mathcal{L} = \sqrt{2}$ and $\mathcal{L} = \sqrt{3}$. The case of $\mathcal{L} = \sqrt{1}$, the modular group, was presented earlier, in section 3.2.2. The deformation for general $\mathcal{L}$ was introduced in section 4.2 and our results are presented in sections 5.4.3 and 5.4.4.

5.4.1 The scattering matrix for $\mathcal{L} = \sqrt{2}$

In this case $n = 4$ in (4.4) and the group is generated by the specific matrices

$$S = \begin{pmatrix} 0 & -1 \\ 1 & 0 \end{pmatrix}, \quad T = \begin{pmatrix} 1 & \sqrt{2} \\ 0 & 1 \end{pmatrix}. \tag{5.102}$$

Thus the matrix representations of particular group elements take two forms.

$$\sigma = \begin{pmatrix} a & b \\ c & d \end{pmatrix} = \begin{pmatrix} 1+2a' & b'\sqrt{2} \\ c'\sqrt{2} & 1+2d' \end{pmatrix}; \{a', b', c', d' \in \mathbb{Z} | ad - 2b'c' = 1\} \tag{5.103}$$

and

$$\sigma = \begin{pmatrix} a & b \\ c & d \end{pmatrix} = \begin{pmatrix} a'\sqrt{2} & 1+2b' \\ 1+2c' & d'\sqrt{2} \end{pmatrix}; \{a', b', c', d' \in \mathbb{Z} | 2a'd' - bc = 1\}. \tag{5.104}$$

Proceeding as in section 3.2.2 we factor out the left coset Γ_0 since

$$\Gamma_0 = \left\{ \begin{pmatrix} 1 & q\sqrt{2} \\ & 1 \end{pmatrix} \right\}; q \in \mathbb{Z} \tag{5.105}$$

and thus

$$\Gamma_0\sigma = \left\{ \begin{pmatrix} a + q\sqrt{2}c & b + q\sqrt{2}d \\ c & d \end{pmatrix} \right\}, \tag{5.106}$$

which all produce the same $y(\sigma z) = y/\left|cz + d\right|^2$.

Now we consider the Fourier decomposition $\psi = \sum_m a_m(y)\exp(-2\pi\imath mx/\mathfrak{L})$. ψ for this group is periodic with period $\sqrt{2}$ in x so concentrating on a_0 which leads to the S-matrix we get

$$a_0(y) = \frac{1}{\sqrt{2}} \int_0^{\sqrt{2}} \sum_{\sigma \in \Gamma_0 \backslash \Gamma} \frac{y^{1/2-\imath k}}{\left|cz + d\right|^{1-2\imath k}} \mathrm{d}x. \tag{5.107}$$

The identity term in the sum again gives a contribution $y^{1/2-\imath k}$ but there are now two cases to consider when treating the right cosets

$$\sigma\Gamma_0 = \left\{ \begin{pmatrix} a & b + q\sqrt{2}a \\ c & d + q\sqrt{2}c \end{pmatrix} \right\}. \tag{5.108}$$

These are equal only for any σ and $\tilde{\sigma}$ with $\tilde{c} = c$ and $\tilde{d} \equiv d (\mathrm{mod}\, \sqrt{2}c)$. In both cases only one coset representative is required in the sum and the rest are taken into the integral via

$$y(\sigma z) = \frac{y}{\left|cz + d + q\sqrt{2}c\right|^2} = \frac{y}{\left|c(z + q\sqrt{2}) + d\right|^2} \tag{5.109}$$

so that

$$\int_0^{\sqrt{2}} y(\sigma(z))^{1/2-\imath k} \mathrm{d}x = \int_{q\sqrt{2}}^{(q+1)\sqrt{2}} y(z')^{1/2-\imath k} \mathrm{d}x' \tag{5.110}$$

by the simple substitution $x' = x + q\sqrt{2}$.

This brings us to a point where (5.107) can be written as

$$a_0(y) = y^{1/2-\imath k} + \frac{1}{\sqrt{2}} \int_{-\infty}^{\infty} \sum_{\sigma \in \Gamma_0 \backslash \Gamma - \mathbb{I}} \frac{y^{1/2-\imath k}}{\left|cz + d\right|^{1-2\imath k}} \mathrm{d}x. \tag{5.111}$$

Substituting $\rho = x + d/c$ this becomes

$$\begin{aligned} a_0(y) &= y^{1/2-\imath k} + \frac{1}{\sqrt{2}} \int_{-\infty}^{\infty} \sum_{\sigma \in \Gamma_0 \backslash \Gamma_{-\mathbb{I}}} \frac{1}{|c|^{1-2\imath k}} \frac{y^{1/2-\imath k}}{|\rho + \imath y|^{1-2\imath k}} \mathrm{d}\rho \\ &= y^{1/2-\imath k} + \frac{1}{\sqrt{2}} \sum_{\sigma \in \Gamma_0 \backslash \Gamma_{-\mathbb{I}}} \frac{1}{|c|^{1-2\imath k}} \int_{-\infty}^{\infty} \frac{y^{1/2-\imath k}}{(\rho^2 + y^2)^{1/2-\imath k}} \mathrm{d}\rho. \end{aligned} \quad (5.112)$$

In the first case considered above, the $\sqrt{2}$ factor is contained in c and the determinant constraint $ad - 2b'c' = 1$ still means c' is coprime to d since ad is odd. Thus we have to sum over all

$$c = \sqrt{2}c',\ c' \in \mathbb{Z} \quad (5.113)$$

and the sum over d is over all odd integers less than $2c'$ and coprime to c'. Since $2c'$ is even, this is just $\phi(2c')$, the number of integers less than $2c'$ and coprime to $2c'$.

In the second case, the $\sqrt{2}$ is contained in d so we have to sum over all *odd* integers c, and the sum over d ranges over all integers d' that are less than c. Thus we get a contribution $\phi(c)$ from the sum over d, since the determinant constraint $2a'd' - bc = 1$ now means that d' is coprime to c (bc is odd).

(5.112) now reads

$$\begin{aligned} a_0(y) = y^{1/2-\imath k} &+ \frac{1}{\sqrt{2}} \int_{-\infty}^{\infty} \frac{y^{1/2-\imath k}}{(\rho^2 + y^2)^{1/2-\imath k}} \mathrm{d}\rho \\ &\times \left(\sum_{0<c' \in \mathbb{Z}} \frac{\phi(2c')}{2^{1/2-\imath k} c'^{(1-2\imath k)}} + \sum_{0 \le c' \in \mathbb{Z}} \frac{\phi(1+2c')}{(1+2c')^{1-2\imath k}} \right) \end{aligned} \quad (5.114)$$

Putting $s = 1/2 - \imath k$ we have two sums to consider in the arithmetic factor (substituting c for c' as the dummy index);

$$\sum_{0<c \in \mathbb{Z}} \frac{\phi(2c)}{2^s c^{2s}} \quad (5.115)$$

and

$$\sum_{0 \le c \in \mathbb{Z}} \frac{\phi(1+2c)}{(1+2c)^{2s}}. \quad (5.116)$$

Splitting the first sum into even and odd parts and using

$$\phi(2c) = \begin{cases} \phi(c) & c \quad \text{odd} \\ 2\phi(c) & c \quad \text{even} \end{cases} \tag{5.117}$$

we obtain

$$\sum_{0<c\in\mathbb{Z}} \frac{\phi(2c)}{2^s c^{2s}} = \frac{1}{2^s}\left(\sum_{c\,\text{odd}} \frac{\phi(c)}{c^{2s}} + 2\sum_{c\,\text{even}} \frac{\phi(c)}{c^{2s}}\right). \tag{5.118}$$

So the total arithmetic term in (5.114) becomes

$$\left(1+\frac{1}{2^s}\right)\sum_{c\,\text{odd}} \frac{\phi(c)}{c^{2s}} + \frac{2}{2^s}\sum_{c\,\text{even}} \frac{\phi(c)}{c^{2s}}. \tag{5.119}$$

The even terms can be removed from the sum over all integers by removing the term which generates factors of 2 in (3.19)

$$\begin{aligned} \sum_{c\,\text{odd}} \frac{\phi(c)}{c^{2s}} &= \frac{(1-1/2^{(2s-1)})}{(1-1/2^{(2s)})} \prod_p \left\{ \frac{\left(1-\frac{1}{p^{(2s-1)}}\right)+\left(\frac{1}{p^{(2s-1)}}-\frac{1}{p^{2s}}\right)}{\left(1-\frac{1}{p^{(2s-1)}}\right)} \right\} \\ &= \frac{(1-1/2^{(2s-1)})\zeta(2s-1)}{(1-1/2^{(2s)})\zeta(2s)}, \end{aligned} \tag{5.120}$$

and the even sum is obtained simply by

$$\sum_{c\,\text{even}} \frac{\phi(c)}{c^{2s}} = \frac{\zeta(2s-1)}{\zeta(2s)}\left(1-\frac{(1-1/2^{(2s-1)})}{(1-1/2^{(2s)})}\right) \tag{5.121}$$

using (3.20) for the full sum.

Putting all this together finally gives

$$\begin{aligned} &\left(1+\frac{1}{2^s}\right)\sum_{c\,\text{odd}} \frac{\phi(c)}{c^{2s}} + \frac{2}{2^s}\sum_{c\,\text{even}} \frac{\phi(c)}{c^{2s}} = \\ &\frac{\zeta(2s-1)}{\zeta(2s)}\left(\left(1+\frac{1}{2^s}\right)\frac{(1-1/2^{(2s-1)})}{(1-1/2^{(2s)})} + \frac{2}{2^s}\left(1-\frac{(1-1/2^{(2s-1)})}{(1-1/2^{(2s)})}\right)\right). \end{aligned} \tag{5.122}$$

This reduces to $\frac{\zeta(2s-1)}{\zeta(2s)}$ times

$$\left(\frac{(1+1/2^s)\,(1-1/2^{(2s-1)})2^s+2\left(1-1/2^{(2s)}-(1-1/2^{(2s-1)})\right)}{2^s(1-1/2^{(2s)})}\right)=$$
$$\left(\frac{2^s\left(1+1/2^s-1/2^{(2s-1)}-1/2^{(3s-1)}\right)+2\left(-1/2^{(2s)}+1/2^{(2s-1)}\right)}{2^s(1-1/2^{(2s)})}\right)=$$
$$\left(\frac{2^s\left(1+1/2^s-1/2^{(2s-1)}-1/2^{(3s-1)}\right)+1/2^{(2s-1)}}{2^s(1-1/2^{(2s)})}\right)=$$
$$\left(\frac{\left(1+1/2^s-2/2^{(2s)}\right)}{(1-1/2^{(2s)})}\right)=\frac{(1+2/2^s)\,(1-1/2^s)}{(1-1/2^s)(1+1/2^s)}=$$
$$\frac{(1+2/2^s)}{(1+1/2^s)}=\frac{(2+2^s)}{(1+2^s)}. \tag{5.123}$$

So we have in this case an S-matrix the same as for the modular case, up to a unitary factor (resubstituting $s=1/2-\imath k$ and remembering the factor $1/\sqrt{2}$ from (5.114))

$$\frac{1}{\sqrt{2}}\frac{(2+2^{1/2-\imath k})}{(1+2^{1/2-\imath k})}=2^{\imath k}\frac{(\sqrt{2}+2^{-\imath k})}{(\sqrt{2}+2^{\imath k})}. \tag{5.124}$$

Thus

$$S(k)=2^{\imath k}\frac{(\sqrt{2}+2^{-\imath k})}{(\sqrt{2}+2^{\imath k})}\frac{\pi^{-\imath k}\Gamma(1/2+\imath k)\zeta(1+2\imath k)}{\pi^{\imath k}\Gamma(1/2-\imath k)\zeta(1-2\imath k)}, \tag{5.125}$$

which has poles on the line $\Im(k)=-1/4$, positioned at the non-trivial zeros of the Riemann zeta function divided by two, and at

$$k=r-\imath/2,\quad r=(1+2n)\pi/(\ln 2),\quad n\in\mathbb{Z}. \tag{5.126}$$

5.4.2 The scattering matrix for $\mathcal{L}=\sqrt{3}$

In this case $n=6$ in (4.4) and the group is generated by the specific matrices

$$S=\begin{pmatrix}0&-1\\1&0\end{pmatrix},\quad T=\begin{pmatrix}1&\sqrt{3}\\0&1\end{pmatrix}. \tag{5.127}$$

Thus the matrix representations of particular group elements now take four forms.

$$\sigma = \begin{pmatrix} a & b \\ c & d \end{pmatrix} = \begin{pmatrix} 1+3a' & b'\sqrt{3} \\ c'\sqrt{3} & 1+3d' \end{pmatrix} \text{or} \begin{pmatrix} 2+3a' & b'\sqrt{3} \\ c'\sqrt{3} & 2+3d' \end{pmatrix}; \\ \{a', b', c', d' \in \mathbb{Z} | ad - 3b'c' = 1\}, \tag{5.128}$$

and

$$\sigma = \begin{pmatrix} a & b \\ c & d \end{pmatrix} = \begin{pmatrix} a'\sqrt{3} & 2+3b' \\ 1+3c' & d'\sqrt{3} \end{pmatrix} \text{or} \begin{pmatrix} a'\sqrt{3} & 1+3b' \\ 2+3c' & d'\sqrt{3} \end{pmatrix}; \\ \{a', b, c, d' \in \mathbb{Z} | 3a'd' - bc = 1\}. \tag{5.129}$$

The task of calculating the scattering coefficient proceeds almost exactly as in section 5.4.1 for the case $n = 4$. Taking a Fourier decomposition of (3.5) with period $\sqrt{3}$ and factoring out the left cosets brings us to an expression for the constant Fourier coefficient,

$$a_0(y) = y^{1/2-\imath k} + \frac{1}{\sqrt{3}} \sum_{\sigma \in \Gamma_0 \backslash \Gamma - \mathbb{I}} \frac{1}{|c|^{1-2\imath k}} \int_{-\infty}^{\infty} \frac{y^{1/2-\imath k}}{(\rho^2+y^2)^{1/2-\imath k}} \mathrm{d}\rho. \tag{5.130}$$

The sum naturally splits into two parts over the two classes of matrices described in (5.128) and (5.129),

$$a_0(y) = y^{1/2-\imath k} + \frac{1}{\sqrt{3}} \int_{-\infty}^{\infty} \frac{y^{1/2-\imath k}}{(\rho^2+y^2)^{1/2-\imath k}} \mathrm{d}\rho \\ \times \left(\sum_{0<c\in\mathbb{Z}} \frac{\phi(3c)}{3^{1/2-\imath k} c^{1-2\imath k}} + \sum_{0<c\in\mathbb{Z}|(c,3)=1} \frac{\phi(c)}{(c)^{1-2\imath k}} \right). \tag{5.131}$$

Performing these sums as done earlier for the case $\mathfrak{L} = \sqrt{2}$ in (5.120), but now removing all factors of 3 from the full sums rather than factors of 2, the expression for the scattering coefficient reduces to $\frac{\zeta(2s-1)}{\zeta(2s)}$ times the unitary factor

$$3^{\imath k} \frac{(\sqrt{3} + 3^{-\imath k})}{(\sqrt{3} + 3^{\imath k})}, \tag{5.132}$$

Thus

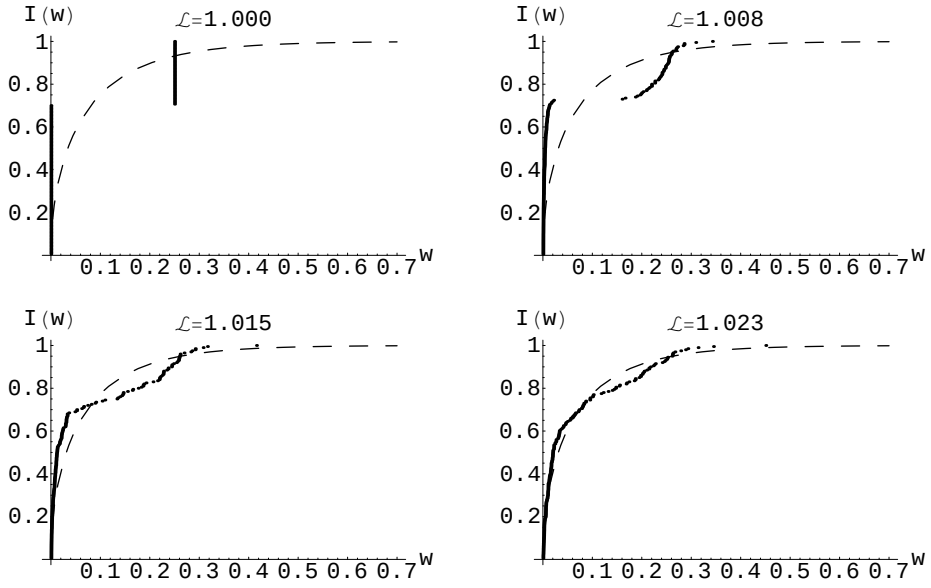

Figure 5.24: Integrated width density of 200 resonances for $\mathcal{L}$ between 1.000 and 1.023. The dashed curve is the integrated Porter-Thomas distribution. The case $\mathcal{L} = 1.000$ corresponds to the Hecke group with $\theta = \pi/3$.

$$S(k) = 3^{\imath k} \frac{(\sqrt{3} + 3^{-\imath k})}{(\sqrt{3} + 3^{\imath k})} \frac{\pi^{-\imath k}\Gamma(1/2 + \imath k)\zeta(1 + 2\imath k)}{\pi^{\imath k}\Gamma(1/2 - \imath k)\zeta(1 - 2\imath k)}, \tag{5.133}$$

which has poles on the line $\Im(k) = -1/4$, positioned at the non-trivial zeros of the Riemann zeta function divided by two, and at

$$k = r - \imath/2,\ r = (1 + 2n)\pi/(\ln 3),\ n \in \mathbb{Z}. \tag{5.134}$$

5.4.3 The widths

Figures 5.24 to 5.33 show the numerical integrated width density $I(w)$ as it evolves in the range $1.000 \leq \mathcal{L} \leq \sqrt{3}$. The dashed line is again the integrated Porter-Thomas distribution

$$I(w) = \mathrm{erf}(\sqrt{w_n/2}), \tag{5.135}$$

where $\mathrm{erf}(x)$ is the error function.

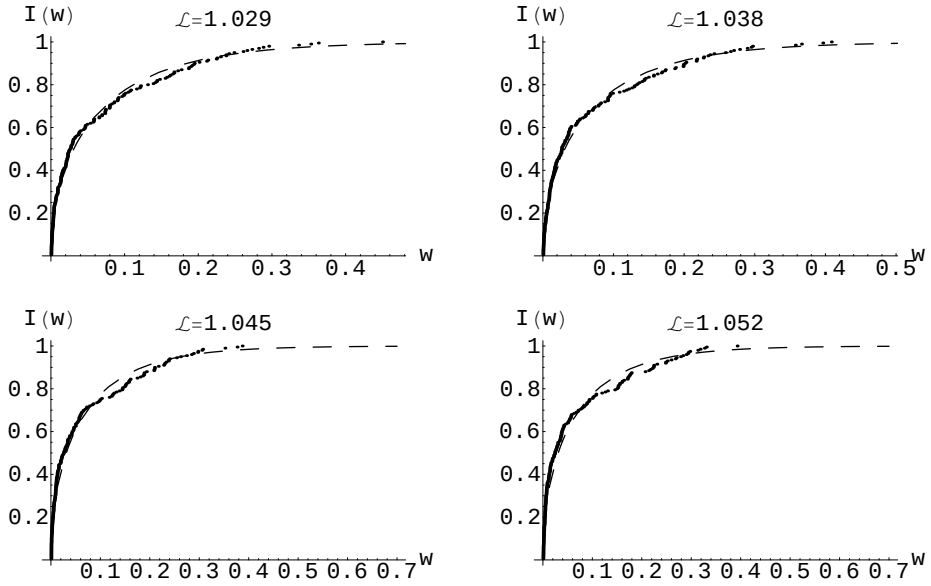

Figure 5.25: Integrated width density of 200 resonances for $\mathcal{L}$ between 1.029 and 1.052. The dashed curve is the integrated Porter-Thomas distribution.

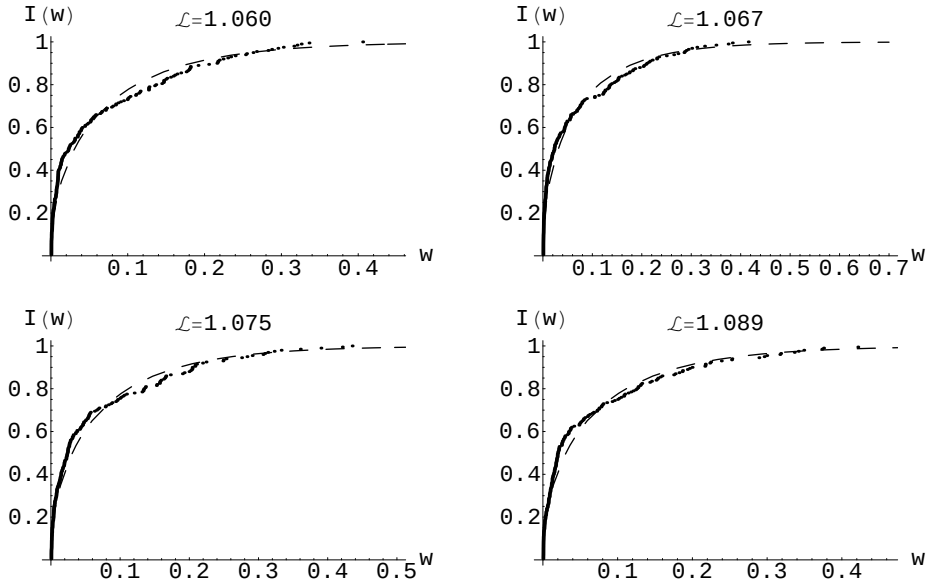

Figure 5.26: Integrated width density of 200 resonances for $\mathcal{L}$ between 1.060 and 1.089. The dashed curve is the integrated Porter-Thomas distribution.

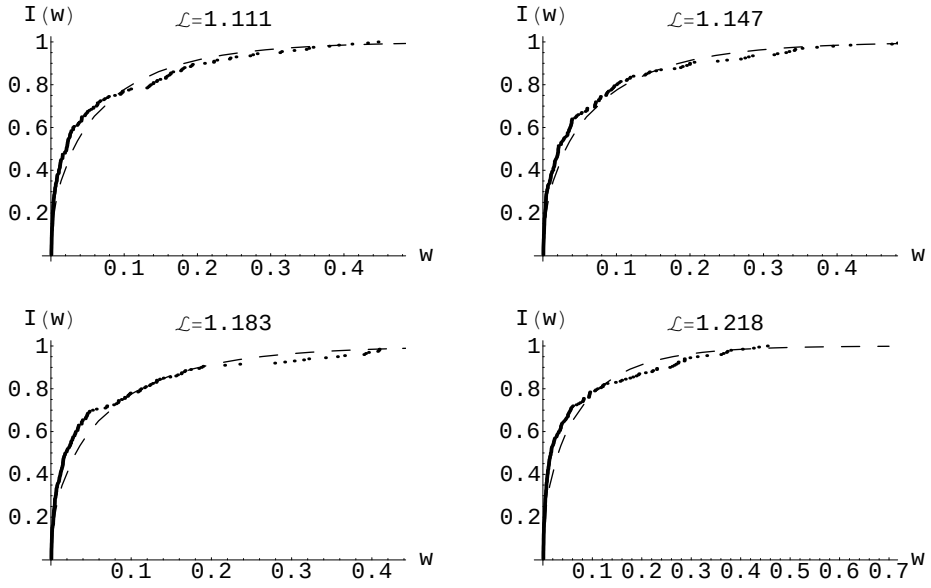

Figure 5.27: Integrated width density of 200 resonances for $\mathcal{L}$ between 1.111 and 1.218. The dashed curve is the integrated Porter-Thomas distribution.

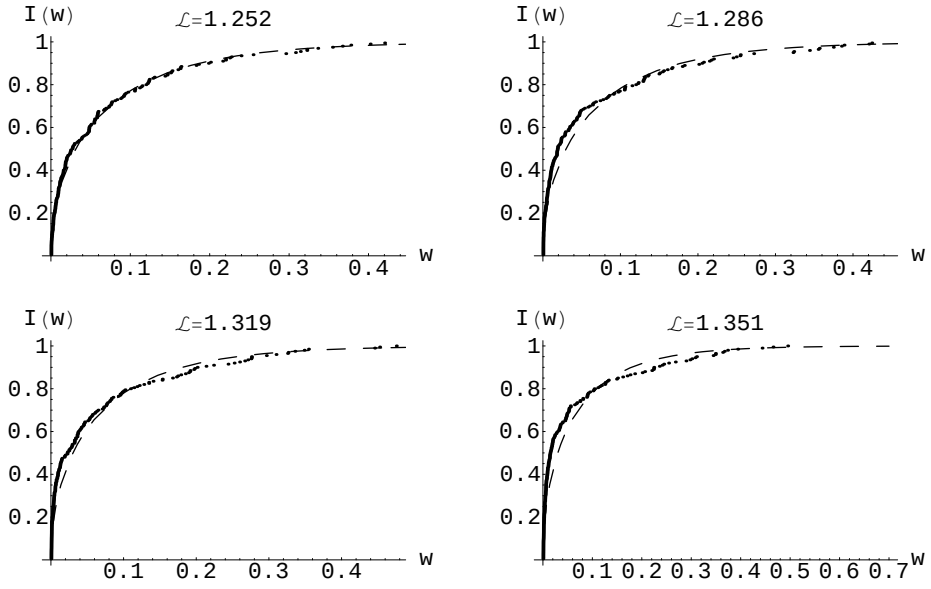

Figure 5.28: Integrated width density of 200 resonances for $\mathcal{L}$ between 1.252 and 1.351. The dashed curve is the integrated Porter-Thomas distribution.

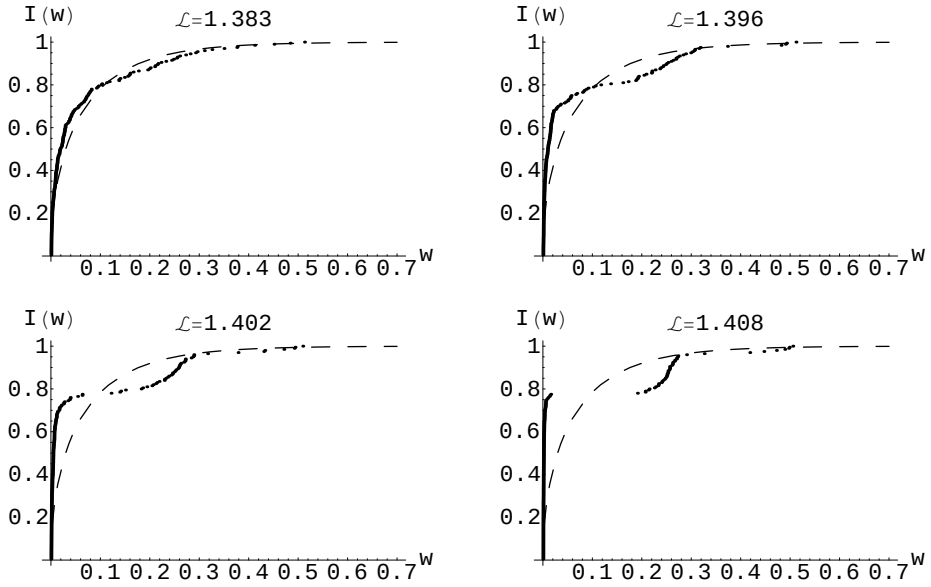

Figure 5.29: Integrated width density of 200 resonances for $\mathfrak{L}$ between 1.383 and 1.408. The dashed curve is the integrated Porter-Thomas distribution.

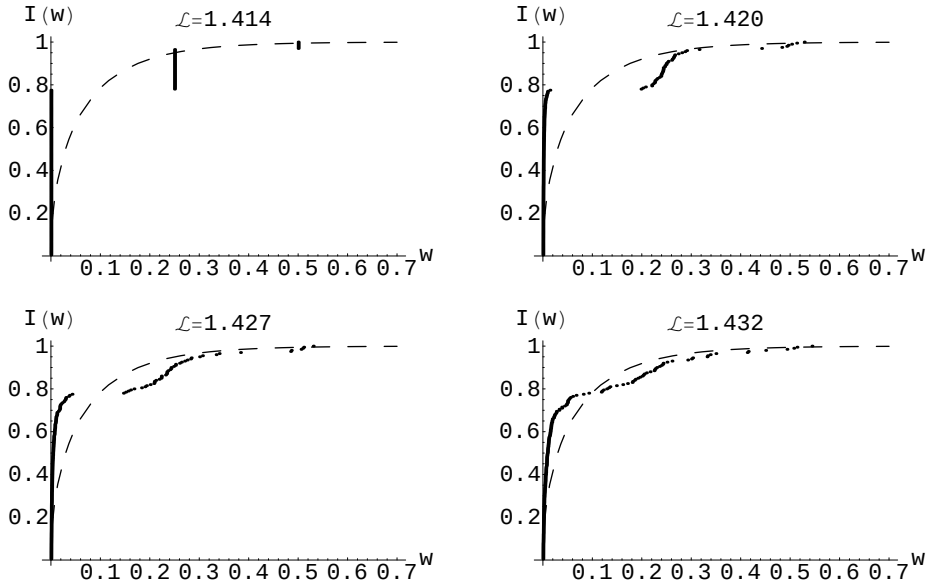

Figure 5.30: Integrated width density of 200 resonances for $\mathfrak{L}$ between 1.414 and 1.432. The dashed curve is the integrated Porter-Thomas distribution. The case $\mathfrak{L} = 1.414$ corresponds to the Hecke group with $\theta = \pi/4$.

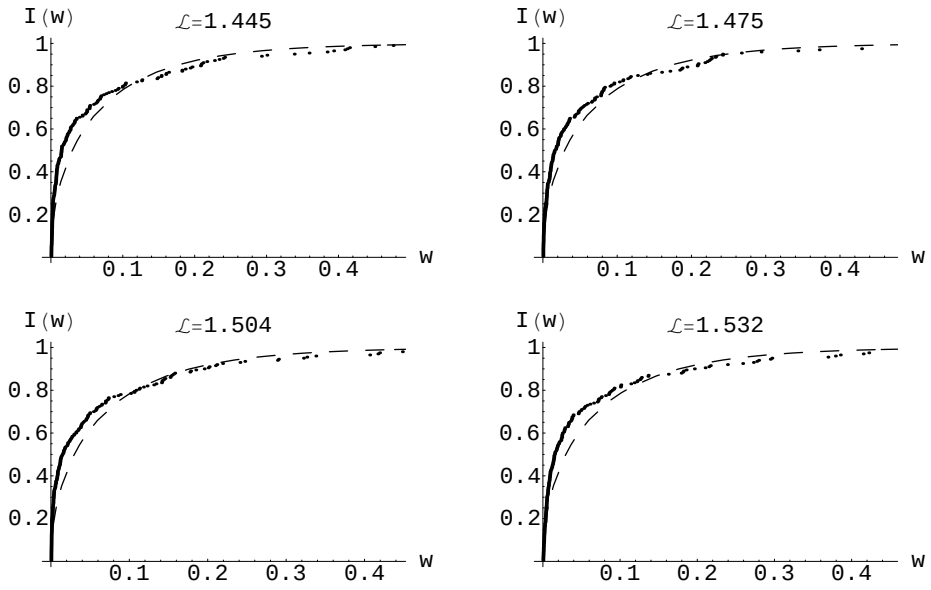

Figure 5.31: Integrated width density of 200 resonances for $\mathcal{L}$ between 1.445 and 1.532. The dashed curve is the integrated Porter-Thomas distribution.

Figures 5.24, 5.30 and 5.33 show the transition to arithmetic chaos near the special cases of arithmetic groups at $\mathcal{L} = \sqrt{1}, \sqrt{2}$ and $\sqrt{3}$, corresponding to $\theta = \pi/3, \pi/4$ and $\pi/6$ respectively. In these cases it is good to see the predictions of sections 5.4.2 and 5.4.1 confirmed in the existence of a class of states with imaginary part equal to $-\frac{1}{4}$ positioned at the Riemann zeros halved, as in the case of section 3.2.2, and moreover the class with imaginary part equal to $-\frac{1}{2}$ positioned at regular intervals of $\frac{\pi}{\ln(\mathcal{L})}$. As $\mathcal{L}$ is varied away from these particular cases, the three groups merge again and the χ^2 distribution is again recovered in the intermediate regions (see figures 5.26 and 5.31). There appears to be no significant correlation between which states fall into which class at different values of $\mathcal{L}$, in fact states often switch class during the intermediate deformation. The phenomenon seen here is again attributed purely to arithmetic chaos due to the underlying groups' structure. The best agreement with RMT appears to be for $\mathcal{L} = 1.252$. In figure 5.32 the case $\mathcal{L} = 1.618, \theta = \pi/5$ is seen to agree reasonably well with the generic RMT case, although clearly there is some discrepancy for shorter widths.

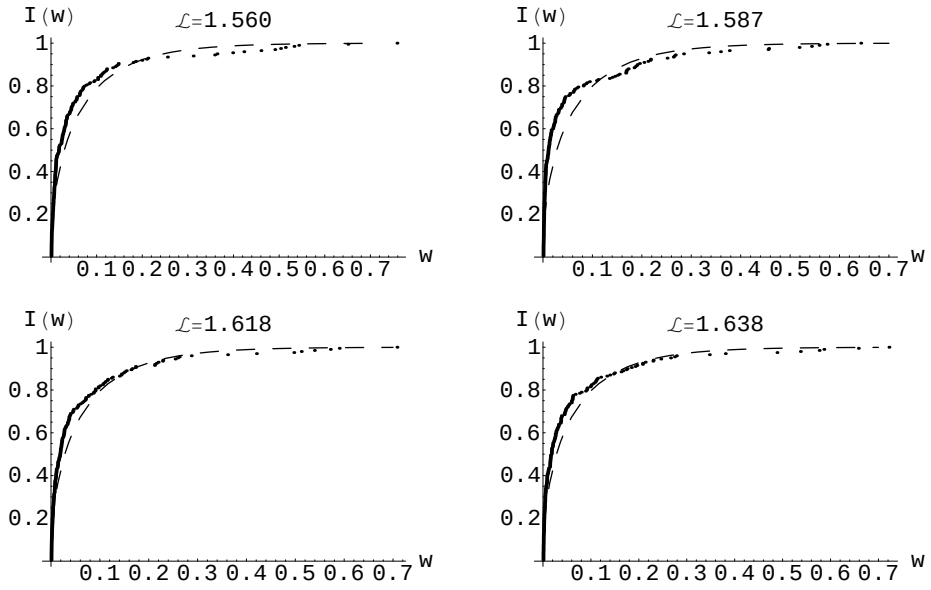

Figure 5.32: Integrated width density of 200 resonances for $\mathfrak{L}$ between 1.560 and 1.638. The dashed curve is the integrated Porter-Thomas distribution. The case $\mathfrak{L} = 1.618$ corresponds to the Hecke group with $\theta = \pi/5$. This is not an arithmetic group, but it tiles the plane.

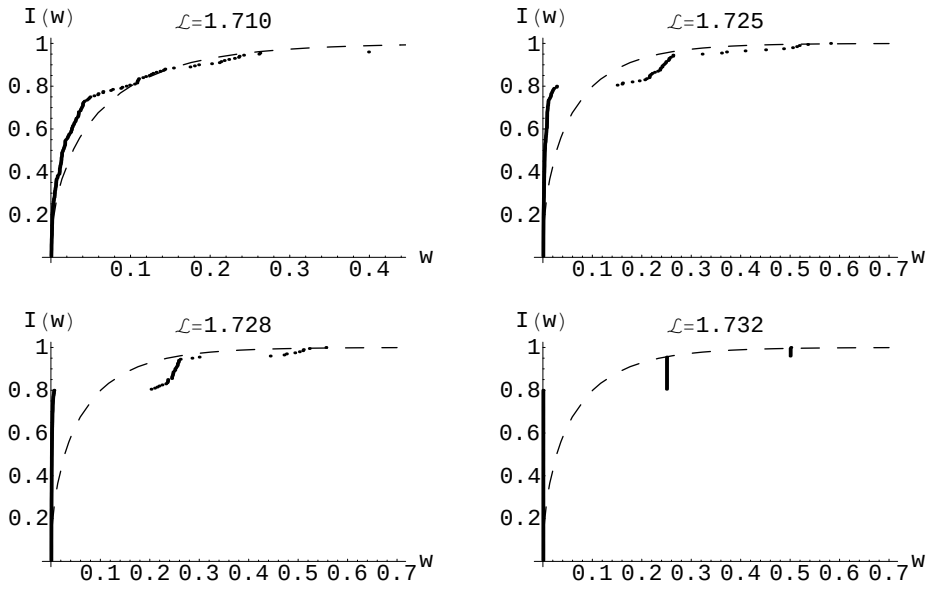

Figure 5.33: Integrated width density of 200 resonances for $\mathcal{L}$ between 1.710 and 1.732. The dashed curve is the integrated Porter-Thomas distribution. The case $\mathcal{L} = 1.732$ corresponds to the Hecke group with $\theta = \pi/6$.

5.4.4 Level-spacing statistics

Again the nearest-neighbour distribution for the statistics of the unfolded eigenmomenta is considered. Behaviour similar to that observed in section 5.3.4 is seen, except that now the underlying classical system is always fully chaotic, and the transitions observed are purely due to arithmetic factors. Figures 5.34 to 5.36 show the distributions of level-spacings for the three arithmetic cases, and demonstrate the return to GOE behaviour in between. The case of $\mathcal{L} = 1.618, \theta = \pi/5$ shows reasonably good agreement with GOE statistics. The billiard with $\mathcal{L} = 1.252$ appears to agree best with the GOE, as was the case for the widths. In all the graphs, we also plot the Poissonian (dashed line) distribution (5.93) and the integrated Wigner surmise for both the GOE (finely dashed line) (5.94) and the GUE (solid line) (5.95).

We also follow the variation of the Brody parameter, given by (5.96), for the entire $\mathcal{L}$ range in figure 5.37. The three transitions to arithmetic chaos are dramatically displayed as the sharp drops at $\mathcal{L} \in \{1, \sqrt{2}, \sqrt{3}\}$. These are due

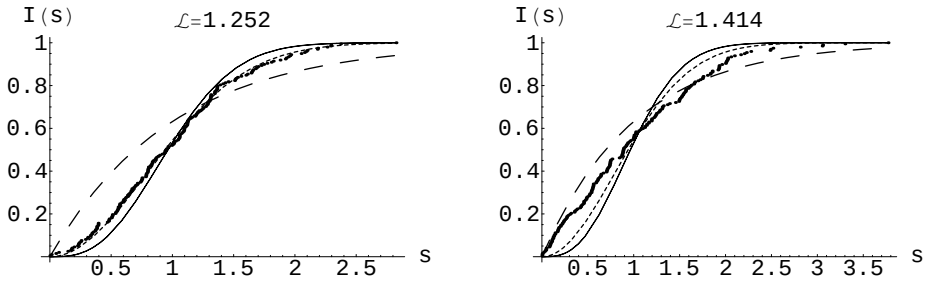

Figure 5.34: Integrated level-spacing distribution of 200 resonances for $\mathcal{L} = 1.252$. and for $\mathcal{L} = \sqrt{2} \simeq 1.414(\theta = \pi/4)$. The dashed line is the integrated Poisson distribution, the finely dashed line is the GOE prediction and the solid line is the GUE prediction.

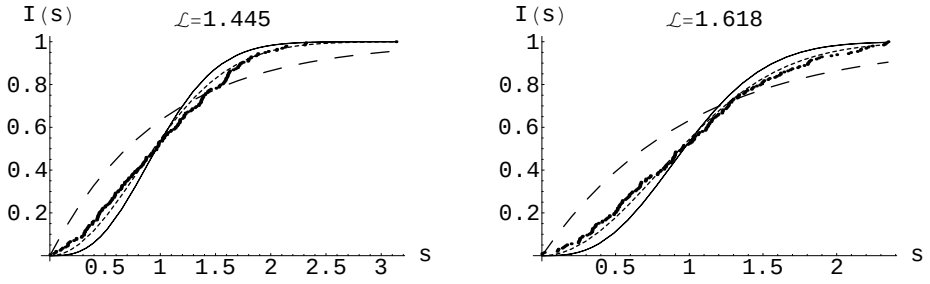

Figure 5.35: Integrated level-spacing distribution of 200 resonances for $\mathcal{L} = 1.445$. and for $\mathcal{L} = 1.618(\theta = \pi/5)$. The dashed line is the integrated Poisson distribution, the finely dashed line is the GOE prediction and the solid line is the GUE prediction.

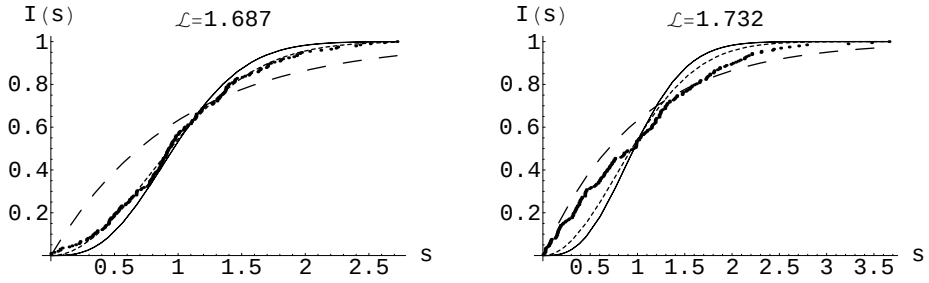

Figure 5.36: Integrated level-spacing distribution of 200 resonances for $\mathcal{L} = 1.687$. and for $\mathcal{L} = \sqrt{3} \simeq 1.732(\theta = \pi/6)$. The dashed line is the integrated Poisson distribution, the finely dashed line is the GOE prediction and the solid line is the GUE prediction.

to the large set of cusp forms with zero width and Poissonian statistics at these values. There appear to be lesser drops away from these special cases, but the current amount of data available does not make it possible to say much about them.

For bound systems, i.e. the odd spectrum, Bogomolny et al. have shown that the non-generic behaviour displayed by arithmetic systems can be interpreted in terms of the Selberg trace formula, as being due to an exponential degeneracy in the number of periodic orbits with the same period [BGGS92]. Although such degeneracies persist for the Hecke group with $n = 5$, they are not large enough to affect the statistics, which are predicted to have generic RMT behaviour. Our results indicate that the same holds true for open systems, i.e. the even spectra.

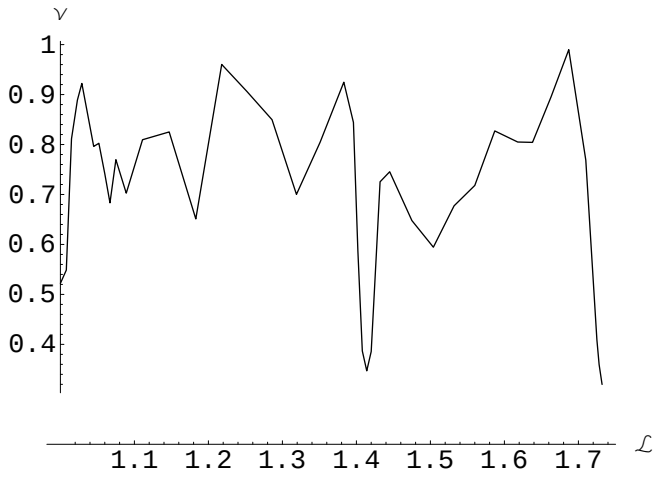

Figure 5.37: Variation of the Brody parameter ν with $\mathfrak{L}$.

Chapter 6

Conclusions

We have studied the behaviour of resonances for two linked classes of billiard system on the Poincaré half-plane. In particular we have followed how the positions and widths of the resonances move as the shape of Artin's billiard is perturbed both by varying its width and by deforming the lower boundary. The main results were presented in chapter 5, where the variation of the statistical properties of the spectra were focussed on. Of particular interest were transitions in the statistics of the widths near particular values of the perturbation parameters which correspond to the underlying billiard being a fundamental domain for some arithmetic group. Analytic solutions for the resonances in these particular arithmetic systems were derived in section 5.4. While for most values of the perturbation parameters the resonant energies distribute randomly according to the predictions of RMT, in these special cases three classes of resonance were observed: those which have zero imaginary part and become pseudo-bound cusp forms; those with imaginary part equal to $-\frac{1}{4}$ positioned at half the magnitude of the Riemann zeros; and the class with imaginary part equal to $-\frac{1}{2}$ positioned at regular intervals of $\frac{\pi}{\ln(\mathcal{L})}$.

A specific numerical technique based on basis expansion collocation methods was developed for this purpose and excellent agreement was obtained with the theory and the results of other groups, where they exist (see table 5.1). In the vast majority of parameter space there are no other results in the literature and the statistical behaviour of resonant states in arithmetic systems under deformation has not been studied numerically before, to the best of our knowledge. Away from

the arithmetic systems, both generic and non-generic behaviour according to the predictions of RMT was observed, deviations occurring particularly in the long range statistics, and it is of interest to continue research into the origin of such anomalies. We also followed the variation of the Brody parameter characterizing the variation of the nearest-neighbour distribution of the resonance positions, and the scaling of this parameter under transitions to arithmetic chaos would also be of interest for further study. Preliminary results agreed well with those obtained elsewhere [CGSV94] for bound systems.

In presenting these billiard systems as models of perturbed arithmetic scattering systems, we made an investigation in section 5.1 of the classical phase space underlying the dynamics and investigated the stability of a certain family of periodic orbits. Under perturbation of the lower boundary, a transition from integrable to fully-chaotic dynamics was observed and all periodic orbits considered were shown to become more unstable as varying the parameter led to higher percentages of chaotic phase space. Semiclassical WKB theory was used to produce accurate wavefunctions and eigenvalues for the integrable billiard that lies at one extreme of the perturbation parameter space. Additionally, in chapters 4 and 5 we derived other explicit methods of calculation, first for the behaviour of the resonant wavefunctions energies based on perturbation theory, and secondly for the S matrix, building on knowledge of the Green's function for a closed version of the system.

It has been seen that a spectral reorganisation occurs in the arithmetic cases where the S matrix can be calculated analytically but not the cusp forms. This leads to non-generic statistics for the resonance levels and their widths. At first sight the classical mechanics in arithmetic billiards seem no different in that both have fully chaotic phase spaces. However, Bogomolny et al. have shown [BGGS92] that in arithmetic cases there is an exponential degeneracy in the number of periodic orbits with the same period. This affects the Selberg trace formula (3.46) and hence the distribution of energy levels, leading to in particular, Poissonian statistics for the cusp forms (they only studied bound systems). In addition, although there is remaining exponential degeneracy for non-arithmetic cases, e.g. for the Hecke group with $n = 5$ above, they showed that the statistics in those cases appeared to be generic. For the open systems studied here, we find

that both the level spacing statistics and the widths follow RMT reasonably well. Interesting questions remain as to the exact role of exponential degeneracy in the trace formula (3.46) for open systems.

Appendix A

Change of variables in the equation for the free Green's function

To solve the equation for the free Green's function in the Poincaré half-plane (2.37), we considered a change of variables in the equation

$$(y^2\left(\frac{\partial}{\partial x^2}+\frac{\partial}{\partial y^2}\right)+\lambda)G_0(z,z';\lambda)=\delta(z-z'), \tag{A.1}$$

with $z=x+iy$. Since the expression for G_0 should not depend on the precise points involved on the half-plane, but only on their hyperbolic separation

$$\rho(z,z')=\cosh^{-1}\left(1+\frac{|z-z'|^2}{2yy'}\right), \tag{A.2}$$

we change to the variable

$$\xi=\cosh\rho(z,z')=1+\frac{(x-x')^2+(y-y')^2}{2yy'}. \tag{A.3}$$

To do this we need the first and second partial derivatives with respect to x and y in terms of those with respect to ξ. These are

$$\left.\frac{\partial}{\partial x}\right|_y=\left.\frac{\partial\xi}{\partial x}\right|_y\left.\frac{\partial}{\partial\xi}\right|_y=\frac{x-x'}{yy'}\left.\frac{\partial}{\partial\xi}\right|_y \tag{A.4}$$

and

$$\left.\frac{\partial}{\partial y}\right|_x = \left.\frac{\partial \xi}{\partial y}\right|_x \left.\frac{\partial}{\partial \xi}\right|_x = \left(\frac{y-y'}{yy'} - \frac{(x-x')^2+(y-y')^2}{2y^2y'}\right)\left.\frac{\partial}{\partial \xi}\right|_x$$
$$= \frac{y-y'\xi}{yy'}\left.\frac{\partial}{\partial \xi}\right|_x . \tag{A.5}$$

Applying each of these twice to G_0 gives

$$\frac{\partial^2 G_0}{\partial x^2} = \left(\frac{x-x'}{yy'}\right)^2 \frac{\mathrm{d}^2 G_0}{\mathrm{d}\xi^2} + \frac{x-x'}{yy'}\frac{\mathrm{d}G_0}{\mathrm{d}\xi}\frac{1}{yy'}\frac{yy'}{x-x'} \tag{A.6}$$

and

$$\frac{\partial^2 G_0}{\partial y^2} = \left(\frac{y-y'\xi}{yy'}\right)^2 \frac{\mathrm{d}^2 G_0}{\mathrm{d}\xi^2} + \frac{y-y'\xi}{yy'}\frac{\mathrm{d}G_0}{\mathrm{d}\xi}\left(\frac{-y'}{yy'} + \frac{1}{yy'}\frac{yy'}{y-y'\xi} - \frac{1}{y}\right). \tag{A.7}$$

Combining these two expressions then gives

$$\frac{\partial^2 G_0}{\partial x^2}+\frac{\partial^2 G_0}{\partial y^2} = \frac{(x-x')^2+(y-y'\xi)^2}{y^2y'^2}\frac{\mathrm{d}^2 G_0}{\mathrm{d}\xi^2}+\frac{\mathrm{d}G_0}{\mathrm{d}\xi}\left(\frac{1}{yy'} - \frac{y-y'\xi}{y^2y'} + \frac{1}{yy'} - \frac{y-y'\xi}{y^2y'}\right) \tag{A.8}$$

and inserting this into the left hand side of (A.1) yields

$$y^2\left(\frac{\partial^2 G_0}{\partial x^2} + \frac{\partial^2 G_0}{\partial y^2}\right)+\lambda G_0 = \frac{(x-x')^2+(y^2-2yy'r+y'^2r^2)}{y'^2}\frac{\mathrm{d}^2 G_0}{\mathrm{d}\xi^2}+2\xi\frac{\mathrm{d}G_0}{\mathrm{d}\xi}+\lambda G_0. \tag{A.9}$$

Finally collecting terms in the first bracket on the right-hand side brings us to

$$(\xi^2-1)\frac{\mathrm{d}G_0}{\mathrm{d}\xi^2} + 2\xi\frac{\mathrm{d}G_0}{\mathrm{d}\xi} + \lambda G_0 = 0, \quad \xi \neq 0, \tag{A.10}$$

which is (2.39) with $\lambda = -l(l+1)$, as required.

Appendix B

Derivation of Gauss's theorem in hyperbolic geometry

Gauss's theorem is a tensor equation identifying the integral over an arbitrary finite area A of the divergence of a vector field to the integral around the perimeter S of A of the outward-pointing component of that vector field.

$$\int_A \mathrm{div}\mathbf{V}\,\mathrm{d}A = \oint_A \mathbf{V}\cdot\hat{\mathbf{n}}\,\mathrm{d}S. \tag{B.1}$$

$\mathbf{V}\cdot\hat{\mathbf{n}}$ is the normal component of the vector $\mathbf{V}$, where $\hat{\mathbf{n}}$ is the unit normal to the perimeter. Since this is a tensor identity, it's validity in frames of reference other than Euclidean rectangular coordinates is trivial, but a proof is still reassuring at least.

Consider first a small (we shall consider the limit of its dimensions tending to zero) rectangular area G with its bottom left corner at coordinates (x_o, y_0) in the half-plane (see figure B.1). It extends δx in the horizontal coordinate and vertically by δy, thus having non-Euclidean area $\frac{\delta x\delta y}{y_0^2}$ and perimeter $\frac{2}{y_o}(\delta x+\delta Y)$, using the formulae from chapter 2 for area and length in this geometry.

In evaluation of the left hand side of (B.1) we note that the arbitrary vector field $\mathbf{V}$ has components v^x and v^y, and that $\mathrm{div}\mathbf{V} = v^i_{;i}$, where Einstein's summation notation is used for the index i (which can take values x and y). ; indicates the covariant derivative

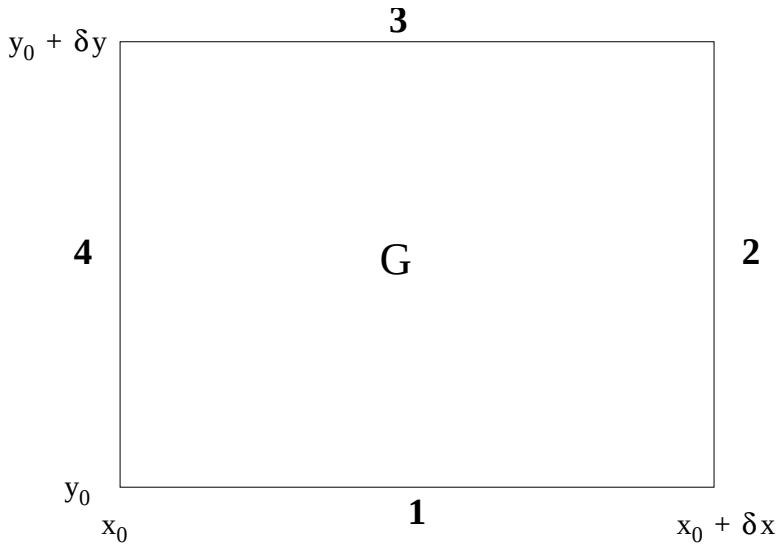

Figure B.1: Region G, considered in proof of Gauss's theorem

$$v^i_{;j} = \frac{\partial v^i}{\partial x^j} + v^k \Gamma^i_{kj}, \tag{B.2}$$

where i, j, k are indices taking values x and y, $x^x = x$ and $x^y = y$, and Γ^i_{kj} are the Christoffel symbols introduced in (2.7). Thus

$$\mathrm{div}\mathbf{V} = v^i_{;i} = \frac{\partial v^x}{\partial x} + v^x\Gamma^x_{xx} + v^y\Gamma^x_{yx} + \frac{\partial v^y}{\partial y} + v^y\Gamma^y_{yy} + v^x\Gamma^y_{xy} = \frac{\partial v^x}{\partial x} + \frac{\partial v^y}{\partial y} - \frac{2v^y}{y}. \tag{B.3}$$

Hence for small δx and δy, the left hand side of (B.1) for region G gives

$$\int_G \mathrm{div}\mathbf{V}\,\mathrm{d}G \simeq \frac{\delta x \delta y}{y_0^2}\left[\frac{\partial v^x}{\partial x}(x_0, y_0) + \frac{\partial v^y}{\partial y}(x_0, y_0) - \frac{2v^y(x_0, y_0)}{y_0}\right]. \tag{B.4}$$

Next examining the right hand side of (B.1), we consider each side in turn.

- On side 1, $\hat{\mathbf{n}} = \begin{pmatrix} 0 \\ -y_0 \end{pmatrix}$; $\mathrm{d}S = \mathrm{d}x/y_0$; $\mathbf{V}\cdot\hat{\mathbf{n}} = -\frac{v^y(x,y_0)}{y_0}$.
- On side 2, $\hat{\mathbf{n}} = \begin{pmatrix} y \\ 0 \end{pmatrix}$; $\mathrm{d}S = \mathrm{d}y/y$; $\mathbf{V}\cdot\hat{\mathbf{n}} = \frac{v^x(x_0+\delta x,y)}{y}$.

- On side 3, $\hat{\mathbf{n}} = \begin{pmatrix} 0 \\ y_0 + \delta y \end{pmatrix}$; $\mathrm{d}S = -\mathrm{d}x/(y_0 + \delta y)$; $\mathbf{V} \cdot \hat{\mathbf{n}} = \frac{v^y(x, y_0+\delta y)}{y_0+\delta y}$.
- On side 4, $\hat{\mathbf{n}} = \begin{pmatrix} -y \\ 0 \end{pmatrix}$; $\mathrm{d}S = -\mathrm{d}y/y$; $\mathbf{V} \cdot \hat{\mathbf{n}} = \frac{v^x(x_0, y)}{y}$.

Performing the integrals in an anti-clockwise direction around S, in the limit of small δx and δy, so that the functions can be approximated by linear expansions in those variables, the right hand side of (B.1) thus gives

$$\oint_A \mathbf{V}\cdot\hat{\mathbf{n}}\,\mathrm{d}S = -\frac{v^y(x_0, y_0)\delta x}{y_0^2} + \frac{v^y(x_0, y_0 + \delta y)\delta x}{(y_0 + \delta y)^2} + \frac{v^x(x_0 + \delta x, y_0)\delta y}{y_0^2} - \frac{v^x(x_0, y_0)\delta y}{y_0^2}. \tag{B.5}$$

Again expanding the vector components linearly in the small distances, that is

$$\begin{array}{rcl} \frac{v^y(x_0,y_0+\delta y)\delta x}{(y_0+\delta y)^2} & \simeq & \frac{\delta x}{y_0^2}\left(v^y(x_0, y_0) + \delta y \frac{\partial v^y}{\partial y}(x_0, y_0)\right)(1 + \frac{\delta y}{y_0})^{-2} \\ & \simeq & \frac{\delta x}{y_0^2}\left(v^y(x_0, y_0)(1 - 2\frac{\delta y}{y_0}) + \delta y \frac{\partial v^y}{\partial y}(x_0, y_0)\right) \end{array} \tag{B.6}$$

and

$$\frac{v^x(x_0 + \delta x, y_0)\delta y}{y_0^2} \simeq \frac{\delta y}{y_0^2}\left(v^x(x_0, y_0) + \delta x \frac{\partial v^x}{\partial x}(x_0, y_0)\right), \tag{B.7}$$

we are left with

$$\oint_A \mathbf{V} \cdot \hat{\mathbf{n}}\,\mathrm{d}S = \frac{\delta x \delta y}{y_0^2}\left[\frac{\partial v^x}{\partial x}(x_0, y_0) + \frac{\partial v^y}{\partial y}(x_0, y_0) - \frac{2v^y(x_0, y_0)}{y_0}\right] \tag{B.8}$$

which is identical with the left hand side as required. It is a simple matter to extend this result for infinitesimal rectangular areas to arbitrary smoothly-bounded regions in the half-plane by covering such an area with infinitesimal rectangles and observing that the surface integrals in the right hand side of (B.1) cancel with those of their neighbours for sides interior to the region, so that only the perimeter of the whole region generates surface terms. The volume integral extends trivially by the definition of an integral as the limit of a sum.

Appendix C

Numerical quadrature

In order to calculate the matrix elements in (5.53) the normal derivative (5.61) must be integrated over the range $0 \leq s \leq s_{\max}$ (see (5.55)) with weight $\sin(n\pi x(s)/\mathcal{L})$. To perform these integrals numerically, a tenth-order method is used, based on methods in [PTVF92]. A rule of quadrature of the form

$$\int_a^b f(x)\mathrm{d}x = \sum_{i=0}^{I-1} a_i f(h(k+i)) \tag{C.1}$$

is sought, where a and b are arbitrary and h is the size of the intervals between different evaluations of the function $f(x)$, which is called at the I points $x = h(k+i)$. By writing down a quadrature rule which is exact for polynomials up to order 9, corrections to this formula will, for general functions, be of higher order. By dividing the range of integration into small equally spaced intervals h, these corrections quickly become vanishingly small. To derive the general i^{th}-order formula, we first write down I equations for the coefficients a_i required to make our rule exact for polynomials of degree $I-1$ or less.

$$w_i = \frac{1}{h^i}\int_a^b x^i \mathrm{d}x = \frac{(b^{i+1}-a^{i+1})}{(i+1)h^i} = \sum_{j=0}^{I-1} a_j (k+j)^i,\ 0 \leq i \leq I-1 \in \mathbb{Z}. \tag{C.2}$$

This linear system is solved by matrix inversion and gives

$$a_i = \sum_{j=0}^{I-1} Q_{ij}^{-1} w_j, \tag{C.3}$$

with $Q_{ij} = (k+j)^i$. Now this formula is applied (for even I) to the specific case of $a = h(k + I/2 - 1)$, $b = h(k + I/2)$. This is the central interval in the range of points that the function has been evaluated at. This leads to a symmetrical set of coefficients a_i with the property $a_i = a_{I-1-i}$. For the order 10 rule, this gives explicitly the vector of a_i values

$$\underline{a} = \frac{h}{7257600} \begin{pmatrix} 2497 \\ -28939 \\ 162680 \\ -641776 \\ 2067169 \\ 2067169 \\ -641776 \\ 162680 \\ -28939 \\ 2497 \end{pmatrix} \tag{C.4}$$

and the formula

$$\int_{h(k+4)}^{h(k+5)} f(x)\mathrm{d}x = \sum_{i=0}^{9} a_i f(h(k+i)) + O(h^{10}) \tag{C.5}$$

for integration over a range h using 10 points equally spread around it.

Repeated application of this rule leads to an extended rule for integration of a function over a large interval. The interval is subdivided into sections of size h, as suggested above, then the rule applied to each in turn. Because the sum of the coefficients (C.4) is 1, away from the end points of the integral terms in (C.1) contribute with unit weight. However, the rule (C.5) cannot be applied to the $I/2 - 1$ points at the extremes of the integral range. For even I, the integral in this range is estimated by another application of (C.1), with $a = hk$ and $b = h(k + I/2 - 1)$ (or $a = h(k + I/2)$ and $b = h(k + I - 1)$ for the end of the range). For $I = 10$ this is solved again, giving the new vector of a_is

$$\underline{a} = \frac{h}{7257600}\begin{pmatrix} 2032128 \\ 11992064 \\ -1607680 \\ 20811776 \\ -10713088 \\ 10790912 \\ -6068224 \\ -2232320 \\ -487936 \\ 48128 \end{pmatrix}. \tag{C.6}$$

Combining this with repeated application of (C.5) gives a general tenth-order formula for the integral (C.1)

$$\int_a^b f(x)\mathrm{d}x = \sum_{i=0}^{I-1} b_i(f(a+ih) + f(b-ih)) + h\sum_{j=I}^{J} f(a+jh). \tag{C.7}$$

J is the point I evaluations from the end of the integral range, $J = (b-a)/h - I$, where h must be chosen to divide $(b-a)$ exactly, which is now an arbitrary range again. The vector of b_is for the case $I = 10$ is

$$\underline{b} = \frac{h}{7257600}\begin{pmatrix} 2034625 \\ 11965622 \\ -1471442 \\ 20306238 \\ -7084288 \\ 18554050 \\ 1053138 \\ 9516362 \\ 6767167 \\ 7305728 \end{pmatrix}. \tag{C.8}$$

Appendix D

Numerical evaluation of Bessel functions

D.1 Uniform asymptotics

The Bessel functions required to find the resonance spectrum of the billiards considered are solutions of the differential equation (5.30), that is

$$y^2 \frac{\mathrm{d}^2}{\mathrm{d}y^2} K_{\imath k}(2\pi m y/\mathcal{L}) + y \frac{\mathrm{d}}{\mathrm{d}y} K_{\imath k}(2\pi m y/\mathcal{L}) + (k^2 - (2\pi m y/\mathcal{L})^2) = 0. \tag{D.1}$$

Putting

$$w = \sqrt{p} K_{\imath k}(kp) \tag{D.2}$$

with

$$p = \frac{2\pi m y}{k\mathcal{L}}, \tag{D.3}$$

this is transformed to

$$\frac{\mathrm{d}^2 w}{\mathrm{d}p^2} = \left(k^2 \frac{p^2 - 1}{p^2} - \frac{1}{4p^2} \right) w, \tag{D.4}$$

which is of the standard form

$$\frac{\mathrm{d}^2 w}{\mathrm{d}p^2} = \left(k^2 f(p) + g(p)\right) w \tag{D.5}$$

if

$$f(p) = \frac{p^2 - 1}{p^2} \tag{D.6}$$

and

$$g(p) = -\frac{1}{4p^2}. \tag{D.7}$$

Starting from this equation, we follow the analysis of chapter 10 in [Olv74] to generate uniform expansions for w valid for all p, except for in the vicinity of the turning points at $f(p) = 0$. Changing to the variables

$$\xi = \int \sqrt{f(p)}\mathrm{d}p = \begin{cases} \sqrt{p^2-1} - \cos^{-1}(1/p); & |p| > 1 \\ -\imath\left(\sqrt{1-p^2} - \cosh^{-1}(1/p)\right); & |p| < 1 \end{cases} \tag{D.8}$$

and

$$W = f(p)^{1/4} w = \begin{cases} \left(\frac{p^2-1}{p^2}\right)^{1/4} w; & |p| > 1 \\ \exp(\imath\pi/4)\left(\frac{1-p^2}{p^2}\right)^{1/4} w; & |p| < 1 \end{cases}, \tag{D.9}$$

we obtain the new differential equation

$$\frac{\mathrm{d}^2 W}{\mathrm{d}\xi^2} = \left(k^2 + \psi(\xi)\right) W \tag{D.10}$$

with

$$\psi(\xi) = \frac{g(p)}{f(p)} - \frac{1}{f(p)^{3/4}} \frac{\mathrm{d}^2}{\mathrm{d}p^2}\left(\frac{1}{f(p)^{1/4}}\right). \tag{D.11}$$

Because we are primarily looking at regions of high momenta, we look for a solution with asymptotic k-behaviour $W(k,\xi) \simeq \exp \pm k\xi$, obtained by neglecting ψ in (D.10). Keeping k and ξ separate, we look for solutions with the form

$$W(k,\xi) = \exp(\pm k\xi) \sum_{s=0}^{\infty} \frac{A_s(\xi)}{(\pm k)^s}. \tag{D.12}$$

Substituting this back into (D.10) and comparing coefficients of k^{-s}, we get

$$2A'_{s+1}(\xi) = -A''_s(\xi) + \psi A_s(\xi), \tag{D.13}$$

making A_0 a constant, which can be chosen as 1. Higher coefficients are obtained recursively by

$$A_{s+1}(\xi) = -\frac{1}{2}A'_s(\xi) + \frac{1}{2}\int \psi(\xi)A_s(\xi)\mathrm{d}\xi, \tag{D.14}$$

which can be written in terms of the original variable p as

$$A_{s+1}(p) = \begin{cases} -\frac{1}{2}\frac{p}{\sqrt{p^2-1}}A'_s(p) - \frac{1}{8}\int \frac{p(4+p^2)}{(p^2-1)^{5/2}}A_s(p)\mathrm{d}p; & |p|>1 \\ \imath\left(-\frac{1}{2}\frac{p}{\sqrt{1-p^2}}A'_s(p) - \frac{1}{8}\int \frac{p(4+p^2)}{(1-p^2)^{5/2}}A_s(p)\mathrm{d}p\right); & |p|<1 \end{cases} \tag{D.15}$$

Noticing that the A_s are functions only of $t = \frac{1}{\sqrt{p^2-1}}$, writing $B_s = i^s A_s$ and $t = \frac{1}{\sqrt{1-p^2}}$ for $|p|<1$, and choosing the arbitrary integration constant so that $A_{s+1} \to 0$ for large p, this is concisely written as

$$\left.\begin{matrix} A_{s+1}(t) \\ B_{s+1}(t) \end{matrix}\right\} = \begin{cases} \frac{1}{2}t^2(1+t^2)A'_s(t) + \frac{1}{8}\int_0^t (1+5t^2)A_s(t)\mathrm{d}t; & |p|>1 \\ \frac{1}{2}t^2(1-t^2)B'_s(t) + \frac{1}{8}\int_0^t (1-5t^2)B_s(t)\mathrm{d}t; & |p|<1 \end{cases} \tag{D.16}$$

Thus we obtain solutions to (5.30) in the form

$$w_\pm(k,p) = \frac{\sqrt{p}}{(p^2-1)^{1/4}}\exp\left(\pm k\left(\sqrt{p^2-1} - \cos^{-1}(1/p)\right)\right)\sum_{s=0}^{\infty}\frac{A_s(t)}{(\pm k)^s} \tag{D.17}$$

for $|p|>1$ and

$$w_\pm(k,p) = \frac{\sqrt{p}}{(1-p^2)^{1/4}}\exp\left(\pm\imath\left(-\frac{\pi}{4} + k\left(\sqrt{1-p^2} - \cosh^{-1}(1/p)\right)\right)\right)\sum_{s=0}^{\infty}\frac{\imath^s B_s(t)}{(\pm k)^s} \tag{D.18}$$

for $|p|<1$. We identify the correct linear combination of these solutions to yield the desired function, $w = \sqrt{p}K_{\imath k}(kp)$ by comparison with the Bessel function's asymptotic behaviour. For large $|p|$ we have

$$\sqrt{p}K_{\imath k}(kp) \simeq \left(\frac{\pi}{2k}\right)^{1/2} \exp(-kp). \tag{D.19}$$

whereas

$$w_{\pm}(k,p) \simeq \exp\left(\pm k\left(p-\pi/2\right)\right), \tag{D.20}$$

so our solution is

$$K_{\imath k}(kp) = \left(\frac{\pi}{2k}\right)^{1/2} \frac{\exp(-k\pi/2)}{(p^2-1)^{1/4}} \exp\left(-k\left(\sqrt{p^2-1}-\cos^{-1}(1/p)\right)\right) \sum_{s=0}^{\infty} \frac{A_s(t)}{(\pm k)^s}. \tag{D.21}$$

Similarly for small $|p|$, we compare to the asymptotic solution found semiclassically in section 5.3.1

$$\sqrt{p}K_{\imath k}(kp) \simeq \left(\frac{\sqrt{p}}{(1-p^2)^{1/4}} \sin(-k(\sqrt{1-p^2}+\cosh^{-1}(1/p))+\frac{\pi}{4})\right), \tag{D.22}$$

and thus take a superposition of $w_+(k,p) - w_-(k,p)$ to give a solution

$$\begin{aligned} &K_{\imath k}(kp) = \\ &\left(\tfrac{\pi}{2k}\right)^{1/2} \tfrac{\exp(-k\pi/2)}{(1-p^2)^{1/4}} \left[\sin\left(-k\left(\sqrt{1-p^2}-\cosh^{-1}(1/p)\right)+\tfrac{\pi}{4}\right) \textstyle\sum_{s=0}^{\infty} \frac{(-1)^s B_{2s}(t)}{(k)^{2s}}\right. \\ &\left. +\cos\left(-k\left(\sqrt{1-p^2}-\cosh^{-1}(1/p)\right)+\tfrac{\pi}{4}\right) \textstyle\sum_{s=0}^{\infty} \frac{(-1)^s B_{2s+1}(t)}{(k)^{2s+1}}\right]. \end{aligned} \tag{D.23}$$

These forms are those found in [CGS91] and originally attributed to Debye [Olv74]. When $\Re(k)$ is large the series can be truncated quickly. Our routines use terms up to the tenth power of t. Coefficients for comparison can be found in [AS65].

D.2 Continued fraction algorithm

Near the turning points $f(p) = 0$ in the above, the series derived there fail. One solution is to use the technique of section 5.3.1 and linearise the differential equation near those points, but the solutions in terms of Airy functions thus

obtained are limited in their applicability too. In fact a very robust numerical method introduced by Nico Temme [Tem75] is found to converge quickly in a wide region of parameter space, including the neighbourhood of the turning points.

The general algorithm is expounded on in [PTVF92] but here a streamlined version is presented, since only the functions $K_{\imath k}(kp)$ are required for our purposes. The method first writes the Bessel function in terms of the confluent hypergeometric function z_0.

$$K_{\imath k}(kp) = \sqrt{\pi}(2kp)^{\imath k} \exp(-kp) z_0(kp), \tag{D.24}$$

where the functions

$$z_n(kp) = U(\imath k + 1/2 + n, 2\imath k + 1, 2kp) \tag{D.25}$$

are the second solutions of the confluent hypergeometric equation

$$xU''(a,c,x) + (c-x)U'(a,c,x) - aU(a,c,x) = 0. \tag{D.26}$$

Primes here denote differentiation with respect to the parameter x.

These functions obey the recurrence relation ([AS65] eq. 13.4.15)

$$z_{n-1}(x) = b_n z_n(x) + a_{n+1} z_{n+1}(x) \tag{D.27}$$

with

$$b_n = 2(n+x) \tag{D.28}$$

and

$$a_{n+1} = -\left[(n+1/2)^2 + k^2\right]. \tag{D.29}$$

Temme introduced a normalisation condition for these functions;

$$\sum_{n=0}^{\infty} C_n z_n = \left(\frac{1}{2x}\right)^{\imath k + 1/2}, \tag{D.30}$$

with

$$C_n = \frac{(-1)^n \Gamma(\imath k + 1/2 + n)}{n! \Gamma(\imath k + 1/2 - n)} \tag{D.31}$$

which obey the recurrence relation with $C_0 = 1$

$$C_{n+1} = -\frac{a_{n+1}}{n+1} C_n = \left[n + \frac{k^2 + 1/4}{n+1} \right] C_n. \tag{D.32}$$

To prove the relation (D.30), one uses the integral representation of the hypergeometric function

$$\Gamma(a) U(a, b, z) = \int_0^\infty \exp(-zt) t^{a-1} (1+t)^{b-a-1} \mathrm{d}t, \tag{D.33}$$

which here is used as

$$C_n z_n = \frac{(-1)^n}{n! \Gamma(\imath k + 1/2 - n)} \int_0^\infty \exp(-2zt) t^{\imath k - 1/2 + n} (1+t)^{\imath k + 1/2 + n} \mathrm{d}t. \tag{D.34}$$

Summing over n and taking the sum inside the integral, we observe that the sum can be written as a prefactor times a series expansion of $\left(\frac{1}{1+t}\right)^{\imath k - 1/2} = (1-q)^{\imath k - 1/2}$, in powers of $q = \frac{t}{t+1}$;

$$\frac{t^{\imath k - 1/2} (1+t)^{\imath k - 1/2}}{\Gamma(\imath k + 1/2)} \sum_{n=0}^\infty q_n, \tag{D.35}$$

with

$$q_{n+1} = \frac{-t(\imath k - 1/2 - n)}{(n+1)(t+1)} q_n, \; q_0 = 1. \tag{D.36}$$

Thus

$$\sum_{n=0}^\infty C_n z_n = \frac{1}{\Gamma(\imath k + 1/2)} \int_0^\infty \exp(-2zt) t^{\imath k - 1/2} \mathrm{d}t. \tag{D.37}$$

Substituting $r = 2zt$, this gives

$$\sum_{n=0}^\infty C_n z_n = \left(\frac{1}{2z} \right)^{\imath k + 1/2} \frac{1}{\Gamma(\imath k + 1/2)} \int_0^\infty \exp(-r) r^{\imath k - 1/2} \mathrm{d}r. \tag{D.38}$$

The integral remaining is a representation of the Gamma function in the denominator and (D.30) results. Although the integral definition of the hypergeometric function (D.33) is only valid for $\Re(a) > 0$, thus $\Im(k) < 1/2$, which is not always the case in our algorithm, the relation (D.30) can be seen to hold for all k. The C_n are invariant under the transformation $k \mapsto -k$, as are the coefficients in the recursion relations (D.27). Using the property of the Bessel function $K_\nu = K_{-\nu}$, valid for all ν, and the definition of the Bessel function in terms of the hypergeometric function (D.24), the z_n are seen to transform as

$$z_n(k) = (2z)^{-2k} z_n(-k). \tag{D.39}$$

Thus

$$\sum_{n=0}^{\infty} C_n(-k) z_n(-k) = (2z)^{2k} \sum_{n=0}^{\infty} C_n(k) z_n(k) = \left(\frac{1}{2x}\right)^{-\imath k+1/2} \tag{D.40}$$

and thus the relation (D.30) still holds when $k \mapsto -k$, hence for the whole k-plane.

Writing

$$S = \sum_{n=1}^{\infty} C_n \frac{z_n}{z_0} \tag{D.41}$$

and using (D.24), the Bessel function can be expressed as

$$K_{\imath k}(kp) = \left(\frac{\pi}{2kp}\right)^{1/2} \exp(-kp) \frac{1}{1+S}. \tag{D.42}$$

The task is now to evaluate the sum $1 + S$. Putting

$$S = \sum_{i=1}^{\infty} \prod_{j=1}^{i} Y_j \tag{D.43}$$

with

$$Y_n = \frac{C_n z_n}{C_{n-1} z_{n-1}}, \tag{D.44}$$

the sum can be evaluated in reverse, assuming it has converged above some maximum N. Seeding with the arbitrary value $Y_N = 1$, previous values are obtained by

working backwards through the continued fraction representation of z_1/z_0. Using successive terms from (D.27),

$$\frac{z_1}{z_0} = \frac{1}{b_1 + a_2\frac{z_2}{z_3}} = \frac{1}{b_1+}\frac{a_2}{b_2+}\cdots \tag{D.45}$$

one obtains

$$Y_n = \frac{C_n/C_{n-1}}{b_n + a_{n+1}\frac{z_{n+1}}{z_n}} = \frac{(n-1) + \frac{(k^2+1/4)}{n}}{2x + 2n - (n+1)Y_{n+1}}. \tag{D.46}$$

If N steps are to be taken, the scaling prefactor for the Bessel function is divided into N portions, so each individual Y_n scales appropriately to the whole as

$$Y_n \to Y_n \left(\frac{\pi}{2kp}\right)^{-1/2N} \exp(kp/N), \tag{D.47}$$

thus precision overflow is avoided during the calculation.

Format of references

Entries in the references section appear alphabetically sorted, by the initial of each author's surname in turn. This is followed by the title of the referred work, then publication details including the journal title and volume published in for an article, or the publishing house for a book. A relevant page range may be given and this is followed by the year of publication. Finally an index of pages in this thesis where each reference was cited is given. In the text a citation can be identified by its code, which consists of the first letters of the author's (authors') surname(s), and the last two digits of the publication year.

References

[ABB+99] E. Anderson, Z. Bai, C. Bischof, S. Blackford, J. Demmel, J. Dongarra, J. Du Croz, A. Greenbaum, S. Hammarling, A. McKenney, and D. Sorensen. *LAPACK Users' Guide*. Society for Industrial and Applied Mathematics, third edition, 1999. 109

[ADG+99] H. Alt, C. Dembowski, H.-D. Gräf, R. Hofferbert, H. Rehfeld, A. Richter, and C. Schmit. Experimental versus numerical eigenvalues of a Bunimovich stadium billiard: A comparison. *Phys. Rev. E*, 60:2851–2857, 1999. 106

[AGG+97] H. Alt, H.-D. Gräf, T. Guhr, H. L. Harney, R. Hofferbert, H. Rehfeld, A. Richter, and P. Schardt. Correlation-hole method for the spectra of superconducting microwave billiards. *Phys. Rev. E*, 55:6674–6683, 1997. 128

[ALST05] R. Aurich, S. Lustig, F. Steiner, and H. Then. Indications about the shape of the universe from the Wilkinson microwave anisotropy probe data. *Phys. Rev. Letters*, 94:021301, 2005. 21, 38

[And58] P. W. Anderson. Absence of diffusion in certain random lattices. *Phys. Rev.*, 109:1492–1505, 1958. 20

[Arf85] G. Arfken. *Mathematical Methods for Physicists*, pages 560–562. Academic Press, Inc., 1985. 55

[Art24] E. Artin. Ein mechanisches System mit quasi-ergodischen Bahnen. *Abh. Math. Sem. d. Hamburgischen Universität*, 3:170–175, 1924. 22, 37

[AS65] M. Abramowitz and I. A. Stegun. *Handbook of Mathematical Functions*. Dover, 1965. 40, 108, 111, 161, 162

[ASS88] R. Aurich, M. Sieber, and F. Steiner. Quantum chaos of the Hadamard-Gutzwiller model. *Phys. Rev. Lett.*, 61:483–487, 1988. 23

[Ave02] H. Avelin. Research announcement on the deformation of cusp forms. Technical report, Uppsala Univ, 2002. UUDM report 2002:26, Uppsala. 24

[Bac03] A. Backer. Numerical aspects of eigenvalue and eigenfunction computations for chaotic quantum systems. In M. Degli Esposti and S. Graffi, editors, *The Mathematical Aspects of Quantum Maps*. Springer, 2003. 109

[BB70] R. Balian and C. Bloch. Distribution of eigenfrequencies for the wave equation in a finite domain I: three-dimensional problem with smooth boundary surface. *Ann. Phys.*, 60:401–447, 1970. 61

[BB86] K. Bartschat and P. G. Burke. Resfit - a multichannel resonance fitting program. *Computer Physics Communications*, 41, 1986. 95

[BB97] M. Brack and R Bhaduri. *Semiclassical Physics*. Addison Wesley, 1997. 20, 115, 116

[BD95] H. Beijeren and J. R. Dorfman. Lyapunov exponents and Kolmogorov-sinai entropy for the Lorentz gas at low densities. *Phys. Rev. Letters*, 74:4412–4415, 1995. 87

[Ber89] M. Berry. Quantum chaology, not quantum chaos. *Physica Scripta*, 40:335–336, 1989. 20

[BGGS92] E. B. Bogomolny, B. Georgeot, M.-J. Giannoni, and C. Schmit. Chaotic billiards generated by arithmetic groups. *Phys. Rev. Lett.*, 69:1477–1480, 1992. 22, 145, 148

[BGS84] O. Bohigas, M. J. Giannoni, and C. Schmit. Characterization of chaotic quantum spectra and universality of level fluctuation laws. *Phys. Rev. Lett.*, 52, 1984. 21, 119

[BGS86] O. Bohigas, M.-J. Giannoni, and C. Schmit. Spectral fluctuations of classically chaotic quantum systems. *LNP Vol. 263: Quantum Chaos and Statistical Nuclear Physics*, 263:18–40, 1986. 22

[BH76] H. P. Baltes and E. R. Hilf. *Spectra of Finite Systems*. Bibliographisches Institut, Mannheim, 1976. 61

[BK99] M. V. Berry and J. P. Keating. The Riemann zeros and eigenvalue asymptotics. *SIAM Review*, 41:236–266, 1999. 24, 119

[Bog06] E. Bogomolny. Quantum and arithmetical chaos. In *Frontiers in Number Theory, Physics and Geometry, Proceedings of Les Houches winter school 2003*. Springer-Verlag, 2006. 39, 64, 68, 70

[Bou01] N. Bouhamou. The use of NAG mesh generation and sparse solver routines for solving partial differential equations. Technical report, NAG Ltd, 2001. Reference no. TR1/01 (NP3615). 104

[Bro73] T. A. Brody. A statistical measure for the repulsion of energy levels. *Lettere Al Nuovo Cimento*, 7:482, 1973. 125

[BSS92] J. Bolte, G. Steil, and F. Steiner. Arithmetical chaos and violation of universality in energy level statistics. *Phys. Rev. Lett.*, 69:2188–2191, 1992. 22, 112

[BT77] M. V. Berry and M. Tabor. Level clustering in the regular spectrum. *Proc. R. Soc. Lond. A*, 356:375–394, 1977. 119, 125

[BTU93] O. Bohigas, S. Tomsovic, and D. Ullmo. Manifestations of classical phase space structures in quantum mechanics. *Physics Reports*, 223:43–133, 1993. 20

[BV86] B. V. Balázs and A. Voros. Chaos on the pseudosphere. *Phys. Rep.*, 143:109–240, 1986. 12, 22, 28, 34, 38, 45, 64, 70

[BV98] E. Balslev and A. Venkov. The Weyl law for subgroups of the modular group. *Geom. Funct. Anal.*, 8(3):437–465, 1998. 24

[CAM+04] P. Cvitanović, R. Artuso, R. Mainieri, G. Tanner, and G. Vattay. *Chaos: Classical and Quantum*, page 555. Niels Bohr Institute, Copenhagen 2005, 2004. Stable version 11. 61

[CE89] P. Cvitanović and B. J. Eckhardt. Periodic-orbit quantization of chaotic systems. *Phys. Rev. Lett.*, 63(8):823–826, 1989. 62

[CGS91] A. Csordás, R. Graham, and P. Szépfalusy. Level statistics of a non-compact cosmological billiard. *Phys. Rev. A*, 44:1491–1499, 1991. 66, 161

[CGSV94] A. Csordás, R. Graham, P. Szépfalusy, and G. Vattay. Transition from Poissonian to Gaussian-orthogonal-ensemble level statistics in a modified Artin's billiard. *Phys. Rev. E*, 49:325–333, 1994. 82, 83, 84, 86, 92, 124, 125, 127, 148

[CM03] N. Chernov and R. Markarian. *Introduction to the Ergodic Theory of Chaotic Billiards*. IMPA, Rio de Janeiro, Brasil, 2003. 87

[Cox65] H. S. M. Coxeter. *Non-Euclidean Geometry*. University of Toronto Press, 1965. 34

[Cre95] P. Crehan. Chaotic spectra of classically integrable systems. *Journal of Physics A*, 28:6389–6394, 1995. 48

[Ein17] A. Einstein. Zum Quantensatz von Sommerfeld und Epstein. *Verhandlungen der Deutschen Physikalischen Gesellschaft*, 19:82–92, 1917. 19

[EMOT53] A. Erdélyi, W. Magnus, F. Oberhettinger, and F. G. Tricomi. *Higher Trascendental Functions: Volume 1*. McGraw-Hill, 1953. 39

[FH65] R. P. Feynman and A. R. Hibbs. *Quantum Physics and Path Integrals*. McGraw-Hill, 1965. 57, 58

[FK97] R. Fricke and F. Klein. *Vorlesungen über die Theorie der automorphen Funktionen*. Teubner, Leipzig, 1897. 47

[FKS05] Y. V. Fyodorov, T. Kottos, and H.-J. Stöckmann, editors. *Special issue on trends in quantum chaotic scattering*, volume 38. Institute of Phyiscs publishing, 2005. 23

[For29] L. Ford. *Automorphic Functions*. McGraw-Hill, 1929. 47

[Fri98] H. Friedrich. *Theoretical Atomic Physics*. Springer, 1998. 24, 56

[FS97] Y. Fyodorov and H.-J. Sommers. Statistics of resonance poles, phase shifts and time delays in quantum chaotic scattering: Random matrix approach for systems with broken time-reversal invariance. *J. Math. Phys.*, 38, 1997. 78, 95, 119, 121

[GHSV91] R. Graham, R. Hübner, P. Szépfalusy, and G. Vattay. Level statistics of a noncompact integrable billiard. *Phys. Rev. A*, 44:7002–7015, 1991. 61, 106, 111, 124

[GR89] P. Gaspard and S. Rice. Semiclassical quantization of the scattering from a classically chaotic repellor. *J. Chem. Phys.*, 90:2242–2254, 1989. 51

[Gut67] M. C. Gutzwiller. Phase-integral approximation in momentum space and the bound states of an atom. *J. Math. Phys.*, 8:1979–2000, 1967. 58

[Gut83] M. C. Gutzwiller. Stochastic behavior in quantum scattering. *Physica D: Nonlinear Phenomena*, 7:341–355, 1983. 50

[Gut90] M. Gutzwiller. *Chaos in Classical and Quantum Mechanics*. springer-verlag, 1990. 20, 38, 46, 58, 112

[Had98] J. Hadamard. Les surfaces à courbures opposés et leurs lignes géodésiques. *J. Math. Pures et Appl.*, 4:27–73, 1898. 22, 45

[HB82] D. A. Hejhal and B. Berg. Some new results concerning eigenvalues of the non-Euclidean Laplacian for PSL$(2, \mathbb{Z})$. Technical report, University of Minnesota, 1982. 110, 111, 112

[Hej92a] D. A. Hejhal. Eigenvalues of the Laplacian for Hecke triangle groups. *Memoirs of the American Mathematical Society*, 97, 1992. 70, 112

[Hej92b] D. A. Hejhal. Eigenvalues of the Laplacian for Hecke triangle groups. *Mem. Amer. Math. Soc.*, 469, 1992. 110, 112

[Hel84] E. J. Heller. Bound-state eigenfunctions of classically chaotic Hamiltonian systems: Scars of periodic orbits. *Phys. Rev. Lett.*, 53:1515–1518, 1984. 21

[HIL+92] F. Haake, F. Izrailev, N. Lehmann, D. Saher, and H.-J. Sommers. Statistics of complex levels of random matrices for decaying systems. *Z. Phys. B*, 88:359–370, 1992. 122

[HMFOU05] P. J. Howard, F. Mota-Furtado, P. F. O'Mahony, and V. Uski. Statistics of resonances for a class of billiards on the Poincaré half-plane. *J. Phys. A*, 38:10829–10841, 2005. 106

[Kea92] J. P. Keating. Periodic orbit resummation and the quantization of chaos. *Proc. R. Soc. Lond. A*, 436:99–108, 1992. 62

[Kub73] T. Kubota. *Elementary Theory of Eisenstein Series*. John Wiley and Sons, 1973. 51

[LLJP86] L. Leviandier, M. Lombardi, R. Jost, and J. P. Pique. Fourier transform: A tool to measure statistical level properties in very complex spectra. *Physical Review Letters*, 56:2449–2452, 1986. 128

[LP76] P. D. Lax and R. S. Phillips. *Scattering Theory for Automorphic Functions*. Princeton University Press, 1976. 41, 51

[LRP06] M. Lyly, J. Ruokolainen, and A. Pursula. Elmer, 2006. http://www.csc.fi/elmer/index.phtml. 101, 103

[LS93] M. Lombardi and T. H. Seligman. Universal and nonuniversal statistical properties of levels and intensities for chaotic Rydberg molecules. *Phys. Rev. A*, 47:3571–3586, 1993. 129, 131

[LSZ03] W. T. Lu, S. Sridhar, and M. Zworski. Fractal Weyl laws for chaotic open systems. *Phys. Rev. Letters*, 91, 2003. 61

[Maj98] A. W. Majewski. Does quantum chaos exist? a quantum Lyapunov exponents approach. *ArXiv Quantum Physics e-prints*, 1998, quant-ph/9805068. 20

[MHB+04] S. Müller, S. Heusler, P. Braun, F. Haake, and A. Altland. Semiclassical foundation of universality in quantum chaos. *Phys. Rev. Lett.*, 93:014103, 2004. 21

[Moi97] N. Moiseyev. Quantum theory of resonances: calculating energies, widths and cross-sections by complex scaling. *Physics Reports*, 302:211–203, 1997. 96

[Mon73] H. Montgomery. The pair correlation of zeros of the zeta function. *Analytic Number Theory (Proceedings of Symposia in Pure Mathematics)*, 24:181–193, 1973. 23

[MS05] F. Mezzadri and N. C. Snaith. *Recent Perspectives in Random Matrix Theory and Number Theory*. Cambridge University Press, 2005. 24

[Odl] A. M. Odlyzko. The first $100,000$ zeros of the Riemann zeta function, accurate to within $3 * 10^{-9}$). http://www.dtc.umn.edu/∼odlyzko/zeta_tables/zeros1. 56, 110, 111, 112

[Odl89] A. M. Odlyzko. The 10^{20}th zero of the Riemann zeta function and 70 million of its neighbours. http://www.dtc.umn.edu/∼odlyzko/unpublished/, 1989. 112, 125, 129

[Olv74] F. W. J. Olver. *Asymptotics and Special Functions*. Academic Press, 1974. 159, 161

[Ott93] E. Ott. *Chaos in Dynamical Systems*. Cambridge University Press, 1993. 20

[PHH06] O. Pironneau, F. Hecht, and A. Le Hyaric. FreeFEM++, 2006. http://www.freefem.org/ff++. 80, 103

[PRSB00] E. Persson, I. Rotter, H.-J. Stöckmann, and M. Barth. Observation of resonance trapping in an open microwave cavity. *Physical Review Letters*, 85:2478–2481, 2000. 122

[PS85] R. S. Phillips and P. Sarnak. The Weyl theorem and the deformation of discrete groups. *Comm. Pure Appl. Math.*, 38:853–866, 1985. 24

[PT56] C. E. Porter and R. G. Thomas. Fluctuations of nuclear reaction widths. *Physical Review*, 104:483, 1956. 21, 121

[PTVF92] W. H. Press, S. A. Teukolsky, W. T. Vetterling, and B. P. Flannery. *Numerical Recipes in FORTRAN - The Art of Scienctfic Computing*. Cambridge University Press, 1992. 110, 155, 162

[RM93] U. V. Riss and H.-D. Meyer. Calculation of resonance energies and widths using the complex absorbing potential method. *J. Phys. B*, 26:4503–4536, 1993. 96, 97, 98

[RM02] L. Ramdas Ram-Mohan. *Finite Element and Boundary Element Applications in Quantum Mechanics*. Oxford University Press, 2002. 104

[Rob86] M. Robnik. A simple separable Hamiltonian having bound states in the continuum. *Journal of Physics A*, 19:3845–3848, 1986. 56

[RV98] M. Robnik and G. Veble. On spectral statistics of classically integrable systems. *Journal of Physics A*, 31:4669–4704, 1998. 125

[SC93] R. Schack and C. Caves. Hypersensitivity to perturbations in the quantum baker's map. *Phys. Rev. Lett.*, 71(4):525–528, 1993. 20

[Sch78] D. Schattschneider. The plane symmetry groups: Their recognition and notation. *Am. Math. Monthly*, 85:439–450, 1978. 47

[Sch80a] C. Schmit. Quantum and classical properties of some billiards on the hyperbolic plane. In *Chaos et Physique Quantique — Chaos and Quantum Physics, Les Houches, ecole d'éte de physique theorique 1989, session LII*. Elsevier Science Publishers B V, 1980. 106, 121

[Sch80b] B. Schutz. *Geometrical Methods of Mathematical Physics*. Cambridge University Press, 1980. 30, 36

[Sch95] R. Schack. Comment on 'exponential sensitivity and chaos in quantum systems'. *Phys. Rev. Lett.*, 75(3):581, 1995. 20

[Sel56] A. Selberg. Harmonic analysis and discontinuous groups in weakly symmetric Riemannian spaces with applications to Dirichlet series. *Journal of the Indian Mathematical Society*, 20:47–87, 1956. 63

[SH00] S. Sahoo and Y. K. Ho. Determination of resonance energy and width using the method of complex absorbing potential. *Chinese Journal Of Physics*, 38:127–138, 2000. 96

[SSCL93] M Sieber, U Smilansky, S C Creagh, and R G Littlejohn. Non-generic spectral statistics in the quantized stadium billiard. *Journal of Physics A: Mathematical and General*, 26(22):6217–6230, 1993. 59

[SSS03] D. Savin, V. Sokolov, and H.-J. Sommers. Is the concept of a non-Hermitian effective Hamiltonian relevant in the case of potential scattering? *Phys. Rev. E*, 67, 2003. 78

[Ste94] G. Steil. Eigenvalues of the Laplacian and of the Hecke operators for $\mathrm{PSL}(2,\mathbb{Z})$. Technical report, DESY, 1994. 110, 111

[Stö99] H.-J. Stöckmann. *Quantum Chaos: an Introduction*. Cambridge University Press, 1999. 38, 119, 125, 127

[SZ89] V. V. Sokolov and V. G. Zelevinsky. Dynamics and statistics of unstable quantum states. *Nuclear Physics A*, 504:562–588, 1989. 122

[Tay72] J. Taylor. *Scattering Theory*. John Wiley and Sons, Inc., 1972. 41, 43

[Tem75] N. M. Temme. On the numerical evaluation of the modified Bessel function of the third kind. *J. Comput. Phys.*, 19:324–337, 1975. 162

[The05] H. Then. Maaßcusp forms for large eigenvalues. *Math. Comp.*, 74:363–381, 2005. 111

[THM96] G. Tanner, K. T. Hansen, and J. Main. The semiclassical resonance spectrum of hydrogen in a constant magnetic field. *Nonlinearity*, 9:1641–1670, 1996. 62

[Tit51] E. C. Titchmarsh. *The Theory of the Riemann Zeta-Function*. Oxford University Press, 1951. 54

[Ven78] A. B. Venkov. Selberg's trace formula for the Hecke operator generated by an involution, and the eigenvalues of the Laplace-Beltrami operator on the fundamental domain of the modular group $\mathrm{PSL}(2,\mathbb{Z})$. *Math. USSR Izvestiya*, 12:448–462, 1978. 61, 64, 65

[vV28] J. H. van Vleck. The correspondence principle in the statistical interpretation of quantum mechanics. *Proceedings of the National Academy of Sciences of the United States of America*, 14:178–188, 1928. 58

[Wat66] G. N. Watson. *A Treatise on the Theory of Bessel Functions*. Cambridge University Press, 1966. 40

[Wey11] H. Weyl. Über die asymptotische Verteilung der Eigenwerte. *Göttinger Nachrichten*, 110, 1911. 60

[WJ89] D. M. Wardlaw and W. Jaworski. Time delay, resonances, Riemann zeros and chaos in a model quantum scattering system. *Journal of Physics A*, 22:3561–3575, 1989. 38, 43, 112

[Wol05] Wolfram Research, Inc. Mathematica, 2005. 110, 114